Polymer Flooding in Uzen Field: A Simulation Study to Design and Analyze the Effect of Operational Parameters

by

Aibek Mukhtarov

THESIS SUPERVISOR

Peyman Pourafshary

Thesis submitted to the School of Mining and Geosciences of Nazarbayev University in Partial Fulfillment of the Requirements for the Degree of **Master of Science in Petroleum Engineering**

Nazarbayev University
18.04.2024

ORIGINALITY STATEMENT

I, Aibek Mukhtarov, hereby declare that this submission is my own work and to the best of my knowledge it contains no materials previously published or written by another person, or substantial proportions of material which have been accepted for the award of any other degree or diploma at Nazarbayev University or any other educational institution, except where due acknowledgement is made in the thesis.

Any contribution made to the research by others, with whom I have worked at NU or elsewhere is explicitly acknowledged in the thesis.

I also declare that the intellectual content of this thesis is the product of my own work, except to the extent that assistance from others in the project's design and conception or in style, presentation and linguistic expression is acknowledged.

Signed on 18.04.2024

_____

ABSTRACT

Enhancing oil recovery in mature oil fields poses a considerable challenge within the oil and gas sector. Despite the prevalent application of waterflooding techniques, significant amount of oil often remains unrecovered. This study focuses on enhancing oil recovery in the Uzen field, through the implementation of polymer flooding alongside hot water flooding and hot polymer flooding methods.

Numerical simulations are employed to evaluate the influence of operational parameters on the efficacy of polymer flooding. Key parameters under scrutiny include the polymer injection rate, duration of flooding, and polymer concentration. The main objective of this investigation is to devise an optimal set of operational parameters specific to the Uzen field, thereby maximizing the effectiveness of polymer flooding.

The outcomes derived from the numerical simulations reveal that the most favorable polymer injection rate is 140 m^3/d, with an optimal polymer flood duration of 20 years, and an optimal polymer concentration of 2500 ppm.

Characterized by a high water cut, the Uzen field represents a prime candidate for the implementation of polymer flooding as a tertiary recovery strategy. By conducting comprehensive experimental and simulation studies, different operational parameters were designed and evaluated. Practical recommendations were provided to enhance oil recovery within the Uzen field, based on an integrated research approach.

DEDICATION

I dedicate this work to my nephews Ayaru, Alizhan, Amir, Aibar, and Asylym.

ACKNOWLEDGMENT

I'd like to express my heartfelt gratitude to everyone who helped to complete this thesis. I am grateful to Peyman Pourafshary, my thesis supervisor, as well as lead RA Mariam Shakeel and Sabber, for their invaluable guidance, encouragement, and constant assistance throughout my research and academic ventures. Their mentorship has had a significant impact on the reservoir simulation activities and laboratory study processes, and I am extremely grateful for their knowledge, advice, and help. I am grateful for their expertise and kindness, which have contributed to my academic development.

Moreover, I express my thanks to the School of Mining and Geoscience at Nazarbayev University for providing me with the opportunity to pursue my studies and conduct research under exceptional conditions.

TABLE OF CONTENTS

LIST OF FIGURES

LIST OF TABLES

1 INTRODUCTION

1.1 Problem Statement

The Uzen field is a mature oil reservoir in Kazakhstan, has been experiencing significant challenges in oil recovery due to early water breakthrough, resulting in excessive water production and declining oil production. The issue lies on conformance problems stemming from reservoir heterogeneity, leading to inefficient displacement of oil during water injection. The continuous waterflooding technique has been inadequate in addressing these challenges, necessitating the exploration of new methods to enhance oil recovery while minimizing water cut levels.

Polymer flooding emerges as a promising solution to mitigate conformance issues and improve oil recovery rates in the Uzen field. Different experimental studies were completed by our team to screen the most effective chemicals at the lab scale. However, there is a lack of study to analyze the effect of the designed approach at the field scale. Therefore, the primary objective of this study is to investigate the efficacy of PF as a tertiary recovery method under the Uzen field condition through simulation-based analysis. The importance of this study is in its ability to address the benefits of the proposed PF method in the Uzen field to achieve a higher oil recovery. By exploring the application of PF, the study aims to provide valuable insights into the feasibility and effectiveness of PF for Uzen field and other similar fields in Kazakhstan, which face high water cut production challenges.

1.2 Background

1.2.1 Oil recovery stages

During the initial phases of oil field development, reservoirs are typically designed to facilitate the natural production of oil through intrinsic energy sources. Recoverable oil is extracted through various natural mechanisms, such as gas cap drive, water drive, solution gas drive, rock and fluid expansion, and gravity drainage, with an average recovery rate of approximately 19%, as illustrated in Figure 1. However, a significant portion of the oil remains unrecovered within the reservoir. To enhance oil recovery beyond these natural

mechanisms, subsequent methods are sequentially employed (Alamooti & Malekabadi, 2018; Jensen et al., 2000).

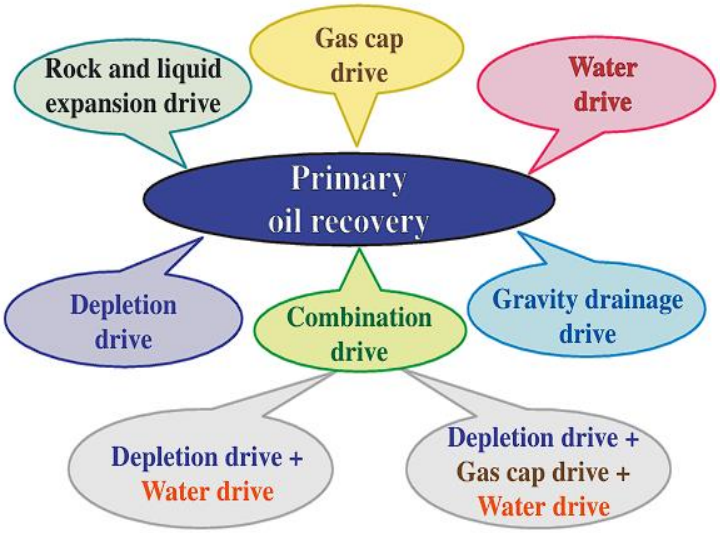

Figure 1. Primary oil recovery drive mechanisms (Vishnyakov et al., 2020)

According to Alamooti and Malekabadi (2018) during the secondary recovery phase, the primary emphasis is placed on maintaining reservoir energy levels. This objective is typically achieved through two main techniques: waterflooding and gas injection, as depicted in Figure 2. Gas injection involves the introduction of gas into the gas cap region of the reservoir to augment the energy required for oil displacement. However, it is widely recognized that gas injection to the gas cap is not as efficient as waterflooding. Consequently, due to the greater effectiveness and widespread utilization of waterflooding as a reservoir energy conservation method, many sources equate waterflooding with the secondary recovery approach.

Vishnyakov et al. (2020) stated that, despite the improvement in oil recovery rates facilitated by these methods, notably through the highly effective oil flooding technique, a significant portion of residual oil remains within the reservoir. According to global data accumulated from various reservoirs, those characterized by low permeability (such as tight oil reservoirs) or containing heavy oils typically exhibit final oil recovery rates ranging from 5% to 10% with primary and secondary oil recovery methods alone. Dissolved gas drive mechanisms recover approximately 10% to 25% of the original oil in place, while partially water-pumping methods, gas injection, or gravitational drive modes recover between 25% and 40% of the oil in place. Moreover, waterflooding, which is widely employed, contributes to

the recovery of more than 40% to 55% of the oil in place. To surpass these recovery rates, tertiary methods, also known as Enhanced Oil Recovery (EOR) methods, are implemented to further enhance hydrocarbon extraction efficiency.

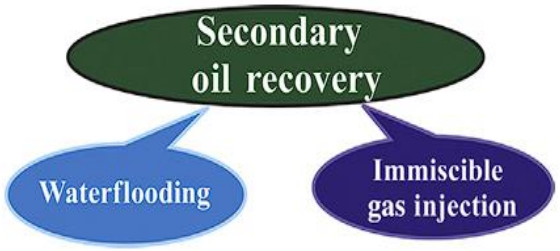

Figure 2. Secondary oil recovery techniques (Vishnyakov et al., 2020)

Tertiary recovery processes encompass all techniques implemented to extract unrecoverable oil following the initial two production stages. It is noteworthy that certain reservoirs, such as those containing highly viscous oil or exhibiting very low permeability, are incapable of yielding oil without tertiary interventions. The majority of procedures categorized within this domain can be further classified into thermal, chemical, microbial, miscible, and immiscible gas injection actions, each employing distinct mechanisms to augment oil recovery, as shown in Figure 3 (Alamooti & Malekabadi, 2018).

Chemical enhanced oil recovery (CEOR) techniques involve the incorporation of chemical additives into injected water to modify the physicochemical properties of the fluid or interfacial tension. Ragab and Mansour (2021) have classified CEOR methods into several categories, including polymer flooding (PF), surfactant flooding (SF), surfactant-polymer flooding (SPF), alkaline flooding (AF), and alkaline-surfactant-polymer flooding (ASPF). PF is aimed at decreasing the mobility ratio of water-oil, thereby enhancing volumetric sweep efficiency. Surfactant flooding, on the other hand, focuses on generating micro emulsions at the interface between oil and water phases, thus mobilizing residual oil and improving oil recovery. In the SPF process, a chemical slug containing water, surfactant, electrolyte (salt), and typically a co-surfactant (alcohol) is injected, followed by polymer-thickened water. Alkaline flooding represents another CEOR method wherein alkaline agents are introduced into the reservoir to induce in situ surfactant production, effectively mimicking the effects of surfactant flooding. ASP flooding combines multiple flooding methods, thereby enhancing oil recovery through the reduction of IFT, improvement of mobility ratio, and enhancement of microscopic displacement efficiency.

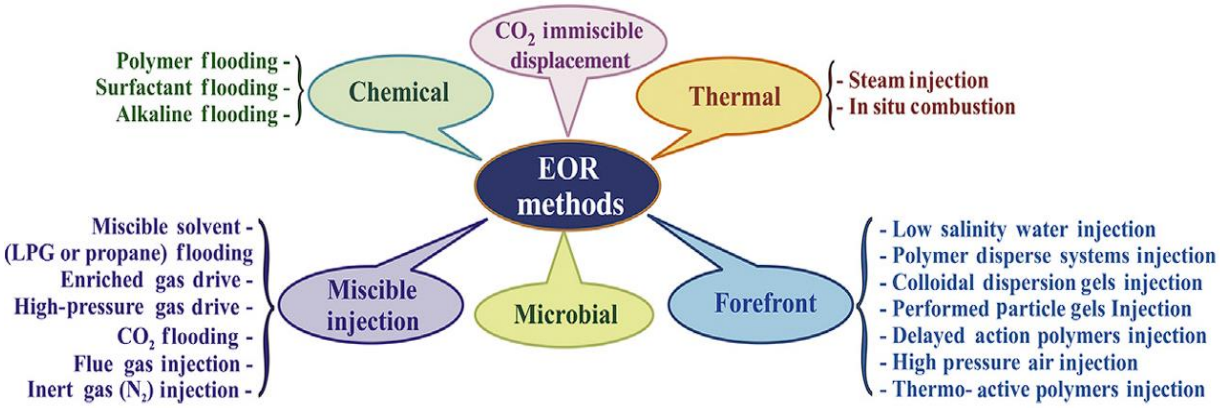

Figure 3. Enhanced oil recovery techniques (Vishnyakov et al., 2020)

The water cut denotes the proportion of water produced relative to the total volume of liquids extracted. High water cut reservoirs are common in oil fields worldwide and present significant challenges for efficient production. As reservoirs mature, the water cut tends to increase, leading to decreased economic viability and operational complexities. Despite facing issues such as extensive water saturation and the widespread dispersion of remaining oil, waterflooding remains a dominant technique in reservoir development due to its price. However, the escalating oil-water ratio escalates production costs, necessitating strategies to mitigate high water cut and optimize economic returns. On this matter Xue et al. (2023) stated that PF is a crucial method for controlling and reducing water cut in reservoirs, particularly those with prolonged production histories. Polymers act as thickening agents, increasing the viscosity of the injected water and reducing its mobility relative to oil, thus promoting more effective displacement of oil from the reservoir. This enhanced mobility control helps mitigate the adverse effects of fingering and channeling, which can result in bypassed oil zones and decreased oil recovery.

1.2.2 Enhanced oil recovery implementation

According to Gharbi et al. (2012), the execution of an EOR project entails a complex and enduring process, delineated by various phases depicted in Figure 4. To optimize efficiency and mitigate the inherent risks and uncertainties associated with project outcomes, it is imperative to establish a comprehensive management framework for the EOR process. This comprehensive approach encompasses several key stages, including the selection of the appropriate EOR method, EOR method design, the execution of pilot tests, and the subsequent implementation across real reservoir.

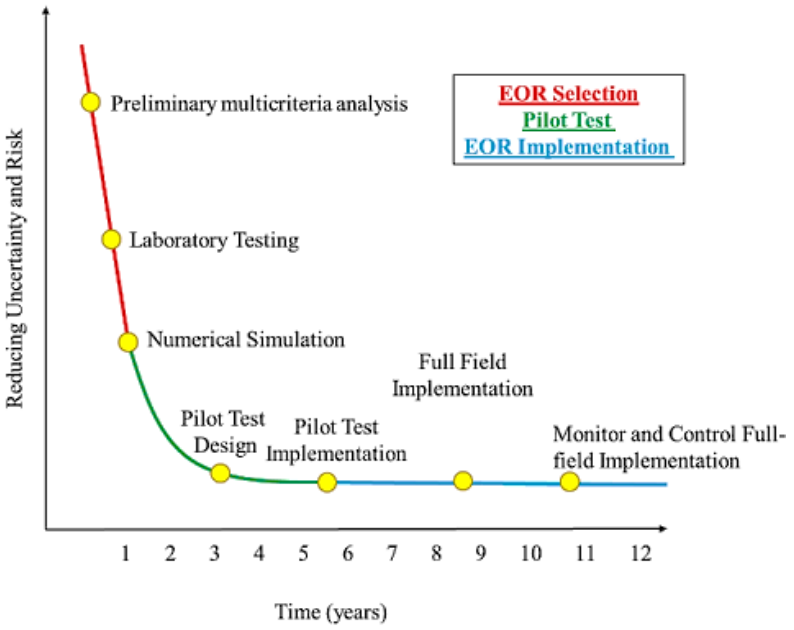

Figure 4. The graph depicts Risk and Uncertainty Analysis across various operational scales (Bigdeli & Delshad, 2023)

Phase 1 involves an initial multi-criteria assessment aimed at evaluating the feasibility of employing suitable EOR methods in a specific oil reservoir. This assessment considers key properties of both fluids and the reservoir itself, comparing them against predefined criteria derived from laboratory findings and the practical outcomes of numerous EOR projects. These properties include oil viscosity and density, oil saturation, reservoir thickness, permeability, porosity, depth, reservoir temperature, pressure, and formation type (Trujillo et al. 2010). Following the selection of an EOR method suitable for implementation in a specific reservoir, the subsequent phase involves conducting comprehensive reservoir studies. These studies entail laboratory testing works and the creation of detailed static geological and dynamic reservoir models. The development of an accurate reservoir model is crucial for gaining insights into reservoir fluid behavior and optimizing production strategies. Numerical simulators are utilized to assess various reservoir recovery strategies and predict reservoir performance under different production conditions. It is essential to highlight the importance of obtaining a thorough understanding of the recovery process associated with the selected EOR method. This understanding is crucial for the development of appropriate reservoir simulation models, which serve as the foundation for predicting a reliable outcome. The subsequent phase involves the design and execution of a pilot test for the selected EOR method, typically conducted at one or more wells. These wells typically include an injection well for fluid injection, an observation well for monitoring and controlling critical operational

parameters, and a production well. Additionally, geophysical well logging is performed in observational wells to analyze changes in oil saturation, providing direct estimates of reservoir characteristics and insights into the movement of the injected fluid front. Following the completion of the pilot test, the planning and full-scale implementation of the EOR project across the entire reservoir ensues. This final stage is informed by the results of the pilot test and the response of the reservoir section where the pilot test was conducted, particularly in terms of incremental oil production. The implementation of an EOR project typically spans 6-10 years, with the initial phase involving the selection of the EOR method, laboratory testing, and process modeling lasting 1-2 years, pilot test implementation taking 2-4 years, and the application of the EOR process across the entire reservoir requiring 3-5 years of EOR process implementation (Bondor, 2011).

1.2.3 Polymer flood implementation

De Sousa Ferreira and Moreno (2018) outline a comprehensive framework for the implementation of PF, comprising several key components. This framework encompasses screening analysis, laboratory investigations, numerical simulations, and field testing, as illustrated in Figure 5. The initial stage of screening analysis is pivotal in determining the suitability of a target oil reservoir for PF application. Laboratory activities are then conducted with the objective of designing the injection solution and characterizing its properties for input into simulation models. The design of the polymer solution entails the selection of various parameters, including the type of polymer to be injected, polymer concentration, injection brine composition, and any additional chemical additives. Concurrently, characterization of the polymer solution involves assessing several factors, such as rheological properties (both bulk and in-situ), polymer retention, solution resistance factor (RF) indicating mobility reduction, residual resistance factor (RRF) indicating permeability reduction, polymer inaccessible pore volume (IAPV), water-oil relative permeabilities, and solution stability. Laboratory analysis procedures encompass a range of tests, including rheology and stability assessments, as well as single-phase and two-phase experiments. These activities contribute crucial data necessary for the design and construction of core scale, sector scale, and reservoir scale model for proper numerical simulations.

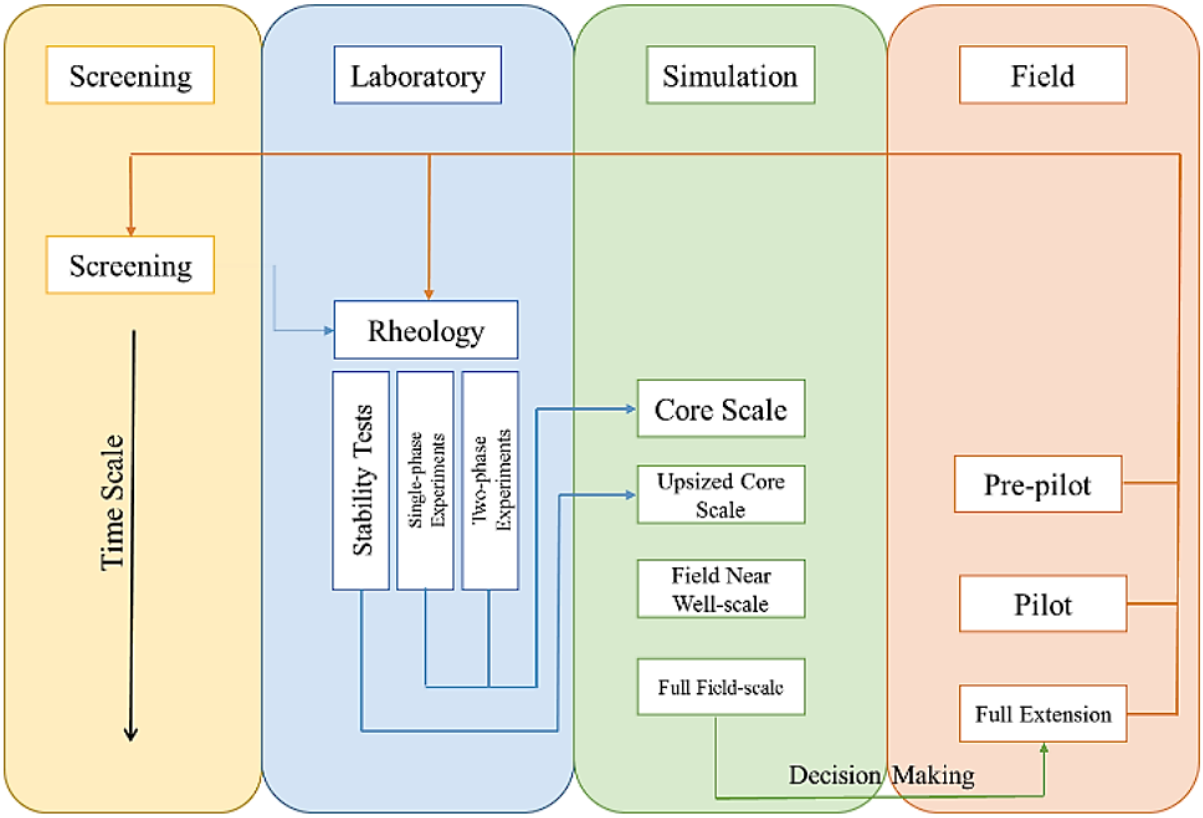

Figure 5. Polymer flooding implementation workflow (Bigdeli & Delshad, 2023)

Numerical simulation entails the meticulous preparation of a highly accurate simulation model, essential for the precise forecasting of field production and economic viability. The development of a comprehensive full-field simulation model hinges upon the integration of geological and fluid data. This study directs its attention towards evaluating the integration of laboratory-derived data into field scale simulations. To accomplish this, it is imperative to undertake a process of history matching, wherein reduced-scale models are aligned with laboratory findings to ensure consistency and accuracy in the simulation outcomes. The numerical simulation phase encompasses several stages, including core-scale, upscaled core-scale, field near-well scale, and full-field scale simulations. Core-scale simulation endeavors to accurately replicate laboratory-measured phenomena within the simulator framework. In this 1D model, all pertinent polymer characterization data from laboratory experiments is integrated, excluding chemical and biological degradation mechanisms due to their longer timescales (Ferreira & Moreno, 2019). Upscaled core-scale simulation involves the enlargement of small-scale laboratory simulations to represent larger-scale processes while preserving their inherent properties (Sanches & Moreno, 2015). This model operates on a larger timescale compared to core-scale simulations, thereby facilitating

the representation of time-dependent degradation mechanisms. The primary objective of the field near-well scale model is to scrutinize the behavior of polymer solutions under reservoir conditions, particularly focusing on injectivity and sweep efficiency, and encompassing all phenomena observed in laboratory experiments (Delamaide, 2014). Finally, in the full-field scale phase, operators engage in pilot and full implementation simulations. Irrespective of the implementation phase, operators must undertake history matching, production forecasting, and risk analysis to inform decision-making processes.

The field-testing phase comprises two key frameworks: pre-pilot and pilot testing. The pre-pilot stage is primarily focused on preparing the field for pilot implementation. This involves meticulous attention to reservoir understanding, well configurations, and surface facilities within the designated pilot area. The pilot testing phase represents a pivotal step in the PF implementation process. During this phase, operators must undertake measures to ensure the success of the pilot. It is imperative to avoid any operations in the wells surrounding the pilot area, as these activities may inadvertently impact the pilot response. Throughout the pilot phase, it is essential to compare collected data with simulation results to refine models and make any necessary adjustments to the pilot operations. Upon completion of the pilot, updating simulation models through history matching of the pilot response becomes imperative to enhance accuracy and reliability (De Sousa Ferreira & Moreno, 2018).

According to Dergano (2021), within the realm of CEOR methods, PF stands out as a particularly notable technique. This method boasts a lengthy commercial history and a track record of proven results, making it a preferred choice for many operators. Thomas (2016) emphasizes the widespread adoption of PF, attributing its popularity to its simplicity and reliability. Over the years, the risk associated with PF applications has remained minimal, while its applicability has significantly expanded, further solidifying its position as a prominent CEOR method in the industry.

2 LITERATURE REVIEW

The literature review section encompasses an examination of the role of polymers in the CEOR process, alongside a comprehensive review of prior experiences and outcomes observed in PF projects conducted in various oil fields. Furthermore, given that the present study is conducted within the specific operational context of the Uzen field, an introduction to the Uzen field itself is provided. This inclusion serves to contextualize the subsequent analysis within the unique geological and operational characteristics of the Uzen field, facilitating a nuanced understanding of the applicability and potential challenges associated with employing PF techniques in this particular reservoir setting.

2.1 Chemical EOR Methods

In light of recent advancements in EOR techniques, CEOR has emerged as a promising strategy for the extraction of residual and trapped oil within reservoirs (Ivanova & Cheremisin, 2022). Residual oil, constrained by capillary forces, and bypassed oil, often occurring due to reservoir heterogeneities or unfavorable mobility ratios between aqueous and oleic phases, constitute the primary targets for CEOR application (Gbadamosi et al., 2019).

According to Thomas (2019), CEOR encompasses a spectrum of methodologies, including polymer (P) injection, surfactant-polymer (SP) injection, alkali-surfactant-polymer (ASP) injection, as well as the utilization of microgels, nanogels, and other chemical formulations. CEOR involves the introduction of specialized formulations into displacing fluids with the aim of modifying the mobility ratio or increasing the capillary number within the reservoir. Modifying the mobility ratio entails thickening injected water by incorporating water-soluble polyacrylamide, thus enhancing reservoir sweep efficiency. Conversely, adjusting the capillary number involves the incorporation of surface-active agents, such as surfactants, to decrease interfacial tension and release trapped residual oil within the reservoir. Alkali flooding, also referred to as caustic flooding, facilitates changes in wettability through chemical reactions, generating in-situ surfactants and reducing interfacial tension between water and oil (Lake, L., 1992).

Microgels and nanogels represent sophisticated chemical solutions comprising tiny polymer particles aimed at mitigating thief zone permeability, redirecting water flow towards previously unswept reservoir zones (Suleimanov & Veliyev, 2017). These formulations

consist of particles capable of adhering to pore walls and potentially obstructing pore throats, thereby impeding water flow through depleted regions and reducing overall permeability. Nevertheless, careful consideration of potential damage and flow capacity loss attributed to the deployment of microgels or nanogels within oil-producing pathways of a reservoir is imperative (Thomas, 2019).

2.2 Polymer flooding

As stated by Ameli et al. (2022), among CEOR techniques, polymer flooding stands out as a widely embraced method for augmenting the oil recovery factor, underscored by numerous successful field implementations. Generally, the inception of PF dates back to the early 1960s, with a notable increase in applications witnessed between 1980 and 1986. Led by the extensive Daqing field PF in China in 1996, polymer flooding has since undergone remarkable innovation (Thomas, 2019). Positioned within the realm of low risk EOR strategies, the utilization of PF has faced a substantial increase in application (Ameli et al., 2022). Moreover, Manrique et al. (2010) delineated PF as a grown technique and emphasized its significance as the primary approach for sandstone reservoirs, based on an extensive analysis.

As outlined by Thomas (2019), PF involves the introduction of powdered or emulsion polymers into the injection water utilized in a waterflood, thereby augmenting water viscosity and reducing its mobility. Even marginal reductions in the mobility of the aqueous phase relative to the oil phase can mitigate the occurrence of viscous instabilities. Furthermore, in addition to enhancing viscosity, certain polymers have the capacity to adhere to reservoir rock, diminishing the permeability of the aqueous phase and resulting in a decreased mobility ratio. Consequently, this promotes increased vertical and areal sweep efficiency within the reservoir, eventually leading to an accelerated and often bigger oil recovery factor at the end of the EOR process, as shown in Figure 6.

A crucial factor to consider during the assessment of PF screening is the mobility ratio denoted as M, encompassing the mobilities of oil and water phases (Ahmed & Meehan, 2012). Typically, discussions on the mobility ratio primarily focus on its ultimate value. Thus, as illustrated in Eq. 1, the relative permeabilities of each fluid are employed at their respective irreducible saturation conditions, specifically, the connate water saturation for oil and residual saturation for water (Thomas, 2019).

$$M = \frac{\lambda_o}{\lambda_w} = \frac{\mu_o / k_{ro(Swe)}}{\mu_w / k_{rw(Sor)}} \quad (1)$$

In this context, λ represent the mobility, μ is viscosity, k_r relative permeabilities, with the subscripts w and o denoting water and oil, respectively.

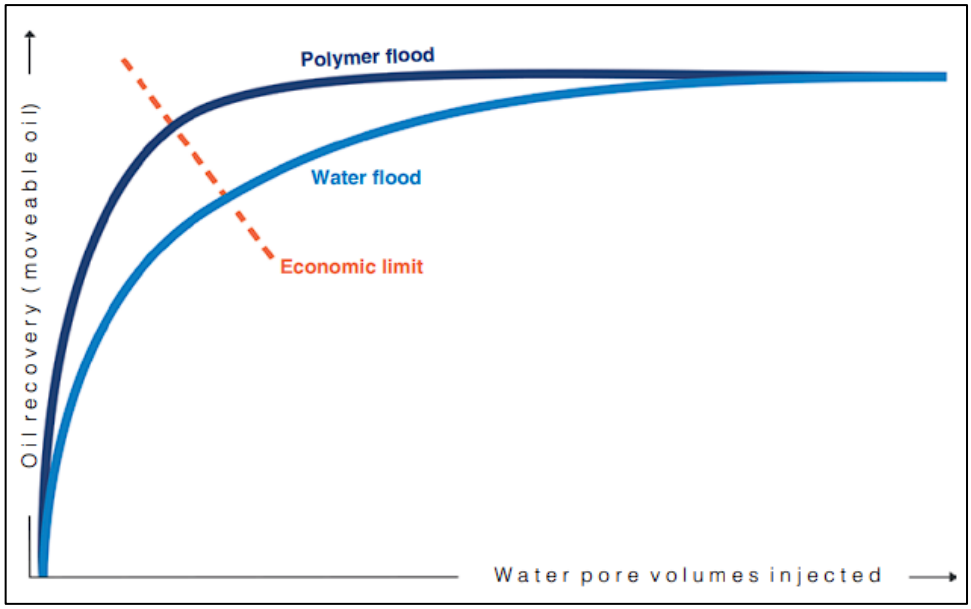

Figure 6. Comparison of water flood and polymer flood oil recovery factors (Thomas, 2019)

Polymer flooding is often utilized as a tertiary recovery technique, typically implemented subsequent to a period of secondary recovery via waterflooding (Kudaivergenov et al., 2015; Thomas, 2019). Consequently, recovery operations unfold under two primary scenarios. First, in instances where the mobility ratio during waterflooding is unfavorable, notably observed in the context of viscous or heavy oils, continuous polymer injection serves to enhance reservoir sweep efficiency, thereby substantially prolonging the duration of the flood. Second, even in cases where the mobility ratio is favorable, the presence of stratigraphic heterogeneities within the reservoir can impede efficient recovery (Xue et al., 2023). Polymer injection aids in mitigating water mobility within high-permeability layers, thereby facilitating the displacement of oil from low-permeability layers. This becomes particularly pertinent in reservoirs characterized by stratigraphic complexities such as bounded layers or vertical equilibrium, where free crossflow is prevalent.

In the first scenario, inefficient macroscopic displacement dynamics often lead to premature water breakthrough, followed by an extended period of two-phase production characterized by escalating water-cut. This situation can be explained using the concept of

viscous fingering, which culminates in the bypassing of oil in reservoir, as shown in Figure 7.

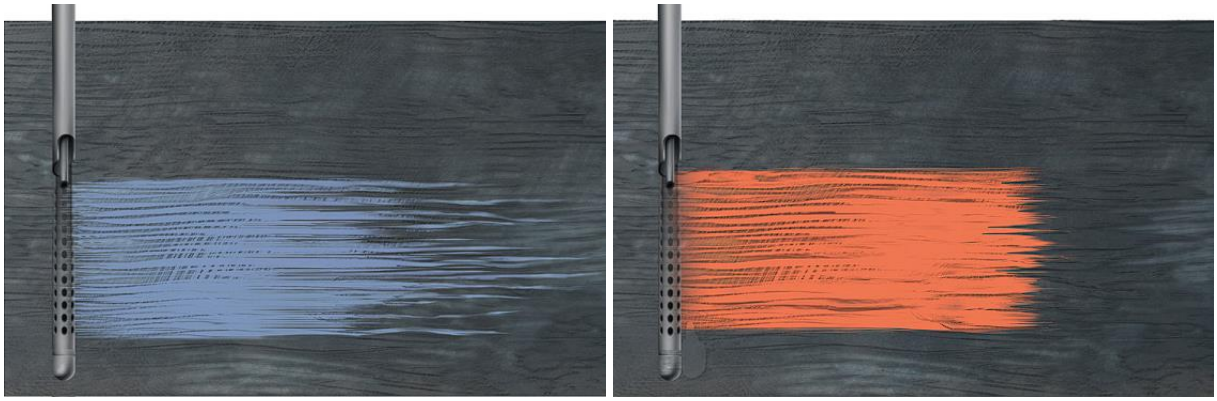

Figure 7. Water (left) and polymer (right) flooding front movement profiles (Thomas, 2019)

As stated in Akın (2005), in the realm of oil production, polymers have been applied in three distinct modes: firstly, as near-well treatments aimed at enhancing the efficacy of water injectors or mitigating watered-out production wells by obstructing high conductivity zones; secondly, as agents capable of being cross-linked in situ to seal off highly conductive zones located at considerable depths within the reservoir; and thirdly, as agents designed to diminish water mobility or the water-oil mobility ratio. The process of PF is particularly well-suited for reservoirs facing challenges with conventional water flooding (WF) methods, typically attributable to either pronounced reservoir heterogeneity or a high water-oil mobility ratio. In such instances, PF is employed to target the extraction of oil from regions within the reservoir that have not been adequately contacted by conventional methods.

The breakthrough time of a polymer within a reservoir is not solely contingent upon the viscosity of the injected solution, rather, it is substantially influenced by factors such as retention levels, encompassing polymer loss attributed to adsorption and entrapment mechanisms, as well as the heterogeneity inherent in the reservoir. The last phenomenon significantly impacts flood dynamics and the overall efficiency of hydrocarbon recovery processes (Al-Hajri et al., 2018; Thomas, 2019; Wang et al., 2003). Consequently, meticulous consideration of these factors is imperative when determining the optimal size of slugs, typically denoted as a certain percentage or fraction of the total pore volume within the reservoir, in order to mitigate potential chemical-rock interactions. Abidin et al. (2012) have noted that conventional PF projects entail the mixing and subsequent injection of polymer over an extended duration until approximately one-third to one-half of the pore volume of the reservoir has been injected.

In a successful case of polymer flood implementation at the Pelican Lake field, located approximately 250 km north of Edmonton, Alberta, Canada, the challenges of a thin formation with high-viscosity oil were addressed through innovative techniques. Initially discovered in 1978, the field's primary recovery stood at less than 7% of its over 6 billion bbl of oil originally in place (OOIP). Vertical wells proved economically unviable due to the reservoir's characteristics until the introduction of horizontal drilling in 1987, significantly enhancing production performance. Despite this improvement, primary recovery remained limited, prompting exploration of enhanced oil recovery (EOR) methods. While thermal methods proved impractical due to heat loss, chemical EOR in the form of polymer flooding emerged as a promising solution. Despite initial skepticism due to prevailing industry beliefs, meticulous reservoir simulation, laboratory studies, and pilot operations demonstrated the viability of polymer flooding. Despite initial setbacks, subsequent adjustments, and learnings from the pilot project, polymer flooding was successfully implemented at scale, significantly increasing the recovery factor to 25% and higher while maintaining a relatively low water cut (JPT.SPE.ORG, 2014).

2.3 Uzen field

The Uzen Field, situated within the South Mangyshlak Sub-basin of onshore western Kazakhstan, was identified in 1960 and commenced production in 1965 (Field Evaluation Report, 2011; Sparke et al., 2005). Renowned as the most extensive field within its basin, Uzen occupies an anticlinal structure spanning approximately 39 km in length and 9 km in width, encapsulating an area of 250 km² (equivalent to 61776 acres). The structural cross-section across the anticline is shown in Figure 8.

The initial pressures within the reservoir exhibit a range of 150 to 180 bars alongside a concomitant reservoir temperature spanning from 54°C to 69°C. The crude oil has a density of 35° API, accompanied by a variable paraffin composition ranging from 10% to 25%, contingent upon the characteristics of the reservoir, thereby yielding a paraffin crystallization temperature ranging between 50°C and 60°C. The viscosity of oil at reservoir condition is 4.5 cp and asphaltene content varies between 13 to 15 wt.% (Yerniyazov et al. 2023). These conditions have engendered operational challenges across the entirety of the production infrastructure (Sparke et al., 2005). The reservoir's permeability exhibits significant variability, ranging from 1 to 1200 mD, with an average value of 235 mD, particularly within extensive amalgamated channel sands reaching thicknesses of up to 43 meters.

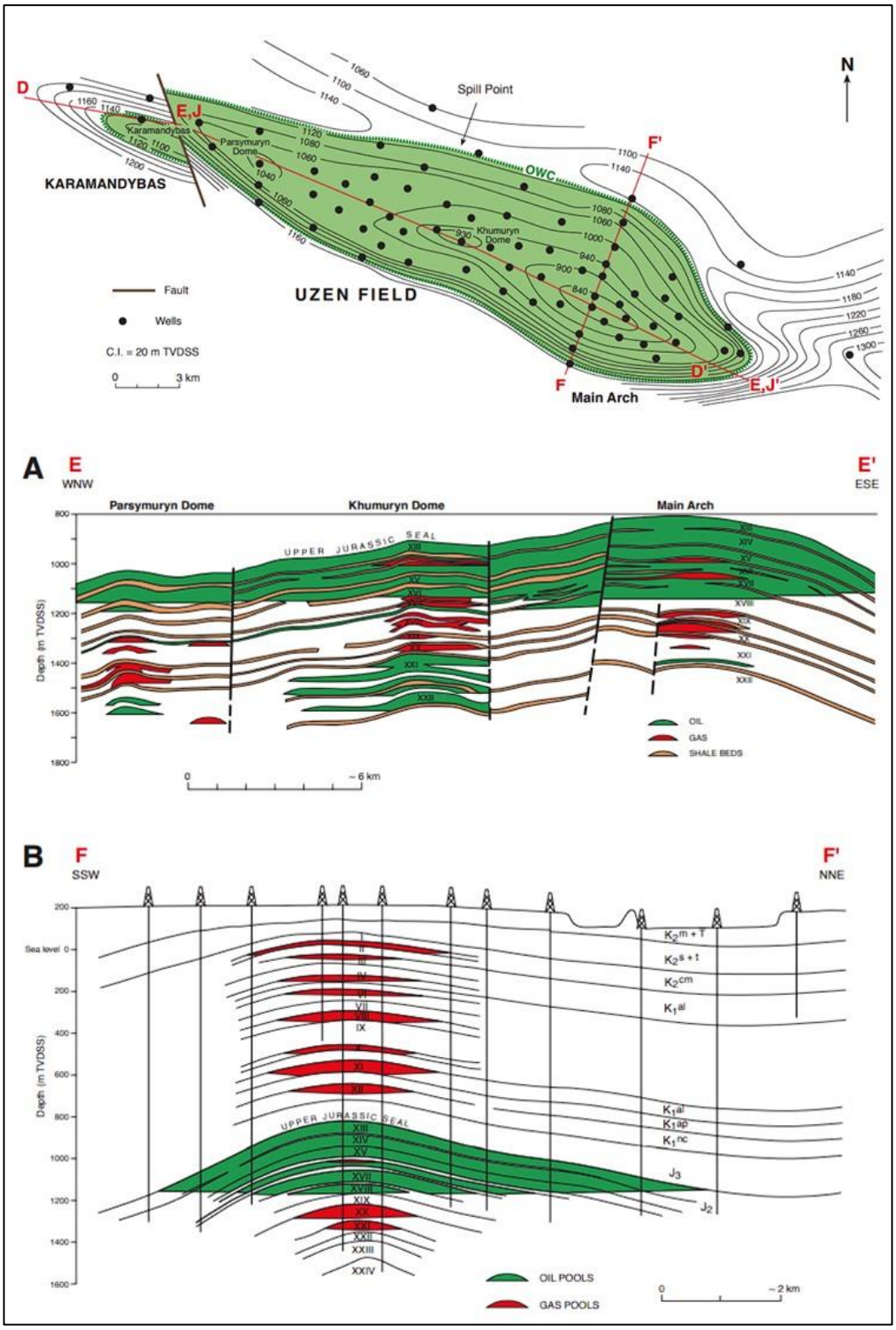

Figure 8. The structural cross-section across the anticline of Uzen Field illustrates the spatial arrangement of oil and gas (Field Evaluation Report, 2011)

The reservoir primarily comprises sandstones and siltstone, exhibiting a notable clay component. The entire reservoir deposit comprises a series of layered and displaced

accumulations, predominantly characterized by a clastic succession. This succession encompasses 25 distinct reservoir layers (XXV), of which 18 have been proved. Reservoir units are characterized by distinct flow layers, featuring pronounced internal heterogeneity and exhibiting limited vertical connectivity. Lateral connectivity follows a predominantly unidirectional pattern dictated by the orientation of the channel formations. The primary oil accumulation is delineated within Units XIII-XVIII (Figure 8), characterized by a shared oil-water contact (OWC) spanning depths ranging from 1124 to 1150 m, with an average depth of 1130 m across the field. These units collectively constitute an oil pool with a maximum oil column height of approximately 320 m from a crestal depth of 830 m (Field Evaluation Report, 2011).

Operational challenges arise due to formation of wax, which precipitates severely hampering production efficiency, weak edge-aquifer drive mechanisms and oil close to saturation point, necessitating water injection from the onset of production. However, the water injection strategy has been moderately successful due to several factors:

1. Delayed implementation allowing for the formation of a secondary gas cap.
2. Premature water breakthrough along high permeability (thief) layers.
3. Inadequacy of the line drive injector pattern for a channelized reservoir.
4. Reservoir cooling caused by injected water resulting in wax accumulation in lower permeability layers.
5. Reduced sweep efficiency due to the adoption of dual-unit completions.

In 1971, an experiment with hot water injection to mitigate wax precipitation within the reservoir was conducted successfully. Subsequently, a fieldwide implementation of hot water injection commenced in 1973, as delineated in Figure 9. Incremental recovery between 1981 and 1992, estimated at 110 million barrels of oil (MMBO), underscored the effectiveness of the approach. Consequently, this endeavor not only attenuated the rate of decline but also contributed significantly to the overall recovery process within the reservoir (Safronov et al., 1993).

According to Offshore Technology Journal (2021), the Uzen field has successfully extracted 66.32% of its total recoverable reserves. Projecting forward based on economic considerations, production operations are anticipated to persist until the field attains its economic threshold in 2063. Currently, the Uzen field contributes approximately 4% to the

Kazakhstans daily oil production. But the field development phase is distinguished by a significant water cut, estimated at approximately 90%, primarily attributed to prolonged waterflooding practices (Imanbayev et al., 2022).

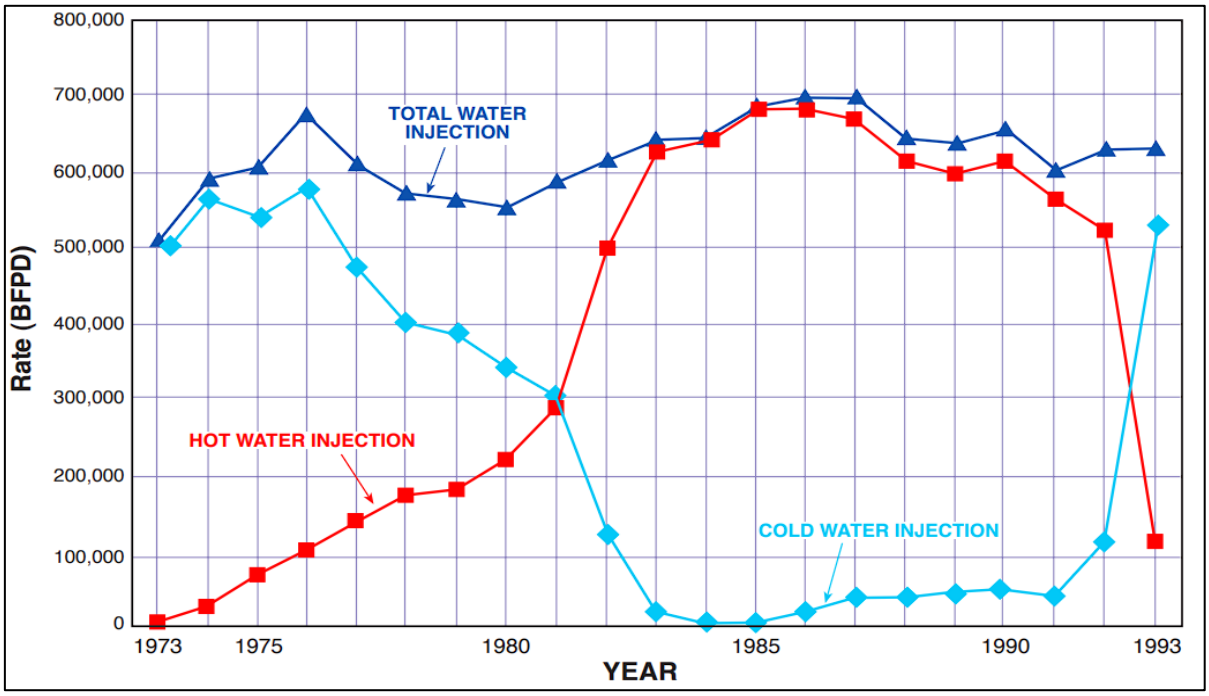

Figure 9. Uzen fields water injection history between 1973 and 1993 (Field Evaluation Report, 2011)

2.4 Polymer screening and design for Uzen field

The process of selecting or designing a polymer solution for certain reservoirs necessitates careful consideration of multiple factors, such as the viscosity of the crude oil expected to be displaced by the polymer. Attaining a mobility ratio below 1 constitutes a critical objective in reservoir engineering, where the viscosity of the polymer solution must match or exceed that of the fluid present under reservoir conditions. This equilibrium is essential for ensuring effective displacement mechanisms within the reservoir and optimizing oil recovery processes (Ezeh et al., 2021; Yerniyazov et al., 2023).

Increasing the viscosity of a polymer solution entails employing various strategies. Principally, adjustments in polymer concentration represent a primary means of influencing viscosity levels. Higher concentrations of polymer within the solution typically correspond to elevated viscosity (D. Wang, 2013). Additionally, manipulation of brine salinity serves as another effective mechanism for altering solution viscosity. Lowering the salinity of the brine

often results in an increase in the viscosity of the polymer solution. Furthermore, the introduction of polymers with higher molecular weights also presents the way for enhancing solution viscosity.

The polymer solution designed for certain reservoir must demonstrate favorable rheological characteristics under reservoir conditions. The rheological properties of polymers are influenced by various factors, including reservoir temperature, salinity levels, and microbial activity (Gaillard et al., 2014, 2015). Elevated salinity levels and the presence of divalent ions can adversely impact the integrity of negatively charged polymer chains, leading to molecular destabilization and consequent viscosity reduction. Furthermore, these conditions may promote increased polymer adsorption onto rock surfaces. Consequently, meticulous selection and optimization of both the type and concentration of polymer employed within a specific field are imperative for the successful execution of mobility control initiatives.

Imanbayev et al. (2022) conducted a thorough examination of the primary geological attributes of the Uzen reservoir to determine the feasibility of employing PF techniques within this specific geological context. The investigation delved into the principal parameters characterizing the Uzen field, thereby assessing their compatibility with the criteria for implementing PF strategies, as depicted in Figure 10. Evidently, the data presented therein reveal an alignment between the values pertaining to the Uzen field and the stipulated ranges deemed necessary across all pertinent characteristics, thereby affirming the suitability of PF within Uzen field.

Yerniyazov et al. (2023) conducted a comprehensive investigation assessing the suitability of PF as a potential strategy for production enhancement within the sandstone formations of the Uzen field. Based on the outcomes of reservoir screening, the Uzen field emerges as a promising candidate for PF, primarily attributable to several factors, foremost among which is its increased water cut. The author conducted a thorough evaluation of various polymers as the subsequent step, aiming to identify the optimal candidate tailored to the requirements of the Uzen field. This assessment considered key attributes such as viscosification potential, thermal stability, propensity for adsorption, resilience against bacterial activity, and tolerance to oxygen exposure.

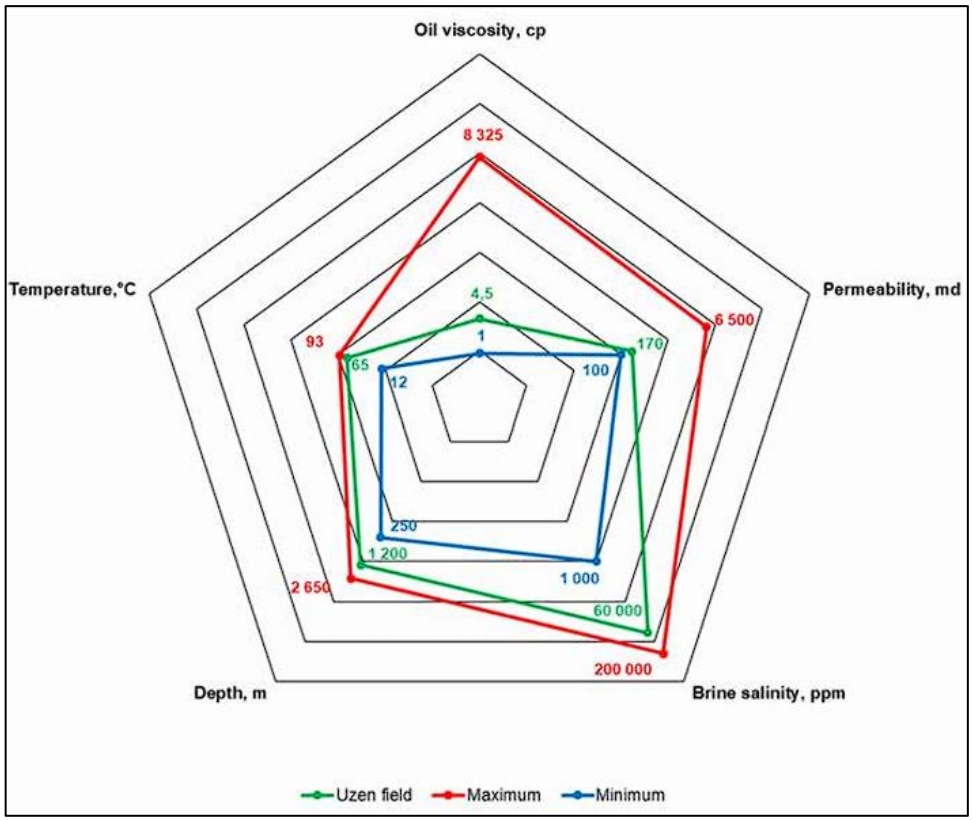

Figure 10. Evaluation graph of the primary parameters of the Uzen field to determine the suitability of polymer flooding (Imanbayev et al. 2022)

Figure 11 presents an analysis of the influence of non-ionic substances on the thermal stability of Polymer 3. The graph delineates the axes of polymer viscosity against time, offering viscosity change profiles for Polymer 3 formulations prepared utilizing both Caspian seawater (CSW) and synthetic water. Examination of the results reveals that the viscosity of Polymer 3 within CSW, after one month, exhibits a marginal decrease of merely 4% compared to its counterpart in synthetic brine. These findings, as depicted in Figure 11, substantiate that Polymer 3 demonstrates better stability in the presence of bacterial components within the makeup brine.

Figure 12 presents a graph of comparative analysis delineating the performance differences between Polymer 2 and Polymer 3, focusing on their resistance to non-ionic materials, oxygen, and propensity for adsorption onto rock surfaces. From the graph, it is discernable that Polymer 3 exhibits better compatibility and lower static adsorption than Polymer 2.

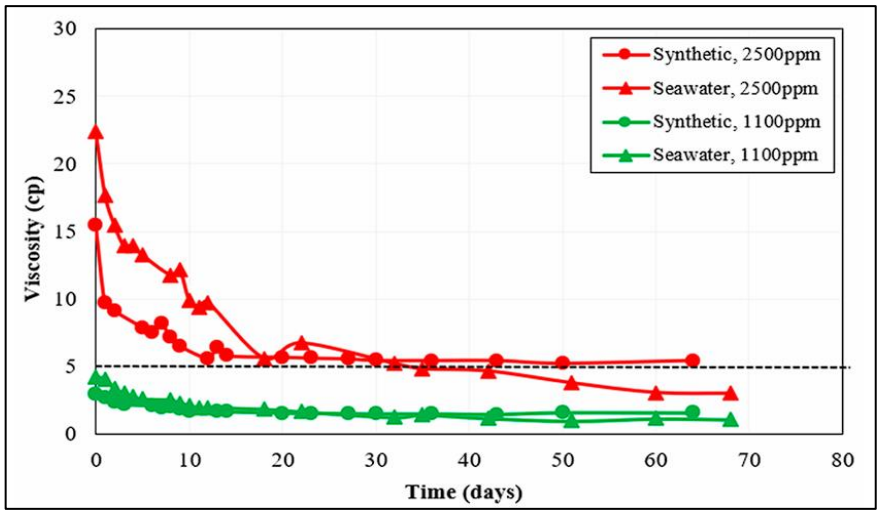

Figure 11. The impact of a non-ionic material on the thermal stability of Polymer 3

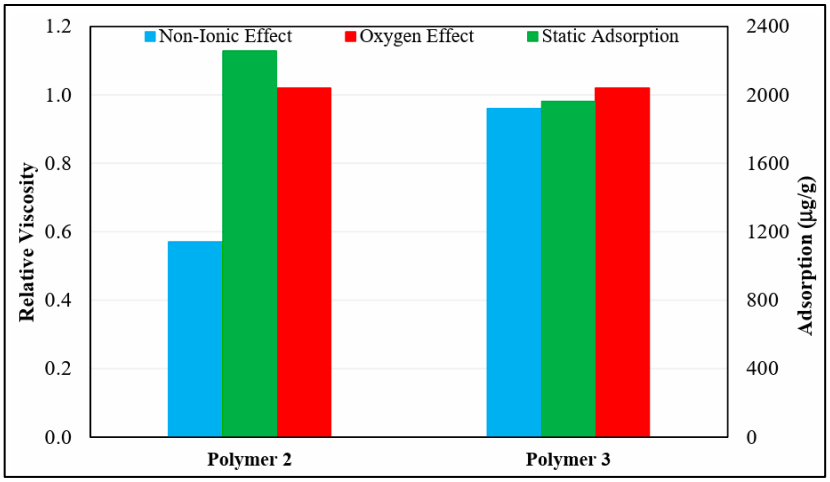

Figure 12. Adsorption and relative viscosity comparison of Polymer 2 and Polymer 3

Table 1. The screening criteria utilized to select the optimal polymer for the Uzen Field (Yerniyazov et al. 2023)

Test	Criterion	Polymer 1	Polymer 2	Polymer 3	Polymer 4	Remarks
Rheology	>5 cp viscosity, No gelling	✗	✓	✓	✓	Polymer 1 appeared more like a gel and was discarded.
Thermal Stability	>5 cp viscosity for at least two weeks aging at 63 °C	-	✓	✓	✗	Polymer 4 was eliminated as it did not meet the set criterion.
Non-Ionic Material (Bacteria)	Little to negligible effect on thermal stability over a month	-	✗	✓	-	Polymer 2 showed higher thermal degradation in presence of bacteria.
Oxygen Content	Little to negligible effect on thermal stability over a month	-	✓	✓	-	Both polymers showed a negligible effect of oxygen present in CSW.
Static Adsorption	Ap < 2000 µg/g	-	✗	✓	-	Static adsorption for Polymer 2 was higher.

The results of the comprehensive polymer evaluations revealed that the polymer sample provided by KMGE (ASP3) is the most optimal for Uzen field, as illustrated in Table

1. Moreover, according to results of laboratory works, the most optimal polymer concentration appropriate to Uzen field condition is 2500 ppm. The designed polymer at concentration of 2500 ppm was studied and confirmed by core flooding experiments.

2.5 Modeling and Simulation of Polymer Flooding

Reservoir simulation is the interdisciplinary field that integrates physics, mathematics, reservoir engineering, and computer programming to create a predictive tool for forecasting hydrocarbon reservoir behavior across different operational strategies (Aziz & Settary, 1979). The concept of reservoir simulation dates back to the inception of petroleum engineering in the 1930s, although the term "numerical simulation" gained prominence only in the early 1960s as predictive techniques advanced into sophisticated computer programs. These programs marked a significant breakthrough as they enabled the solution of complex sets of finite-difference equations characterizing transient, multiphase flow in heterogeneous porous media in two and three dimensions. This progress was facilitated by the rapid development of large-scale, high-speed digital computers and the refinement of numerical mathematical techniques for solving extensive systems of finite-difference equations.

Reservoir simulation enables a comprehensive examination of the reservoir by segmenting it into numerous blocks, sometimes numbering in the thousands. Fundamental equations governing flow in porous media are then applied to each block. The computer programs responsible for conducting such model analyses are referred to as computer models. Thanks to advancements in computer hardware and software technology since the early 1950s, it has become feasible to develop sophisticated models capable of simulating the intricate processes occurring within reservoirs during the implementation of recovery schemes. Reservoir simulation technology undergoes continuous enhancement and refinement, with new models continuously proposed to simulate increasingly complex recovery schemes (Aziz & Settary, 1979).

The fluid flow within porous media is a highly intricate phenomenon. Consequently, obtaining analytical solutions to mathematical models necessitates making simplifications regarding reservoir geometry, properties, and boundary conditions. However, such simplifications often prove inadequate for most fluid flow problems. In many instances, developing analytical solutions for practical issues becomes unfeasible due to the complex behaviors associated with multiphase flow, the nonlinear nature of governing equations, and

the heterogeneity and irregular shape of reservoir systems. Given these challenges, analytical methods are limited, and numerical simulation methods become indispensable for solving these models.

In 2018, Ibiam explored the optimization of PF design parameters using numerical simulation in context of geological uncertainties within reservoir models. By employing an adjoint-based technique, the author aligned model outputs with data from an extended waterflood in the Watt Field, an artificial yet realistic clastic reservoir derived from actual data, encompassing a broad spectrum of geological heterogeneities and uncertainties across various model scenarios. The study's outcomes underscored the advantage of initiating polymer solution injection at the earliest opportunity. It's worth noting that optimized PF could yield an additional net present value (NPV) of $300 million compared to optimized waterflood strategies. This highlights the importance of numerical simulation in informing decision-making processes within reservoir engineering, particularly in optimizing EOR methods.

Fernandes et al. (2019) conducted a study employing an updated iteration of UTCHEM within an adaptive framework, aimed at modeling chemical floods within extensive heterogeneous oil reservoirs. The enhancements introduced facilitated simulations encompassing several million grid blocks, each featuring grid block dimensions were sufficiently small to show physical fidelity. The study presented four cases of PF and SPF, with grid sizes varying from 800,000 to 3.7 million grid blocks. UTCHEM enabled precise and effective large-scale simulations of chemical flooding using mechanistic reservoir models, which was a big challenge in past decades.

Sun et al. (2022) performed a detailed examination of PF within water-flooded reservoirs, particularly within C Block. Through the establishment and calibration of a reservoir model, the researchers investigated the impact of key parameters such as polymer concentration, injection duration, injection rate multiples, and injection timing on reservoir performance. Results revealed a positive relationship between polymer concentration and cumulative oil production, with an optimal concentration of 0.15 wt% that identified based on economic considerations. Moreover, increased injection duration and rate multiples were found to enhance cumulative oil production and incremental recovery compared to traditional WF techniques. Under the optimal PF development strategy for C Block, there was a notable

increase in cumulative oil production compared to WF, with a difference of 1.5042×10^4 m^3, which is 6.3% increase.

2.6 Objectives of the Thesis

The objectives of this study include:

- Modeling the polymer flooding observations for Uzen field at the lab scale;
- Conducting the polymer flooding simulation at the field scale and analyzing the sensitivity of operational parameters;
- Determining the optimal polymer flood parameters.

2.7 Scope of work

The scope of the project encompasses a comprehensive examination of the simulation process involved in polymer flood implementation workflow within the Uzen field. The main chapters of study include:

1. SIMULATION MODEL VALIDATION AND SETUP

This section contains an intricate description of the validation process for the reservoir model, core scale and reservoir scale numerical simulations, as well as the operational parameters of PF design. Additionally, it describes the software used for numerical simulations. Furthermore, it presents a concise outline of the study's design, delineating the sequence of experiments and simulations conducted.

2. RESULTS AND DISCUSSION

This chapter will provide a thorough study of the data received from the numerical simulation. The findings will be extensively examined, and the performance of the PF will be assessed and compared to that of the WF.

3. CONCLUSION AND RECOMMENDATIONS.

The thesis concluded with numerical simulation results-based suggestions, with a focus on selecting the optimum operational parameters for PF implementation in the Uzen field.

3 SIMULATION MODEL VALIDATION AND SETUP

The aim of this research is to develop a PF strategy tailored to the conditions of the Uzen field and evaluate its effectiveness by analyzing various operational factors. Specifically, a hybrid hot polymer flooding (HPF) method will be employed. This chapter is dedicated to presenting an outline of the numerical simulation software used and providing comprehensive descriptions of the procedures carried out. STARS, developed by Computer Modelling Group (CMG), stands as a reservoir simulation software tailored for the intricate modeling and simulation of fluid flow, heat transfer, and chemical reactions within subsurface reservoirs, with specific emphasis on thermal processes.

In this study, the results of previous experimental research by SMG students, were used to construct a core scale model with the STARS software by CMG. The model was employed for simulating core flood experiments, and the accuracy of our developed PF model was validated by comparing the numerical simulation results with real laboratory data, at the core scale.

Following the completion of numerical simulations for the core scale model, reservoir scale numerical simulations were carried out on a sector model of the Uzen field matched and approved by KMGE (Uzen field owner and operator). Once the results of the core scale model were compared and validated, the subsequent step involved designing PF in the reservoir scale model using CMG STARS. Following the design of the PF, a sensitivity analysis of operational parameters such as polymer injection rate, PF duration, and polymer concentration was conducted to assess the design on the performance of the method.

3.1. Numerical Simulation

This subchapter provides information about the results of laboratory core flood along the line with detailed description of core scale and reservoir scale models and conducted numerical simulations. But mathematical equations form the foundation of numerical modeling. These equations describe relationships between variables and are often derived from physical laws or empirical observations.

The numerical model employed in STARS involves the discretization of the reservoir domain into a grid network, where each grid cell represents a distinct volume element. Within

this framework, fluid flow and transport equations, typically governed by Darcy's law and mass conservation principles, are solved iteratively to compute the evolution of fluid properties over time and space. These equations encapsulate the interplay between various physical phenomena such as fluid flow, heat transfer, and phase behavior, thereby capturing the dynamic behavior of the reservoir system. The equations related to conservation term solved by STARS are given in Appendix B.

These equations emerge from representing all important physical phenomena in mathematical form. There is one conservation equation for each chemical component that requires a separate accounting, as well as equations explaining phase equilibrium between phases. Each region of interest has its own set of equations, which is often a discretized grid block. Finally, there is an equation that describes the operational conditions of each injection and production well (STARS User Guide, n.d.).

3.1.1. Model Validation

A numerical simulation of PF at the core scale was performed using core parameters derived from a sample taken from the Uzen field. The main components' parameters for numerical simulation are given Table 1. Previous laboratory studies (Yerniyazov et al., 2023, Maratbekkyzy et al., 2023) yielded the relevant polymer properties, such as dynamic and static polymer adsorption, the best polymer concentration, resistance factor (RF), and residual resistance factor (RRF).

The core model was constructed in STARS software by CMG. The model contains one injector and one producer wells and is made up of a grid arrangement of 10 rows and 1 column, as demonstrated in Figure 13. Each grid has dimensions of 5 cm in width and height, with a length of 0.5 cm, similar to the experiment.

Table 2. Input parameters used in core scale simulation.

Component	Parameter	Value	Unit
Core	A	11.26	cm^2
	L	5.55	cm
	ϕ	0.243	fraction
	k	170	mD
	d	3.8	cm
	$t_{reservoir}$	63	°C

Initial condition	μ_o	8	cp
	μ_{brine}	0.82	cp
	S_{wi}	0.2	fraction
	S_{oi}	0.8	fraction
	OOIP	12.16	cm^3
Polymer	Dynamic adsorption	766.4	µgr/gr
	Concentration	2500	ppm
	μ_{target}	5	cp
	RRF	2.77	

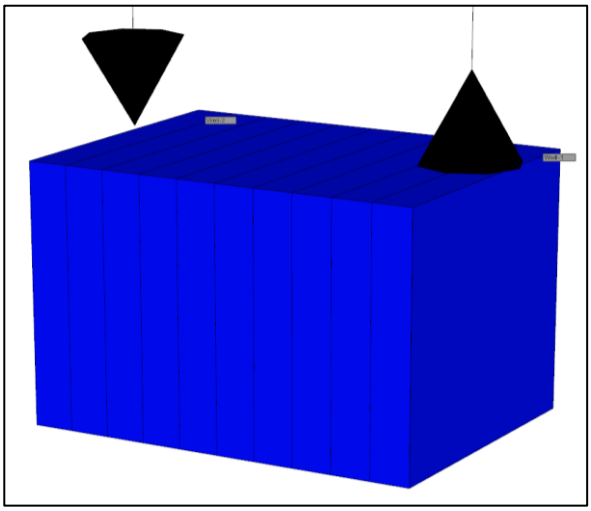

Figure 13. Core model constructed in CMG Stars.

3.1.2. Laboratory core flood and core scale numerical simulation

The laboratory core flood findings depicted in Figure 14 were sourced from the research conducted by Maratbekkyzy et al. (2023). The study details the application of PF in reservoir conditions utilizing core samples from the Uzen fields. Core flooding procedures were conducted under a consistent injection rate, with intervals featuring varied constant injection rates.

The outcomes of the oil displacement test conducted on core samples from the Uzen fields, as illustrated in Figure 14, offer valuable insights into the effectiveness of different flooding stages. Initially, WF, serving as the primary phase, results in an oil recovery of approximately 42%. This signifies the quantity of oil extractable through displacement by water within the reservoir.

Subsequently, the PF phase, designed to augment oil recovery, exhibits a substantial enhancement, yielding an oil recovery rate of 90%. PF involves the injection of polymers into the reservoir to alter fluid flow properties, thereby enhancing oil displacement and overall recovery efficiency.

Following the PF, the post-flush stage contributes to a slight additional increase, with the oil recovery reaching 91%. Post-flush procedures are typically performed to ensure the efficient displacement of any remaining oil and to optimize overall recovery efficiency.

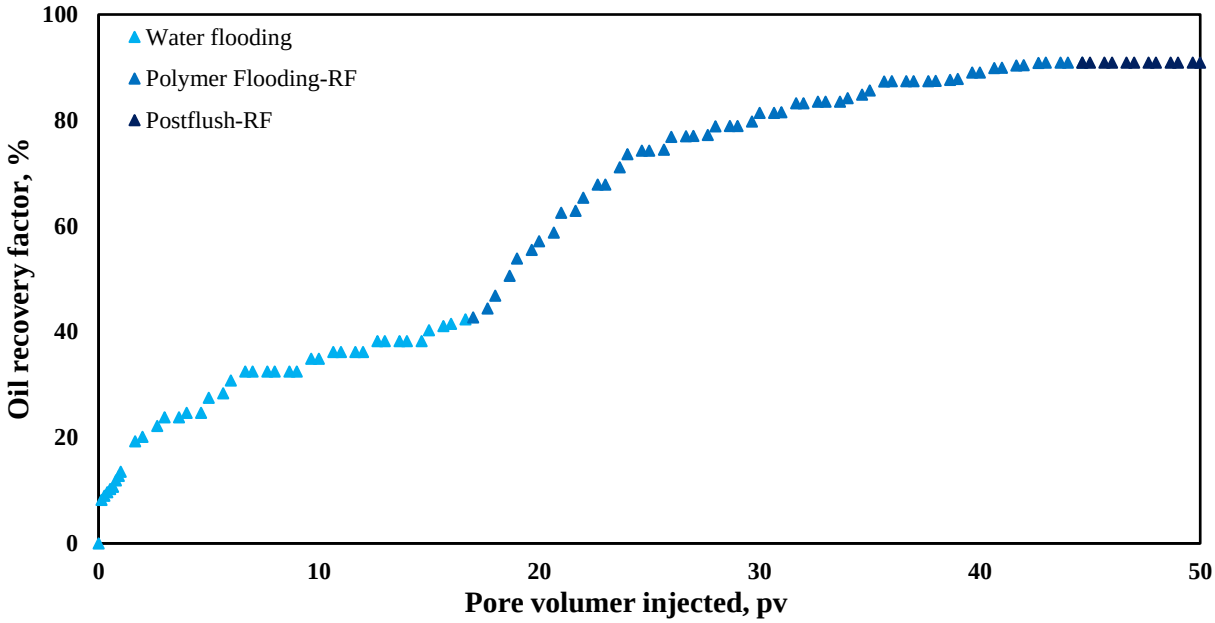

Figure 14. Oil displacement test result in Uzen fields core (Maratbekkyzy et al., 2023).

The incremental oil recovery attributed to the PF, calculated as the difference between the oil recovery at the end of the PF and WF, amounts to approximately 48%. This increment underscores the significant impact of PF in extracting additional oil from the reservoir, highlighting the efficiency of polymer injection as an EOR method in this field.

Numerical simulation was conducted utilizing data obtained from the research conducted by Maratbekkyzy et al. (2023). Figure 15 portrays the water cut observed through numerical simulation of the core model. The graphical representation demonstrates a notable escalation in water cut, peaking at 95% within a 30-minute interval during WF. Subsequently, this upward trend persists until the commencement of polymer injection.

Upon initiation of polymer injection, there is a discernible reduction in water cut, decreasing from 97% to 80%. However, it’s important to note that due to polymer

breakthrough, a subsequent increase in water cut is observed following the polymer injection phase.

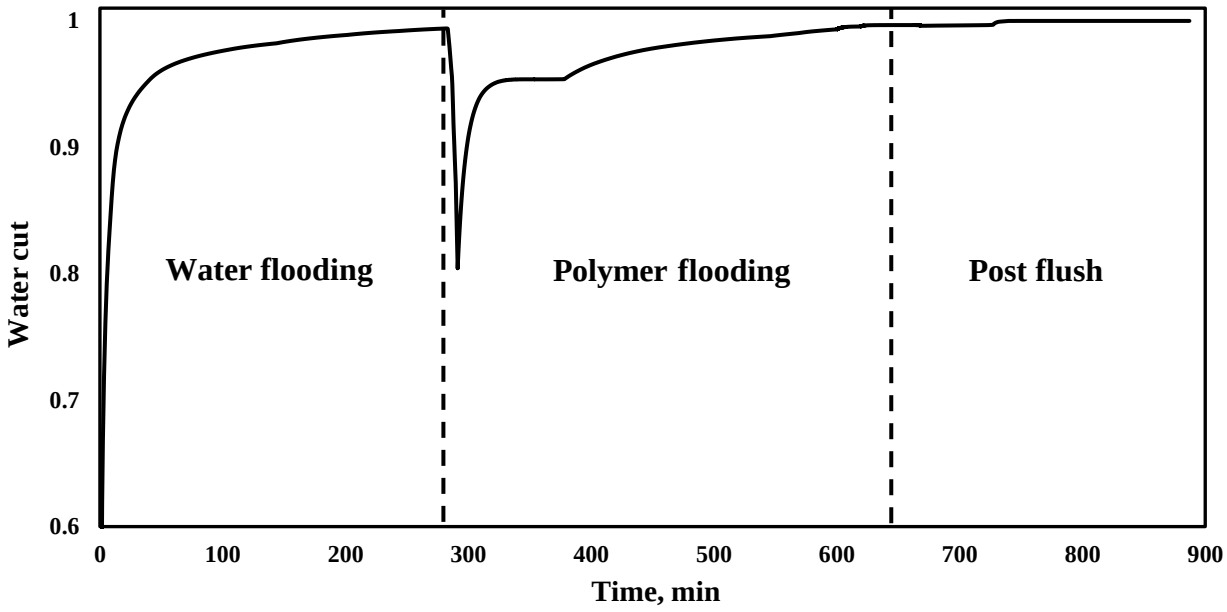

Figure 15. Core scale numerical simulation water cut.

Figure 16 provides a visual comparison of oil recovery factors derived from laboratory core flood experiments (depicted as points) and numerical simulations (illustrated by a solid line). Notably, during the WF phase, both methodologies exhibit close correspondence, indicating a dependable simulation of reservoir dynamics during WF.

Throughout the polymer injection phase, there is a general proximity between the experimental and numerical results. However, towards the conclusion of this phase, a discernible difference becomes apparent. Specifically, the laboratory results indicate a slightly higher recovery rate of 3% compared to the numerical simulation, suggesting some variance in how polymers behave in the physical and simulated core scale environments.

During the post-flush period, no noticeable deviations are observed in either the experimental or numerical results.

In summary, the analogous profile of oil recovery factors observed in the numerical simulation lends support to the notion that the constructed core-scale model effectively reproduces the laboratory findings. This enhances our confidence in the reliability and accuracy of the numerical approach.

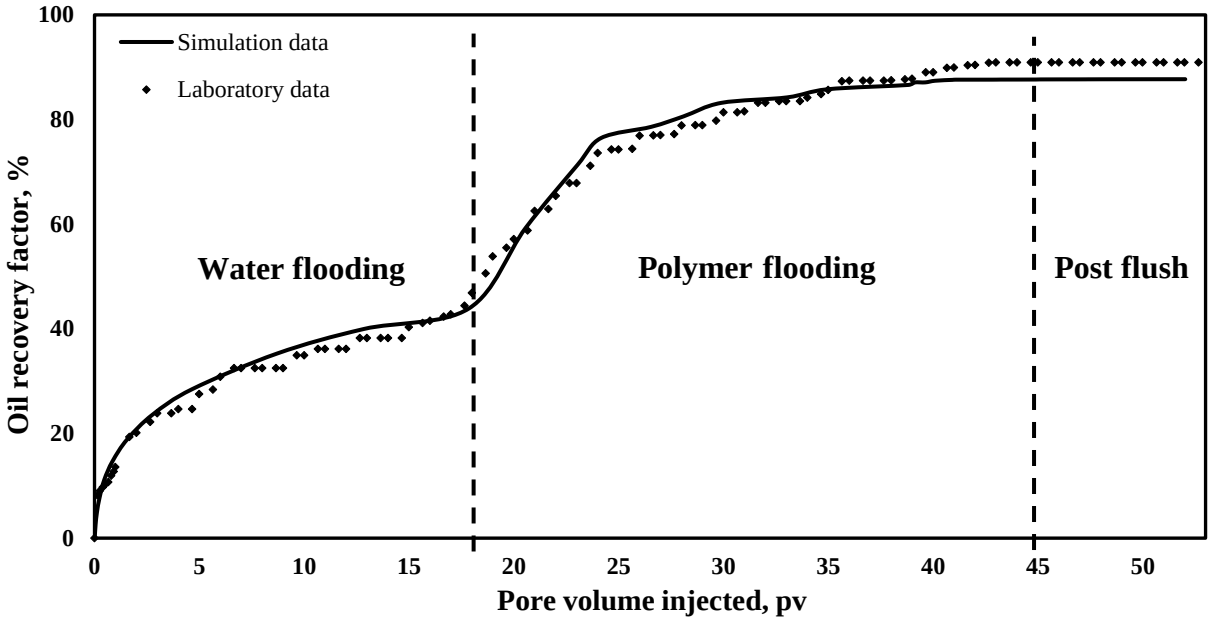

Figure 16. Oil recovery factor of laboratory core flood and simulation core flood.

The comparative analysis between simulated results and experimental results constitutes a crucial stage in the process of model validation. Initially, the Error for each data point on the graph was computed using Eq. 13:

$$Error = \left|\frac{Value_{experiment} - Value_{simulator}}{Value_{experiment}}\right| \times 100\% \quad (13)$$

Once the Error of points calculated, then for the model validation, the Average Error was calculated using Eq. 14:

$$Average\ Error(\%) = \frac{\sum_{i=1}^{N} Error}{N} \quad (14)$$

Consequently, the computed Average Error value, which is 5%, signifies a level of reliability in the model. This implies that the model effectively captures the dynamics of the system, affirming the efficiency of PF.

3.1.3. Reservoir scale model

The numerical simulation of the reservoir-scale model was conducted on Sector 14 of the Uzen field, as illustrated in Figure 17. The reservoir model was constructed using Petrel software and subsequently transferred to CMG Stars for further numerical simulations. This sector model, integral to the study, encompasses six production wells: №9061, №3496,

№8707, №3529, №2917, and №9449, positioned around the periphery, along with a central injection well, №9051. All the wells are operated

The upper and lower boundaries of the sector model exhibit a gradient from lower depths to higher depths. Specifically, the upper boundary ranges from its highest point at 994 m to its lowest point at 955 m, while the lower boundary spans from its highest point at 1058 m to its lowest point at 1022 m. The grid dimensions of the reservoir are characterized by a 15×15×44 configuration, resulting in a total of 9900 grid blocks. Each grid block was manually constructed, with thicknesses ranging from 0.35 to 7.75 m.

The arrangement of wells in this sector model replicates the well pattern and activation years observed in real-field data. Notably, the addition of production well №8707 in 1996 signifies the commencement of oil production in this sector. Subsequently, production wells №2917, №3529, №9061, №9449, and №3496 were added in 2009, 2011, 2012, 2016, and 2011, respectively. Furthermore, injection well №9051 was introduced in 2012 specifically for WF operations.

The investigation of grid cell size variations within the context of optimizing a reservoir model entail examining their impact on the precision and computational effectiveness of simulation outcomes. In this particular reservoir model, the comprehensive sensitivity analysis concerning grid sizes for attaining optimal reservoir model performance was carried out utilizing Petrel software by KMGE.

Figure 18 depicts the distribution of oil saturation across the reservoir. The graphical representation reveals that a greater concentration of oil saturation is situated in the upper strata of the reservoir, contrasting with the lower portion primarily occupied by water influx sourced from the aquifer.

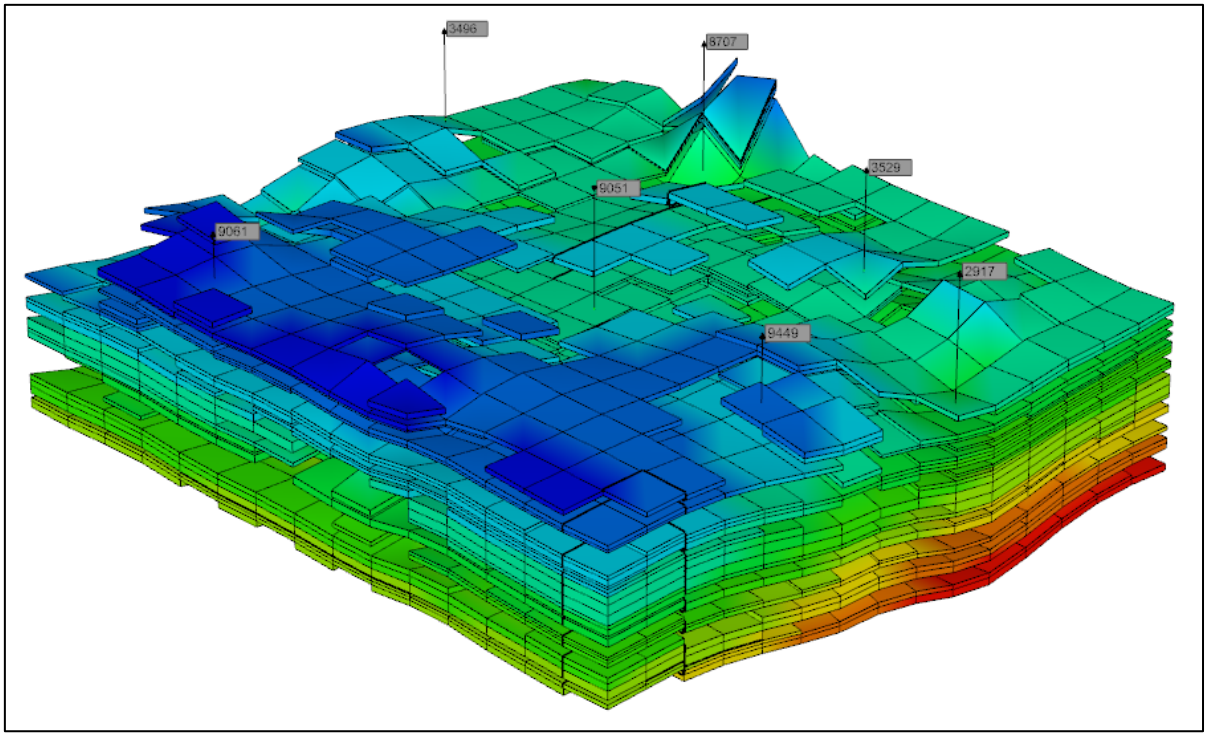

Figure 17. Reservoir model (Sector 14).

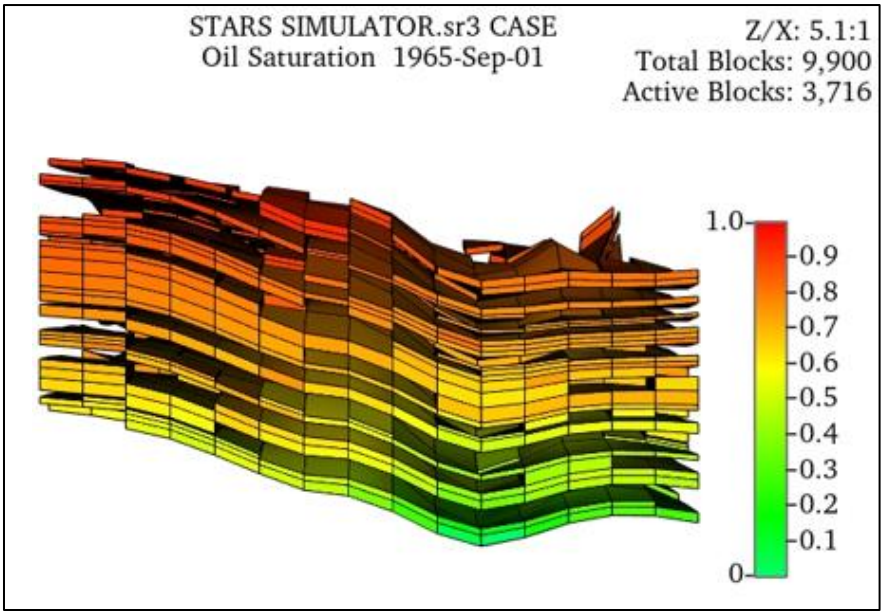

Figure 18. Oil saturation within the reservoir.

Figure 19 presents a histogram delineating the distribution of oil saturation. The graphical depiction indicates that the peak oil saturation value falls within the range of 0.7 to 0.8, encompassing 1202 units.

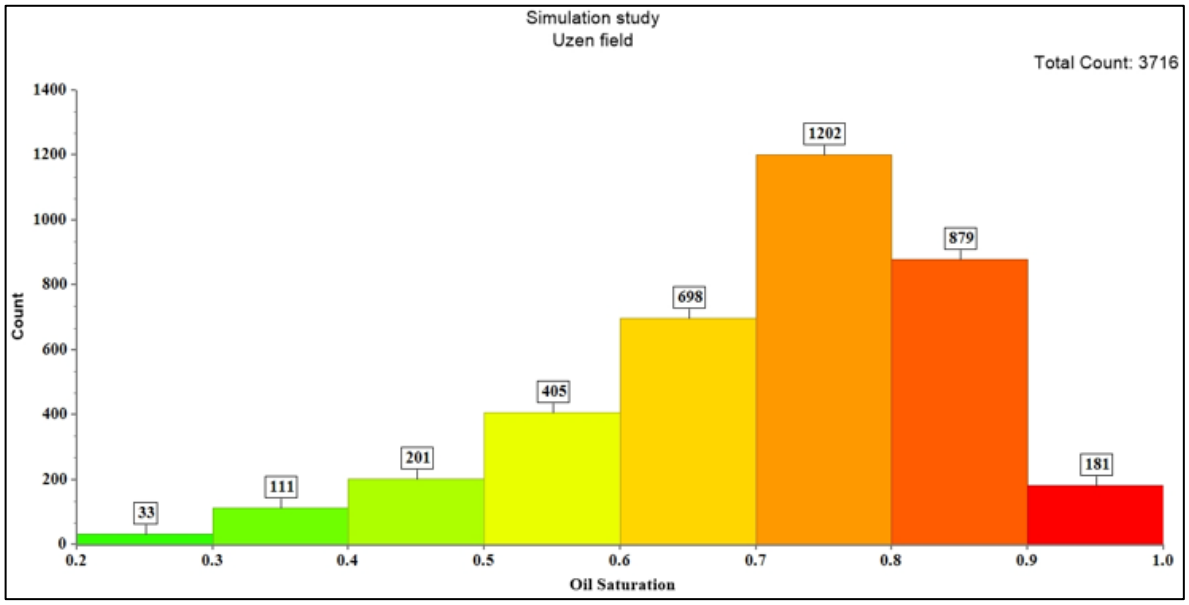

Figure 19. Oil saturation distribution histogram.

Figure 20 illustrates the distribution of water saturation within the reservoir. The graphical depiction indicates a predominant accumulation of water saturation in the lower section of the reservoir, contrasting with the upper region predominantly characterized by the presence of oil.

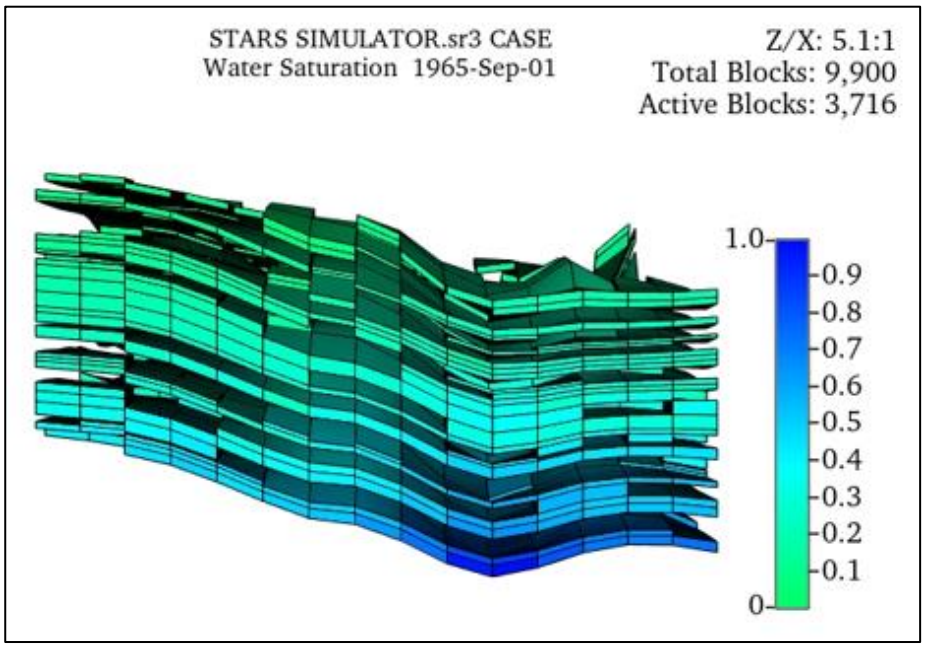

Figure 20. Water saturation within the reservoir.

Figure 21 displays a histogram outlining the distribution of water saturation. The graphical representation reveals that the highest water saturation value is observed within the interval of 0.2 to 0.3, encompassing a total of 1202 units.

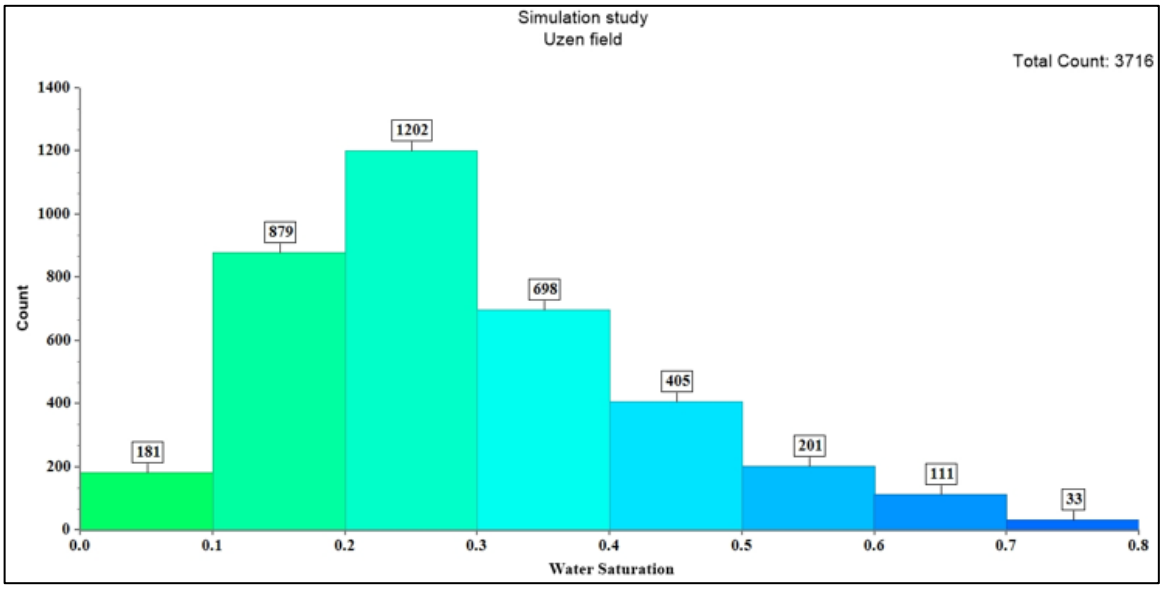

Figure 21. Oil saturation distribution histogram.

3.1.4. Reservoir scale numerical simulation

According to Imanbayev et al. (2022), production activities in the Uzen field commenced in 1965. In addition to waterflooding, the field is currently undergoing development through various methods aimed at enhancing oil production. These methods include hydraulic fracturing, refracturing, drilling of horizontal wells, and the implementation of conformance control measures such as gel treatment in injectors and water shut-off in producers.

As of the conclusion of 2021, cumulative oil production in the Uzen field had reached 361.5 million tonnes, resulting in a recovery factor of 34.6%. Over the past decade, the field has consistently maintained an annual production rate of approximately 4.5 million tonnes, as depicted in Figure 22.

Well № 8707, situated within Sector 14, initiated oil production activities in the sector in the year 2000. Sector 14 encompasses six operational wells and one injection well, with KMGE providing production data from these wells for subsequent utilization in numerical simulations and validation of the sector model. The oil production rate data of well № 8707, sourced from the Uzen field and depicted in Figure 23, reveals fluctuations in production rates

ranging from 1 to 10 m^3/d over the years 2000 to 2021. Analysis of the production rate trend indicates a decline from 9 to 3 m^3/d over a span of 21 years.

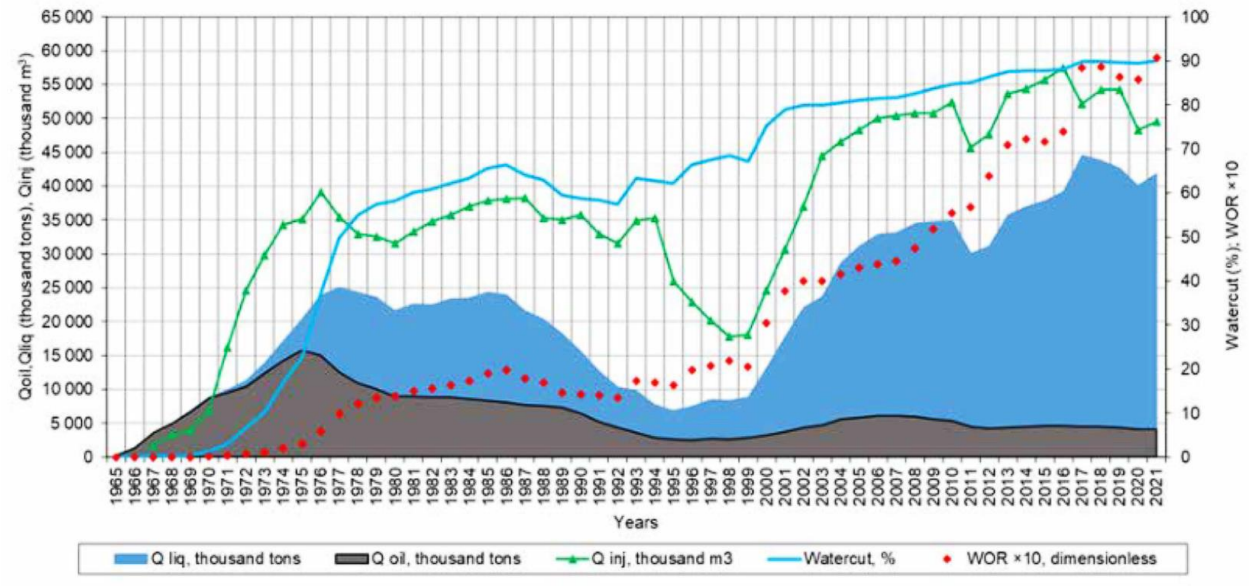

Figure 22. Production history of the Uzen field (Imanbayev et al., 2022).

The model underwent validation and approval by KMGE through history matching of real data and numerical simulation data, ensuring its accuracy and reliability.

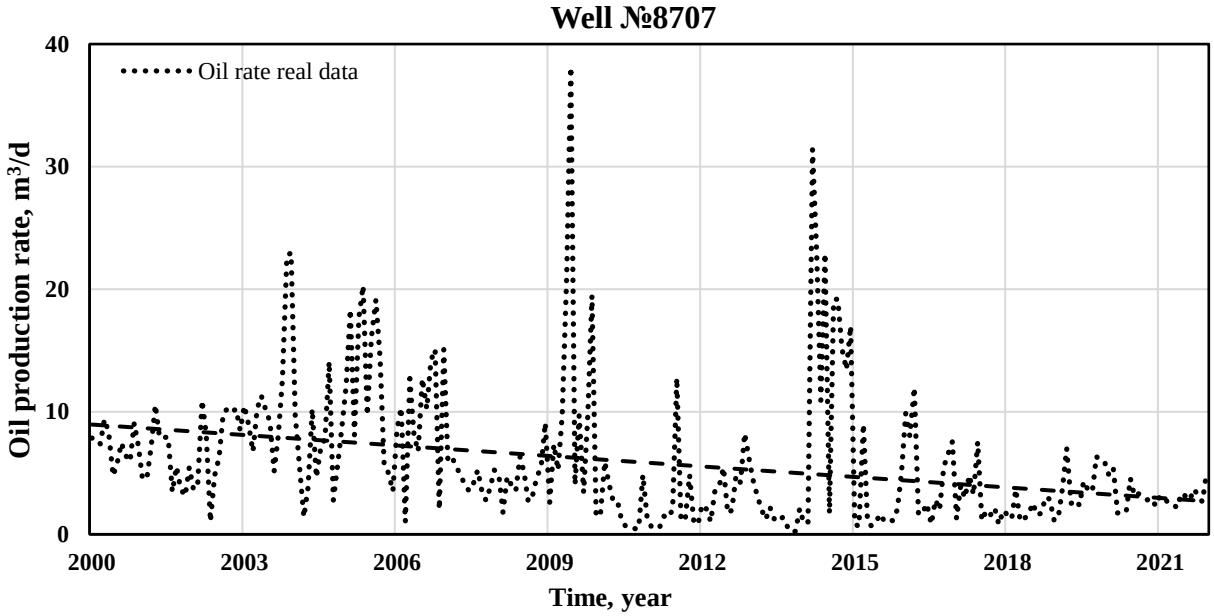

Figure 23. Oil production rate of well №8707 provided by KMGE.

The validation of reservoir-scale models constitutes a crucial step in ensuring the accuracy and reliability of numerical simulation outcomes. Initially, the simulation of WF was conducted to assess the performance of the reservoir-scale model. The results of the WF simulation, encompassing metrics such as well oil rates, cumulative oil production, and sector model cumulative oil production, were then juxtaposed with data from actual field wells.

Figure 24 depicts a comparative analysis of oil production rates derived from numerical simulation results (represented by the solid line) and those obtained from actual field data (illustrated by the dashed line) spanning the years 2013 to 2022. During the initial five-year period from 2013 to 2017, minimal divergence is observed between the oil production rate profiles, with close alignment between the lines. However, in the subsequent five years spanning from 2017 to 2022, the lines exhibit virtually identical behavior. This graphical representation underscores a significant correspondence between the two sets of oil production rates, indicating a robust convergence between numerical simulation results and actual field data.

The Average Error is calculated by Eq. 14 and equal to 7%.

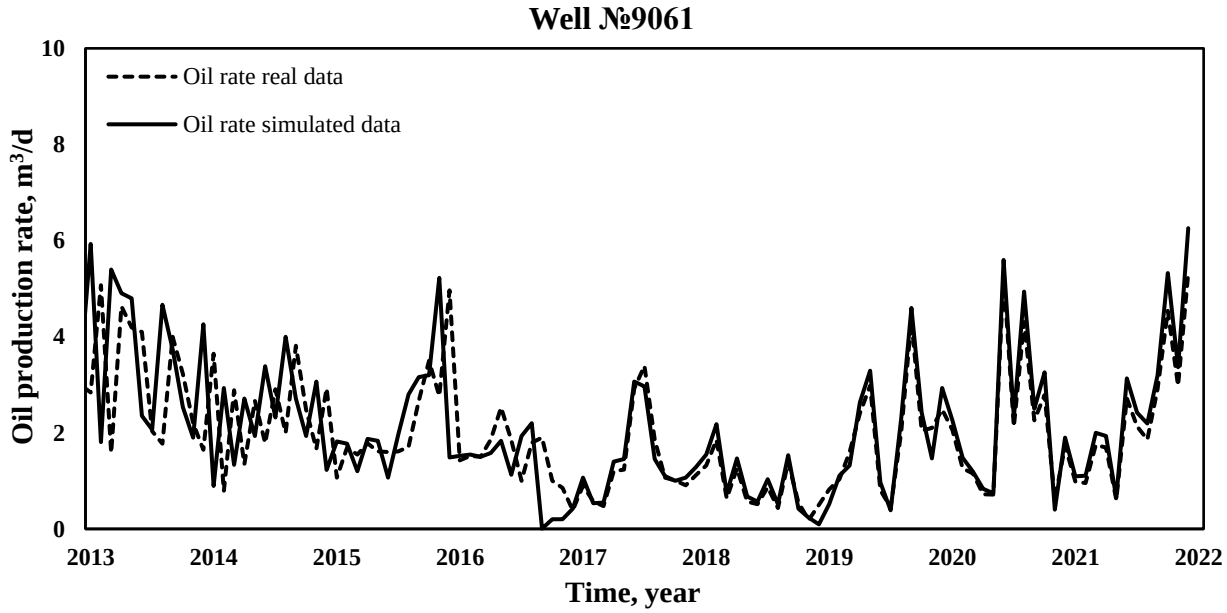

Figure 24. Oil production rate of well №9061 derived from numerical simulation results and real field data.

Figure 25 presents a comparative analysis of cumulative oil production between numerical simulation data (solid line) and real field data (dashed line) from 2012 to 2022. The

graphical depiction reveals a notable consistency between the two datasets, with closely aligned values observed throughout the analyzed period. However, towards the end of the timeframe, the numerical simulation depicts a slightly higher cumulative oil production compared to the real field data.

The calculated Error, as determined by Eq. 14, yields a favorable outcome of 7%. This indicates a strong degree of agreement between the numerical simulation results and the actual field data, underscoring the reliability and accuracy of the reservoir model utilized in the study. Consequently, it can be inferred that the reservoir model demonstrates robustness and dependability in its predictive capabilities.

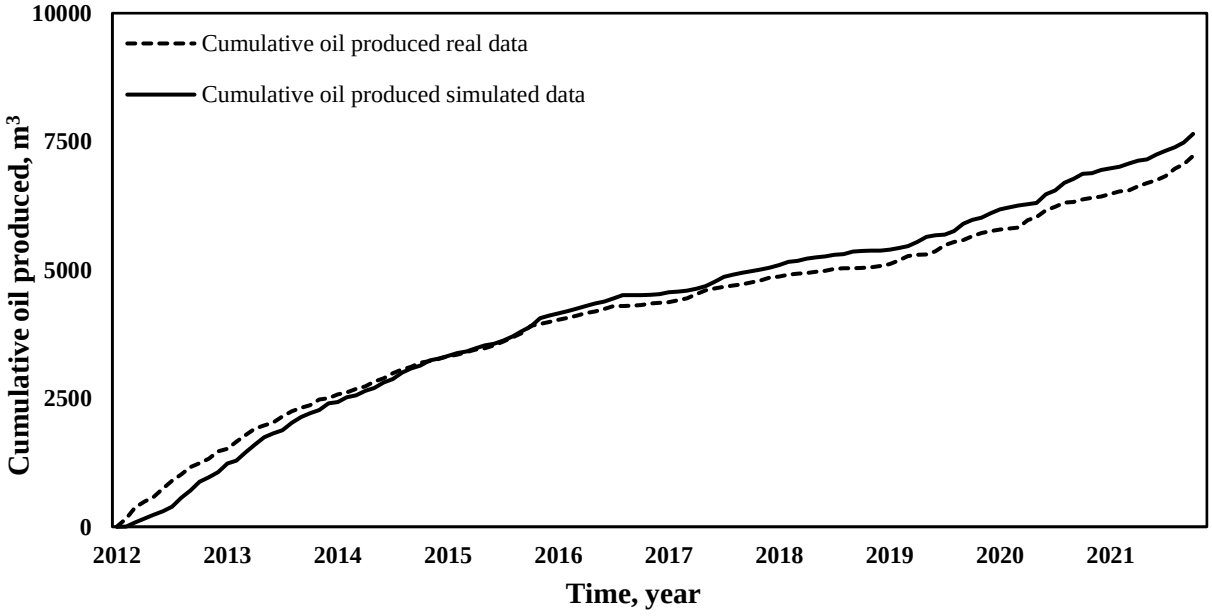

Figure 25. Cumulative oil production of well №9061 derived from numerical simulation results and real field data.

The goal of this comparative analysis was to assess the agreement between simulated and real sector model performance, thereby improving the integrity and accuracy of the reservoir scale model.

3.1.5. Polymer flood design parameters

According to Yerniyazov et al. (2023), the selection or design of a polymer solution requires careful consideration of various parameters. Achieving a mobility ratio of less than one is crucial, and this necessitates ensuring that the viscosity of the polymer solution

matches or exceeds that of the crude oil under reservoir conditions. Modulating the viscosity of the polymer solution can be effectively achieved by increasing the concentration of the polymer.

Based on the findings of Yerniyazov et al. (2023), one of the polymer samples provided by KMGE (ASP3) was identified as the most optimal polymer. Rheological and stability assessments indicated that the optimal concentration for this polymer is 2500 parts per million (ppm).

The polymer injection rate is another crucial parameter in the design of a PF. To effectively compare and emphasize the advantages of PF over WF, water and polymer were injected at the same rate during numerical simulations. The injection rate was determined based on the maximum reservoir pressure achievable by ASP3. Consequently, a sensitivity analysis of polymer injection rate was conducted initially to ascertain the optimal injection rate. This analysis aimed to define the injection rate that would yield the most favorable results in terms of reservoir performance and oil recovery efficiency.

The initial reservoir pressure in the sector model is documented as 11000 kPa. Therefore, the maximum reservoir pressure attained through polymer injection should surpass 11000 kPa. Following an analysis of injection rate sensitivity, it was concluded that the optimal polymer injection rate is 140 m^3/d. Consequently, to enable a more precise comparison, water injection is also executed at a rate of 140 m^3/d.

The size of the polymer slug plays a critical role in the cost, economic considerations, and overall performance of a polymer-flooding project. Inadequate sizing of the injected polymer slug has been identified as a major factor contributing to unsatisfactory outcomes in PF conducted globally. The optimal slug size during a PF is contingent upon reservoir characteristics, the presence of conformance issues within the reservoir, and alignment with the business objectives of the PF. Therefore, careful consideration and analysis are essential in determining the appropriate size of the polymer slug to ensure the success and efficiency of the polymer-flooding project.

Based on the analysis of 12 international polymer-flooding projects, a recommended initial value for designing a polymer waterflooding project would be a polymer solution slug comprising 50% of the pore volume (PV).

In this study, an extended duration of WF was employed to provide a more comprehensive understanding of the impact of PF, given the primary challenge of high water cut in the Uzen field. The initiation of PF was contingent upon reaching a water cut value of 0.72 and an associated oil recovery of 25%, which occurred in the year 2045. This approach was chosen to better illustrate the influence of PF, with a deliberate extension of the WF until a higher water cut value was attained.

The 37kofiskoir-scale numerical simulation scenario begins with the initiation of oil production in 1990, followed by the commencement of water injection in 2012. Water injection continues until the water cut reaches a value of 0.72, at which point PF is introduced. The duration of the PF will be discussed in detail in the subsequent chapter.

4 RESULTS AND DISCUSSION

The findings of the study will be showcased through numerical simulations conducted at the reservoir scale. These simulations encompass sensitivity analyses for polymer injection rate, PF duration, and polymer concentration. Through the elimination of suboptimal values, the study identified the characteristic features of a PF design parameter.

4.1 Polymer injection rate sensitivity analysis.

Figure 26 depicts the influence of varying polymer injection rates on reservoir pressure. Initially, upon the commencement of oil production, the reservoir pressure is recorded at 11000 kPa. Subsequently, as production progresses, a decline in pressure is observed, reaching 8500 kPa until the onset of water injection in 2012. The implementation of WF leads to a notable rise in reservoir pressure, peaking at 15000 kPa, a level sustained until 2045.

From 2045 onward, different scenarios with varying polymer injection rates are examined. This year was selected due to the anticipated undesirable increase in water cut beyond 0.72, as evidenced by the conclusion of WF. To enable direct comparison between WF and PF, both water and polymer injection rates are maintained at a constant 140 m^3/d, with a polymer concentration of 2500 ppm across all scenarios.

Following 5 years of polymer injection, a gradual rise in reservoir pressure commences, culminating in peak values after 25 years, notably in 2070. Numerical simulations reveal distinct peak reservoir pressure values corresponding to different polymer injection rates: 7230, 9300, 13000, 19600, and 27900 kPa, aligned with polymer injection rates of 110, 120, 130, 140, and 150 m^3/d, respectively, as illustrated in Figure 26. In contrast, under continuous WF, from 2045 with an injection rate of 140 m^3/d, reservoir pressure diminishes to 1500 kPa over 15 years, with a gradual ongoing decline thereafter.

The observed pressure profile is influenced by various factors, with one significant contributor being the viscosity of the polymer and its impact on sweep efficiency. When polymer is introduced into the injected fluid, it enhances the fluid’s viscosity, thereby increasing the resistance to flow.

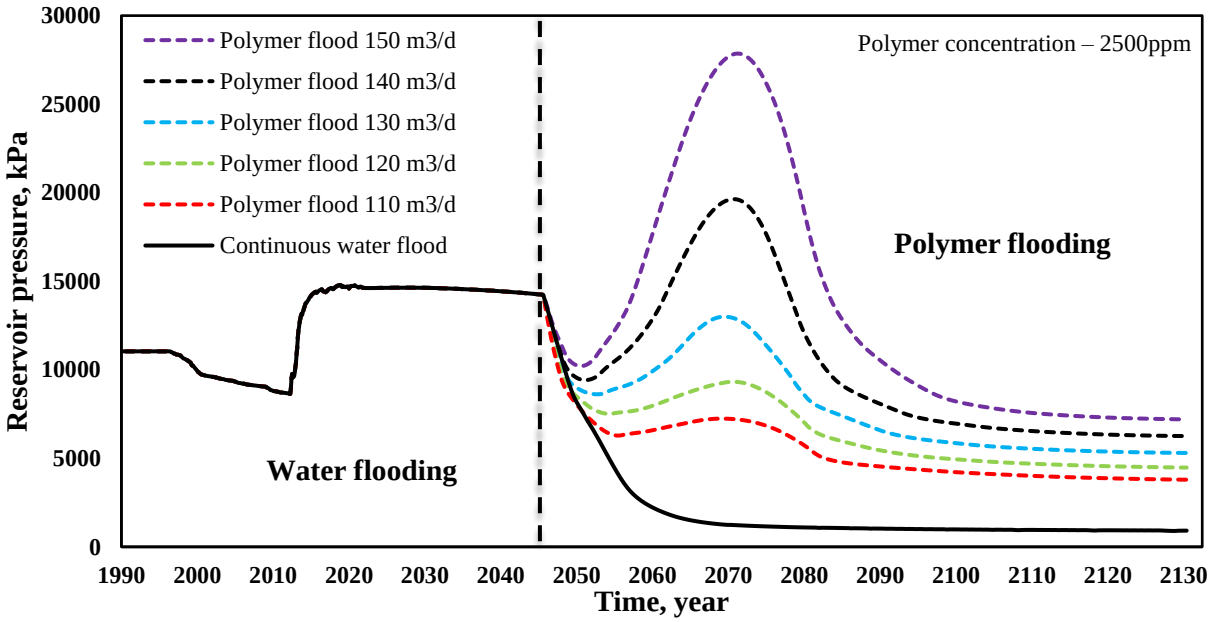

Figure 26. The graph of reservoir pressure at different polymer injection rates.

Figure 27 illustrates the impact of polymer injection rate on water cut. Initially, the water cut undergoes temporal fluctuations and attains a value of 0.72 by the end of the WF phase in 2045. Subsequently, under continuous water injection at a constant rate, the water cut continues to ascend, reaching 0.9 by the year 2060. After 2060, there is a gradual increase that results in a water cut of 0.95 by the end of the simulation period in 2130.

During the PF phase, the water cut experiences an increase, reaching 0.76, in 2050. From the year 2050 onward, the water cut initiates a declining trend, continuing until 2060 and 2065 for various injection rates. Notably, the minimum water cut values recorded are 0.5, 0.52, 0.54, 0.57, and 0.6, corresponding to polymer injection rates of 150, 140, 130, 120, and 110 m^3/d, respectively. At the end of the PF phase, by the year 2130, the water cuts stand at 0.91, 0.92, 0.93, 0.94, and 0.95 for injection rates of 110, 120, 130, 140, and 150 m^3/d, respectively.

Figure 28 delineates the oil recovery trends associated with PF at various injection rates. Initially, during WF, the oil recovery attains a value of 25% by the year 2045. Subsequently, with the ongoing injection of water, the oil recovery exhibits a progressive increase, reaching 32% in 2055 and finally attaining 42% by the end of the simulation period in 2130.

It is imperative to highlight that in the year 2055, the water cut reaches a critical value of 0.85, indicating a substantial proportion of water production. Consequently, the continuation of WF alone leads to the production of primarily water, rendering it ineffective for oil recovery purposes. This underscores the urgent need to introduce EOR methods aimed at mitigating the high water cut.

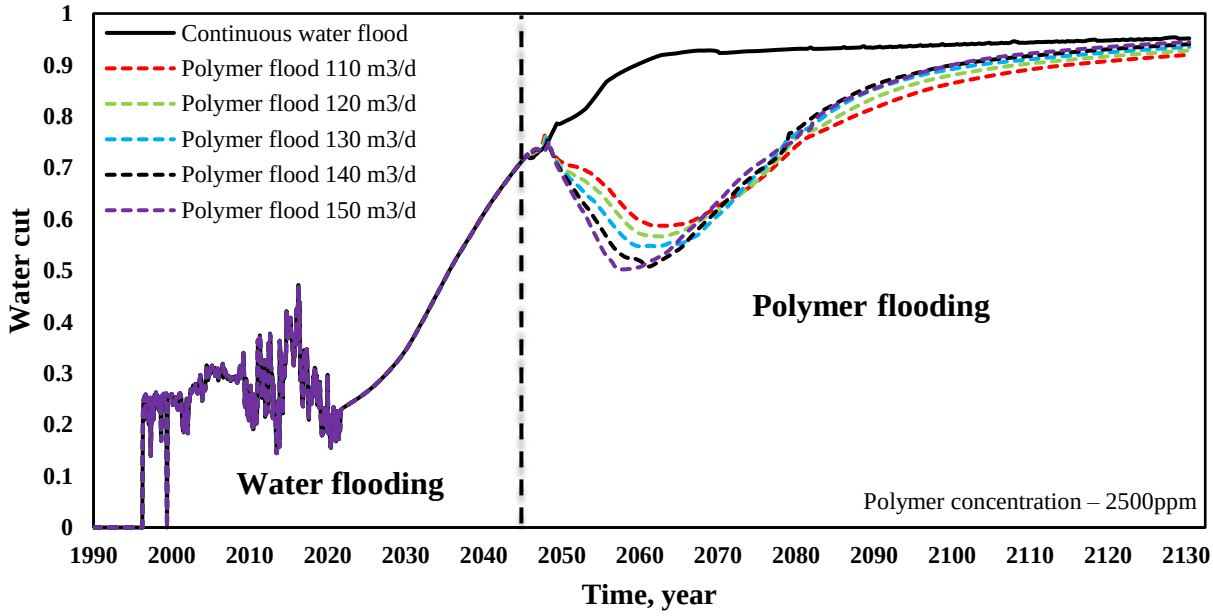

Figure 27. The graph of water cut at different injection rates.

Introducing EOR techniques becomes essential to counteract the escalating water cut and enhance oil recovery efficiency. By implementing appropriate EOR strategies, such as PF, it becomes feasible to effectively manage the reservoir conditions and optimize oil production.

In the context of PF, notable alterations in the slopes of the oil recovery curves are observed in 2080, corresponding to oil recovery of 44%, 46%, 48.5%, 50.5%, and 51% for injection rates of 110, 120, 130, 140, and 150 m^3/d, respectively. Afterwards, from the year 2080 onward, the oil recovery experiences a gradual and sustained increase, culminating in values of 56%, 58%, 60%, 62%, and 64% at injection rates of 110, 120, 130, 140, and 150 m^3/d, respectively, by the year 2130. Notably, the difference between the oil recovery under continuous WF and the minimum polymer injection rate is observed to be 14%.

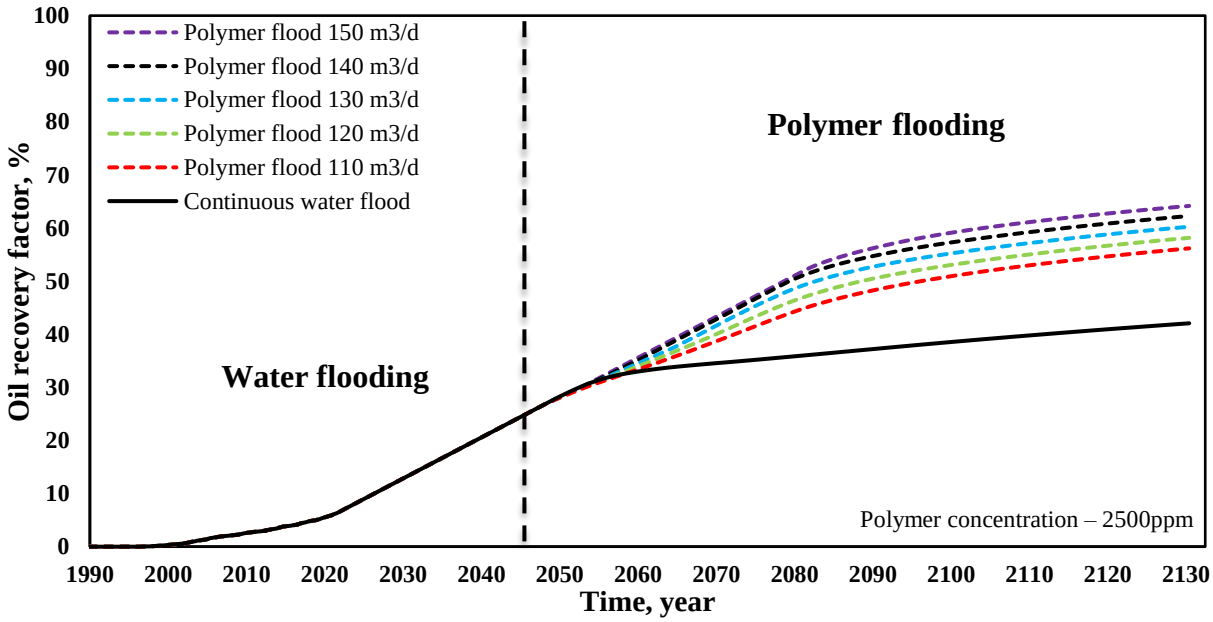

Figure 28. The graph of oil recovery factor at different injection rates.

In the context of EOR, the findings presented in Figure 29 for the years 2070 and 2080 reveal a significant positive correlation between polymer injection rates and reservoir pressure. With a fixed polymer concentration of 2500 ppm, the graph underscores the higher sensitivity of reservoir pressure to higher injection rates. Notably, in 2070, the discernible differences in pressure values between increments of 130 to 140 and 140 to 150 m^3/d suggest that incremental increases in polymer injection rates, particularly in the higher range, exert more pronounced impacts on reservoir pressure.

Conversely, it's essential to note that under the current water injection rates, there is no significant variation in reservoir pressure over a period of 10 years, as illustrated in Figure 30.

The insights drawn from Figure 31, depicting water cut variations in the years 2060 and 2070 at a polymer concentration of 2500 ppm and different rates of polymer injection, hold significant implications. The graph's focus on water cut values proximate to the minimums achieved by respective injection rates sheds light on the varying effectiveness of polymer injection in mitigating water production.

The data depicted in the graph indicates a discernible linear correlation between the polymer injection rate and water cut by the year 2060. In 2070, close values are observed among the same polymer injection rates. It is observed that lower water cut levels are

associated with higher injection rates of polymer. However, by the time, higher injection rates exhibit higher increase in water cut.

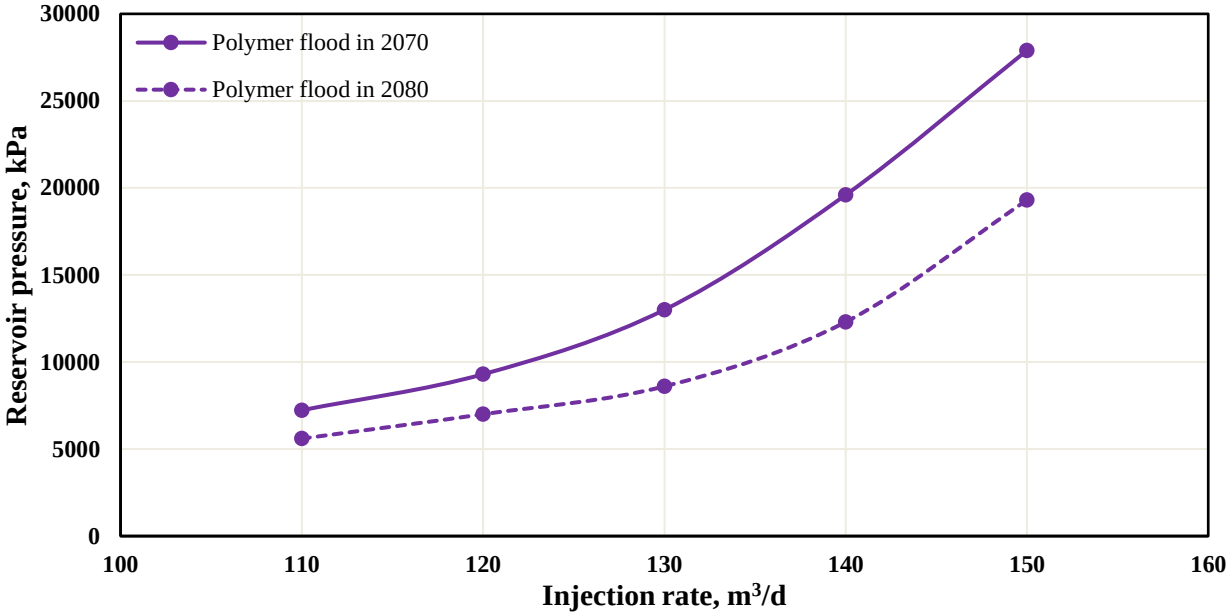

Figure 29. The graph of reservoir pressure at different polymer injection rates in 2070 and 2080 at polymer concentration of 2500 ppm.

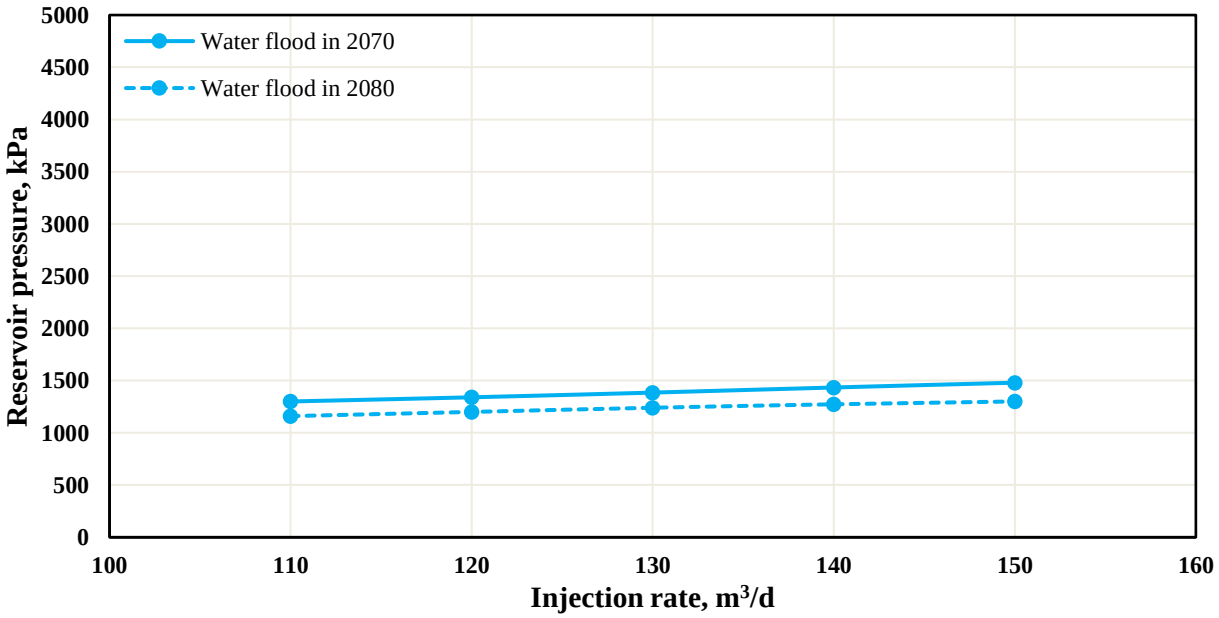

Figure 30. The graph of reservoir pressure at different water injection rates in 2070 and 2080.

In the scenario of continuous WF, there is minimal change in water cut observed over time for injection rates spanning from 110 to 150 m^3/d, as illustrated in Figure 32.

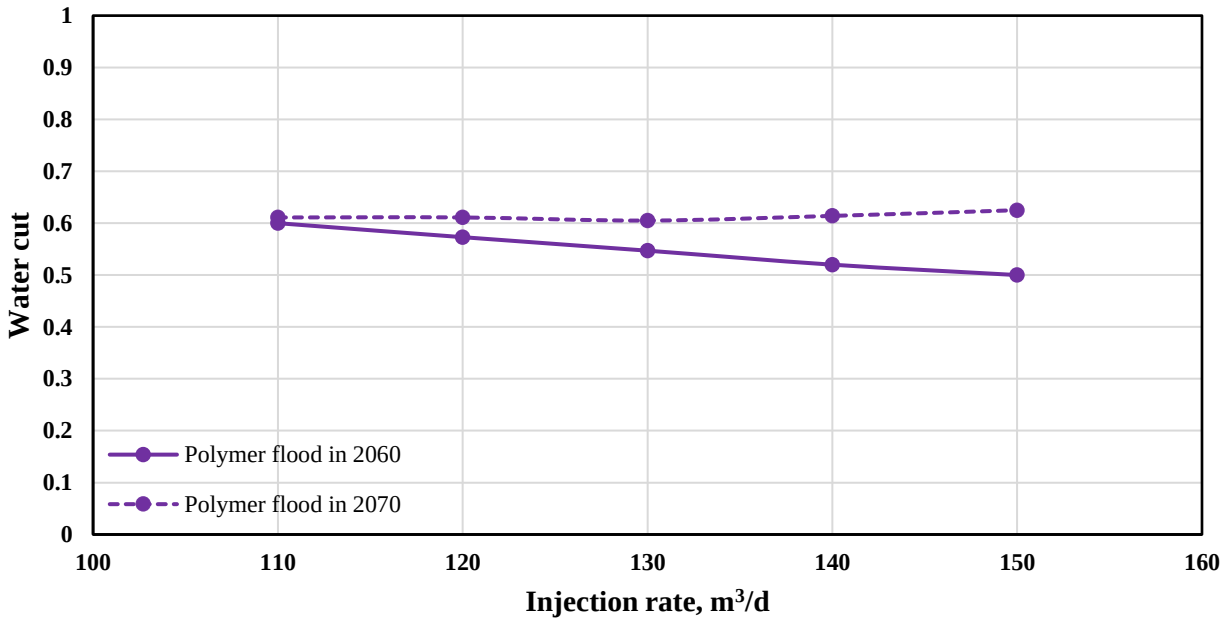

Figure 31. The graph of water cut at different polymer injection rates in 2060 and 2070 at polymer concentration of 2500 ppm.

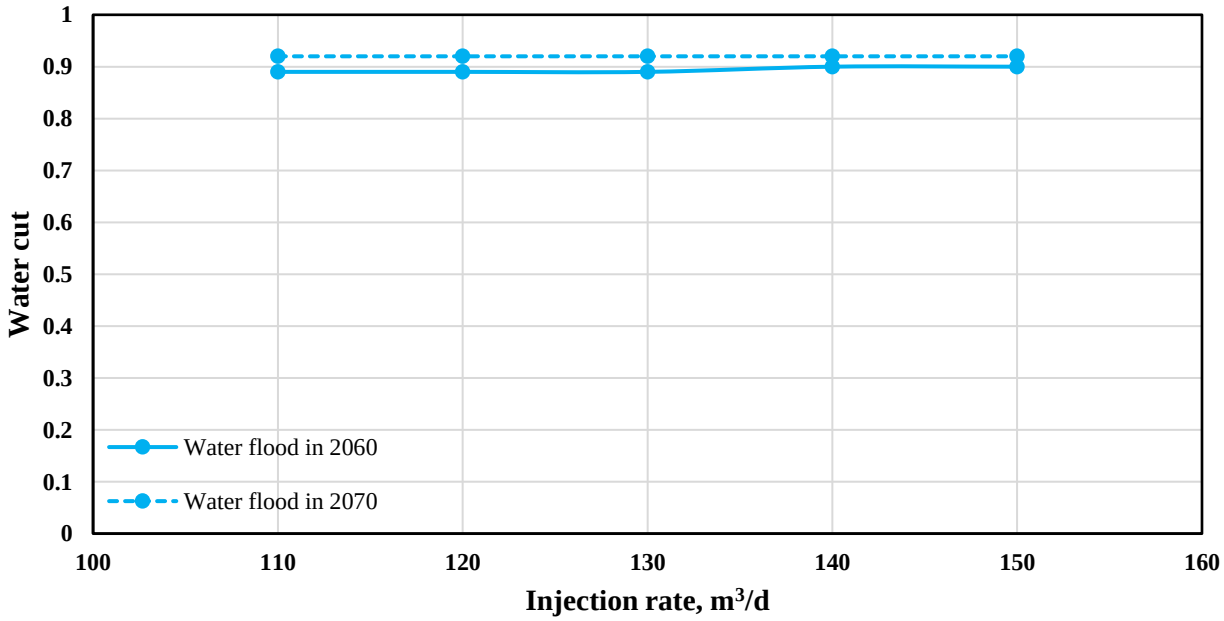

Figure 32. The graph of water cut at different water injection rates in 2060 and 2070.

Figure 33 presents a comparative analysis of oil recovery achieved through PF and continuous WF across injection rates spanning from 110 to 150 m^3/d. The graph reveals a discernible positive correlation between higher injection rates and the oil recovery factor for both PF and WF, indicating a linear relationship in both cases. While the injection rate in WF

demonstrates a minimal effect on oil recovery, the influence of injection rate on PF is notably more pronounced.

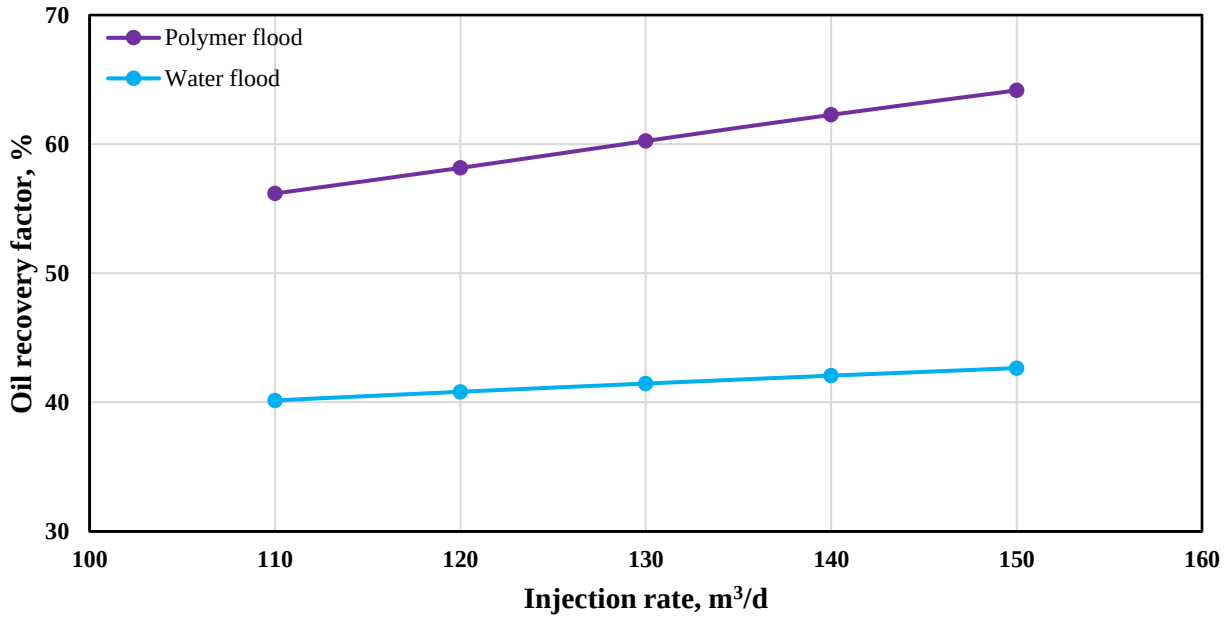

Figure 33. The graph of oil recovery factor at different polymer injection rates at polymer concentration of 2500 ppm and water injection rates.

To establish the optimal polymer injection rate, a comprehensive evaluation of important factors such as reservoir pressure, water cut, and real sector water injection rates is conducted and analyzed.

Analysis of the reservoir pressure profile, in Figure 26, indicates a fluctuating trend following the initiation of polymer injection, characterized by an initial decrease followed by a subsequent increase over time. Specifically, at polymer injection rates below 140 m^3/d, the decline in reservoir pressure outweighs the subsequent increase. Conversely, at injection rates of 140 and 150 m^3/d, the rise in reservoir pressure exceeds the pressure drop. Consequently, it is apparent that the injection pressure should ideally be maintained at 140 or 150 m^3/d. However, a closer examination of reservoir pressure values reveals that an injection rate of 150 m^3/d results in pressure levels approximately 2.5 times higher than the reservoir pressure, posing a significant risk of inducing formation fracturing. Therefore, to mitigate the potential for formation damage and ensure optimal performance, it is recommended that the polymer injection rate be set at 140 m^3/d, as this rate strikes a balance between maximizing oil recovery and minimizing the risk of adverse operational consequences.

In context of water cut, the injection rate of 140 m^3/d stands out as optimal, as it achieves a relatively low water cut of 0.52 in 2060 (Figure 31), in comparison with lower injection rates, and exhibits a comparatively smaller increase in water cut over time compared to higher injection rate.

Figure 34 displays the actual water injection rates of Sector 14, provided by KMGE, spanning the years 2012 to 2021. In determining the optimal injection rate within sector, an analysis of the historical water injection data was conducted. The resultant average water injection rate is 137 m^3/d, a value closely approximating 140 m^3/d. This finding suggests that the optimal polymer injection rate for Sector 14 aligns with the calculated average, indicating that 140 m^3/d serves as the most suitable injection rate for maximizing operational efficiency and oil recovery within this specific sector.

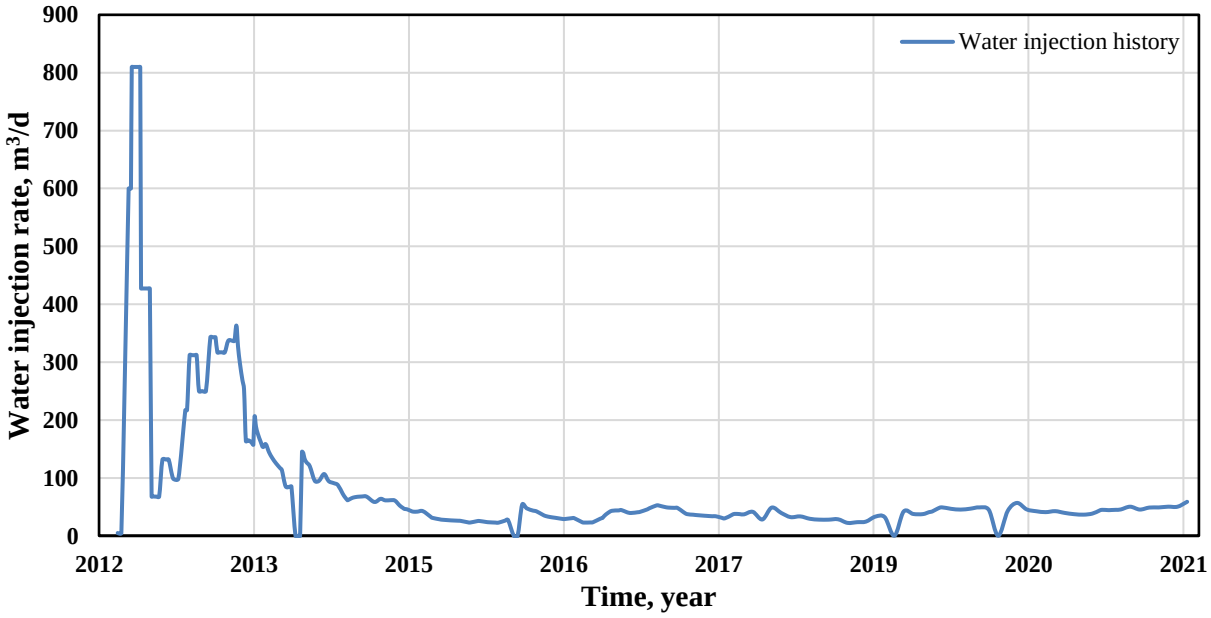

Figure 34. The graph of real water injection rate in Sector 14 (Provided by KMGE).

4.2 Polymer flood duration sensitivity analysis.

Figure 35 delineates the influence of varying durations of PF, while maintaining a constant injection rate, on reservoir pressure. Spanning from the year 2045 onwards, the graph illustrates diverse scenarios of PF durations, with a consistent injection rate of 140 m^3/d and a polymer concentration of 2500 ppm. Following each PF scenario, reservoir pressure was subsequently managed through WF.

Analysis of the graph reveals a distinct pattern wherein reservoir pressure experiences an initial decrease followed by an increase at the onset of PF. The peak reservoir pressure values attained by PF durations of 5, 10, 15, 20, 25, and 30 years, occurring between 2050 and 2070, are observed to be 10300, 14000, 18000, 19450, 19500, and 19500 kPa respectively. Subsequently, reservoir pressure begins to decline after reaching its peak value. Notably, it is emphasized that PF durations of 5 and 10 years exhibit a smaller increase in reservoir pressure compared to the initial decrease, whereas durations of 15, 20, 25, and 30 years demonstrate a more substantial increase in reservoir pressure relative to the initial decrease.

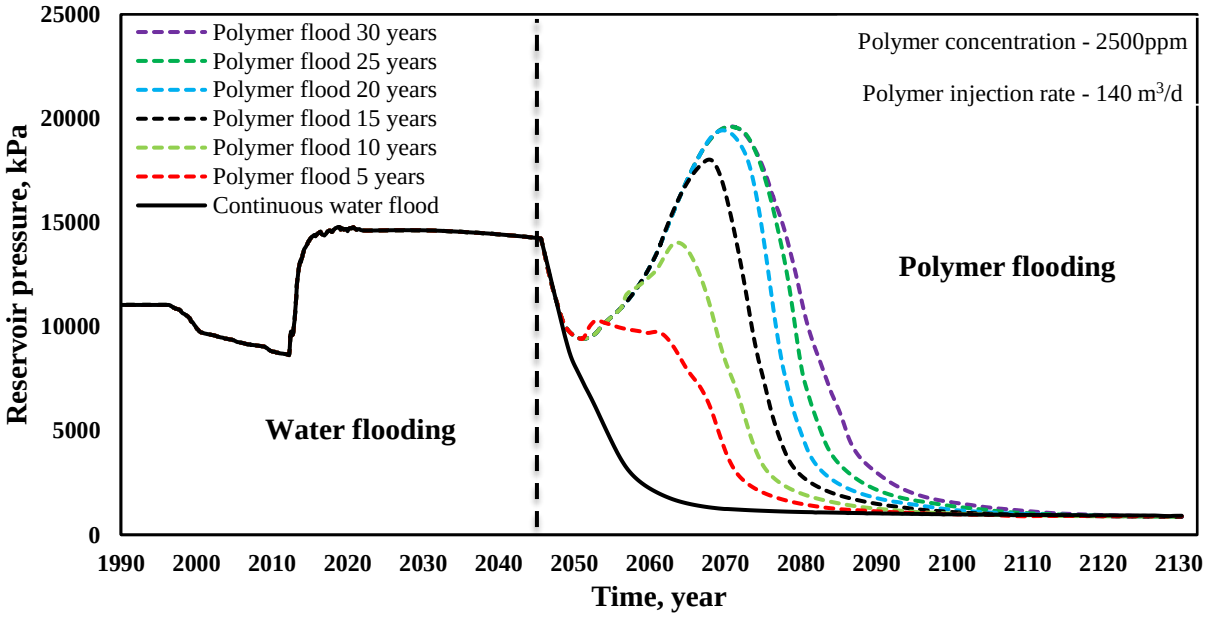

Figure 35. Reservoir pressure at different polymer flood duration.

Figure 36 delineates the influence of varying durations of PF on water cut. Commencing from the year 2045, the graph portrays a range of scenarios depicting water cut dynamics, with a consistent injection rate of 140 m^3/d and a polymer concentration of 2500 ppm.

Upon analysis of the graph, a discernible pattern emerges wherein water cut initially increases and subsequently decreases at the onset of PF. The nadir of water cut values achieved across different PF durations, occurring between 2055 and 2065, are observed to be 0.55, 0.53, 0.51, 0.5, 0.51, and 0.51, respectively. This trend indicates an inverse relationship

between PF duration and water cut, signifying that longer durations of PF result in lower water cut levels.

In essence, the findings suggest that prolonging the duration of PF leads to a reduction in water cut, underscoring the efficacy of extended PF durations in mitigating water production.

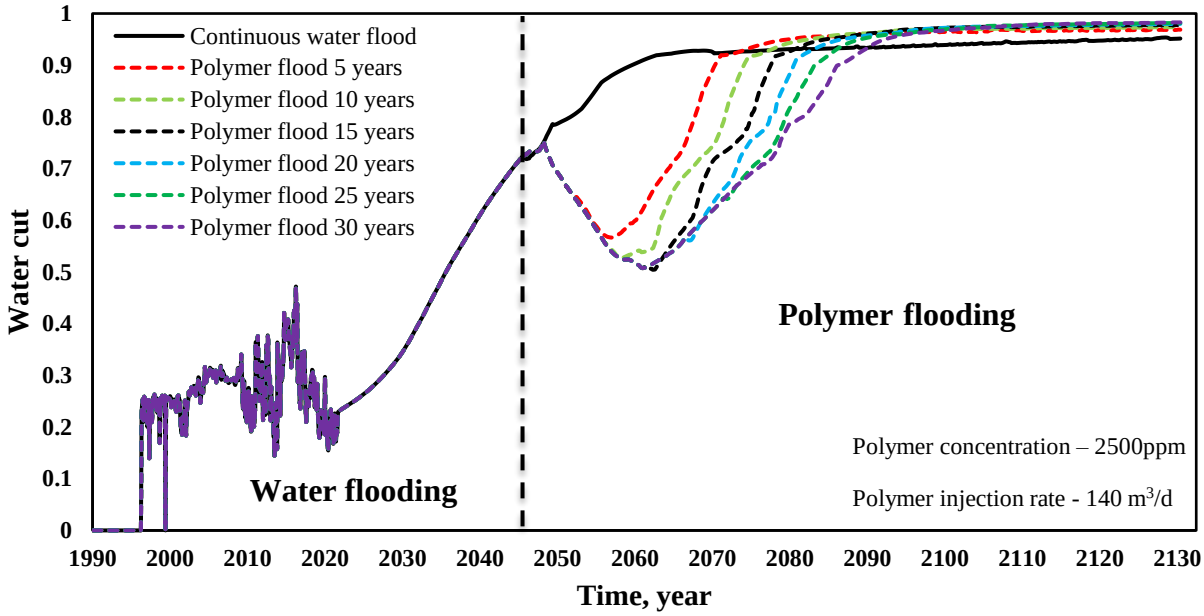

Figure 36. Water cut at different polymer flood durations.

Figure 37 depicts the impact of PF duration on the oil recovery factor. From the commencement of the PF in 2045, the initial ten subsequent years exhibit no discernible change in oil recovery. However, from the year 2055, a clear differentiation between the trajectories of continuous WF and PF are visible. Particularly, this divergence among PF scenarios manifests at distinct time points, specifically in 2070, 2073, 2076, 2080, 2083, and 2085, corresponding to PF durations of 5, 10, 15, 20, 25, and 30 years, respectively.

According to the graph, the oil recovery factors for PF durations of 5, 10, 15, 20, 25, and 30 years are determined to be 48%, 50%, 52%, 54%, 56%, and 57% respectively. These results underscore the substantial influence of PF duration on oil recovery, with longer durations correlating to higher oil recovery factors.

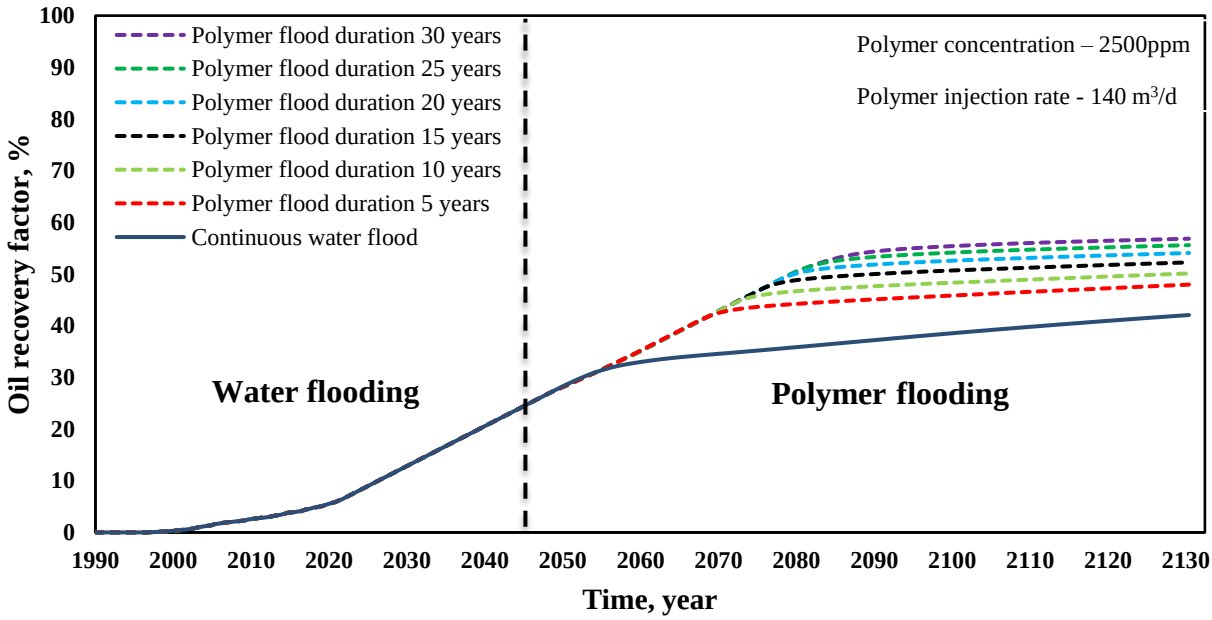

Figure 37. Oil recovery at different polymer flood duration.

Figure 38 illustrates the reservoir pressure values projected for the year 2070 across varying durations of PF operations, spanning from 5 to 30 years, alongside the subsequent changes in reservoir pressure a decade later. The outcomes derived from the numerical simulations depicted in Figure 38 unveil a positive correlation between prolonged PF durations and reservoir pressure, indicating that an extended duration of PF corresponds to higher reservoir pressure levels.

Noteworthy is the observation that the discrepancy in reservoir pressure is particularly pronounced between durations of 5, 10, 15, and 20 years, whereas exhibits minor variations between 25 and 30 years.

The findings imply that a PF duration of 20 years appears to offer an optimal balance between initial pressure augmentation and sustained pressure levels over time.

Figure 39 provides a comparative analysis of water cut levels in 2060 and 2070 across varying durations of PF. The examination of the data reveals a discernible trend: by the time, a more pronounced increase in water cut is observed for shorter durations of PF operations, while longer durations exhibit a comparatively smaller increase.

Regarding the determination of the optimal PF duration, a duration of 20 years emerges as the best solution. This assertion is substantiated by the finding that a 20-year PF

duration yields lower water cut levels in comparison to durations between 5 and 15 years and lower increase in water cut over time.

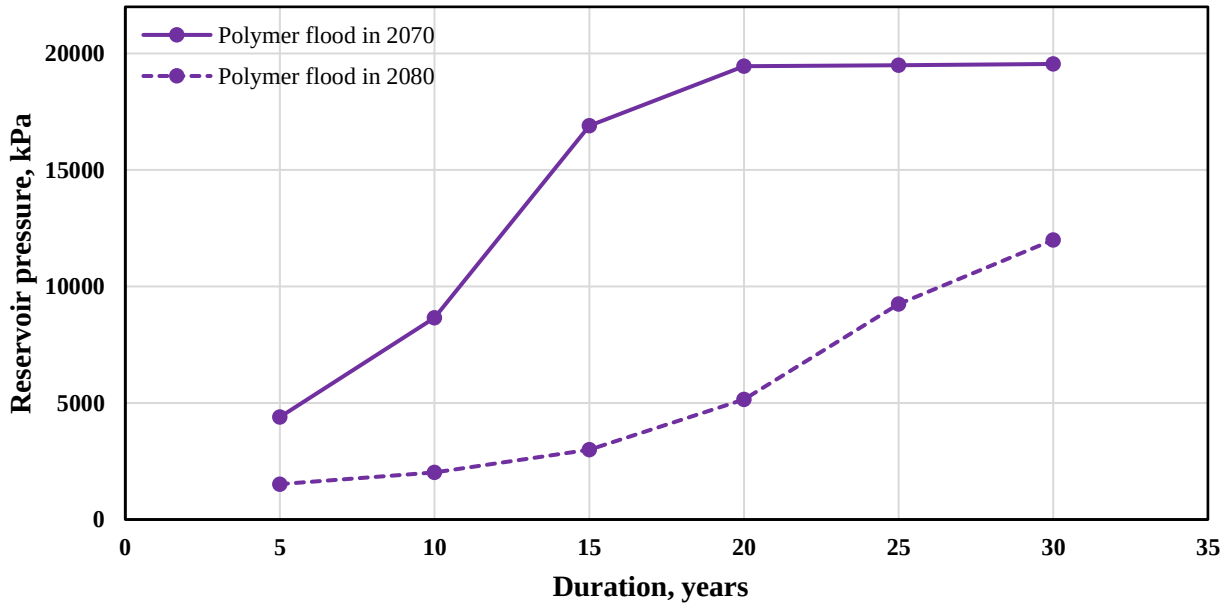

Figure 38. Reservoir pressure at different polymer flood durations in 2070 and 2080 at polymer concentration of 2500 ppm.

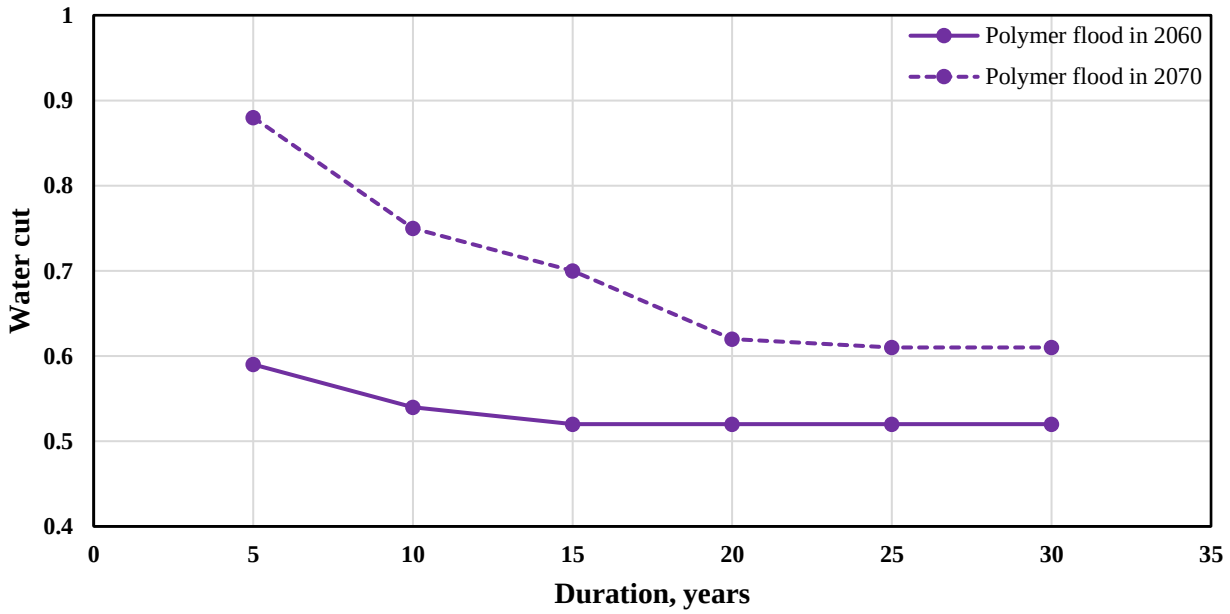

Figure 39. Water cut at different polymer flood durations in 2060 and 2070 at polymer concentration of 2500 ppm.

Figure 40 depicts the influence of PF duration on the oil recovery factor. Analysis of the graph reveals a positive correlation between PF duration and oil recovery factor. However, it is noteworthy that as the duration of PF increases, the discrepancy in oil recovery factor diminishes. Specifically, the disparity in oil recovery factor between 20 and 30 years stands at 2.75%. This suggests that PF durations of 25 and 30 years exhibit reduced effectiveness in enhancing oil recovery. Consequently, a PF duration of 20 years emerges as the most optimal for maximizing oil recovery.

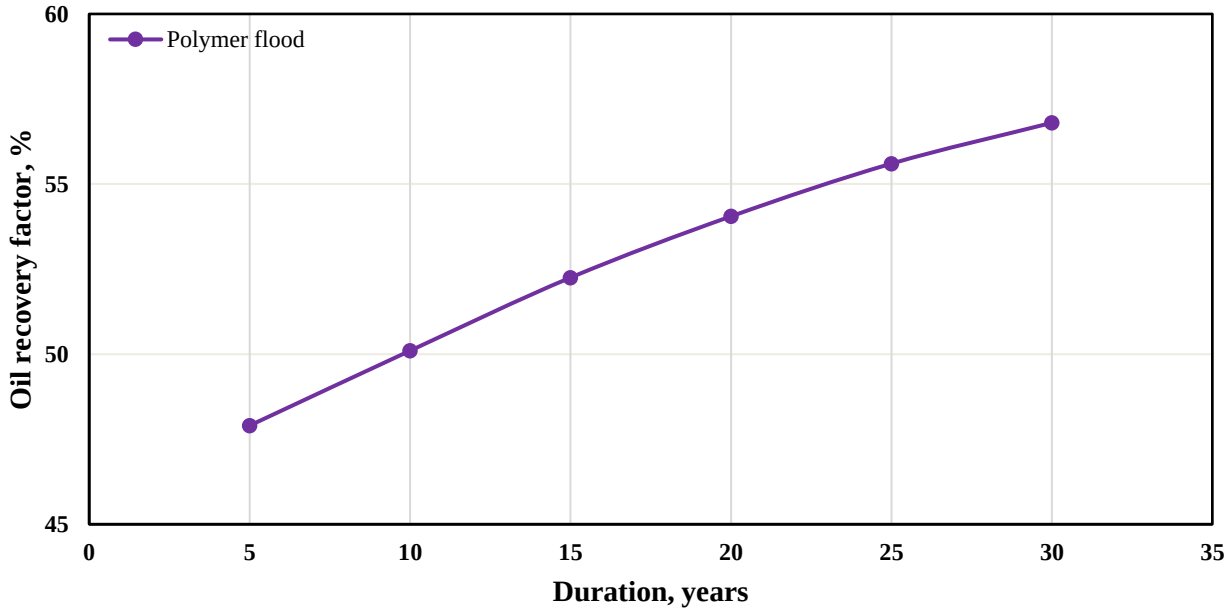

Figure 40. Oil recovery factor at different polymer flood durations at polymer concentration of 2500 ppm.

4.3 Polymer concentration sensitivity analysis

Figure 41 presents how the concentration of polymer impacts the pressure within the reservoir during PF scenarios, all conducted at a consistent injection rate of 140 m^3/d. Starting in 2045 with the initiation of PF, the reservoir pressure initially decreases and then increase reaching its peak values around 2070. Specifically, for polymer concentrations of 500, 1500, 2500, and 3500 ppm, the highest reservoir pressures are observed at 7250, 14150, 19500, and 22550 kPa, respectively.

After 2070, there is a noticeable decline in reservoir pressure following the peak values until 2090. After this point, the rate of decline slows down. By the end of the simulation in 2130, the final reservoir pressures are 2800, 5100, 6300, and 7000 kPa for

polymer concentrations of 500, 1500, 2500, and 3500 ppm, respectively. This information provides a clear picture of how reservoir pressure changes over time in response to different concentrations of polymer during PF scenarios.

Notably, the initial reduction in reservoir pressure at the onset of the PF is notably higher than the subsequent increase in pressure induced by polymer concentrations of 500 and 1500 ppm. Therefore, the concentration range of 2500 to 3500 ppm emerges as the optimal range.

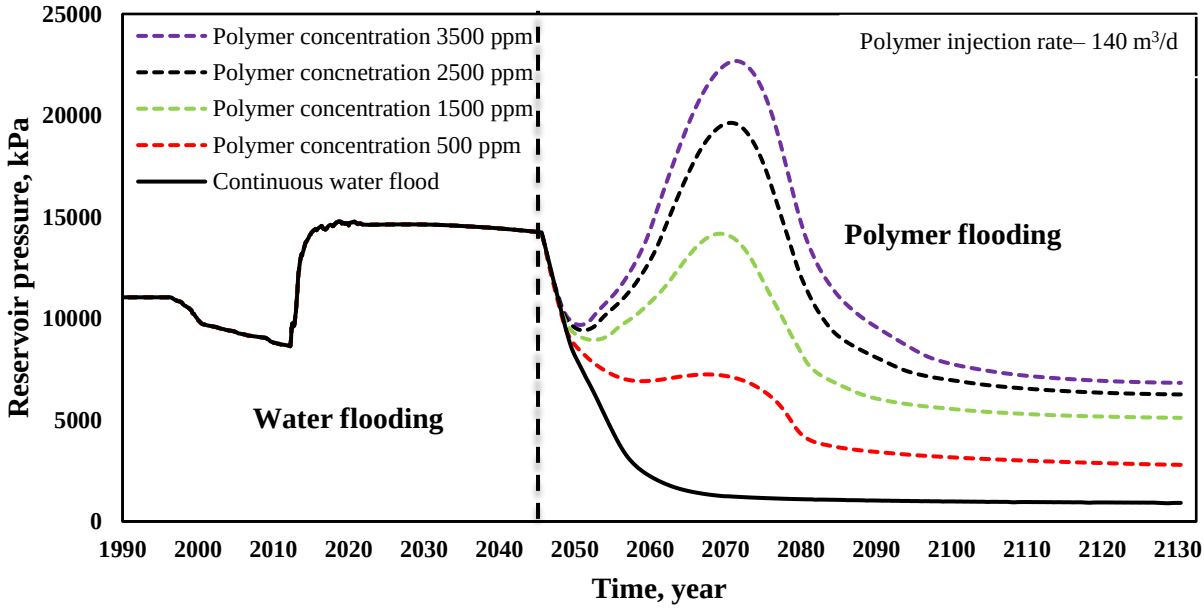

Figure 41. Reservoir pressure at different polymer concentrations.

Figure 42 illustrates how different concentrations of polymer affect water cut. According to the graph, the impact of polymer becomes noticeable 5 years after the start of the PF in 2045. The reduction in water cut begins in 2055, starting from value of 0.77 and reaching its lowest values in 2060, which are 0.66, 0.56, 0.50, and 0.49 for polymer concentrations of 500, 1500, 2500, and 3500 ppm, respectively.

The phenomenon of reaching the lowest water cut in the case of higher polymer concentrations can be attributed to effective residual oil saturation reduction. Higher polymer concentrations are associated with greater reductions in residual oil saturation. This means that a larger proportion of the remaining oil in the reservoir is mobilized and extracted during the subsequent WF. The reduction in residual oil saturation directly correlates with a decrease in water cut.

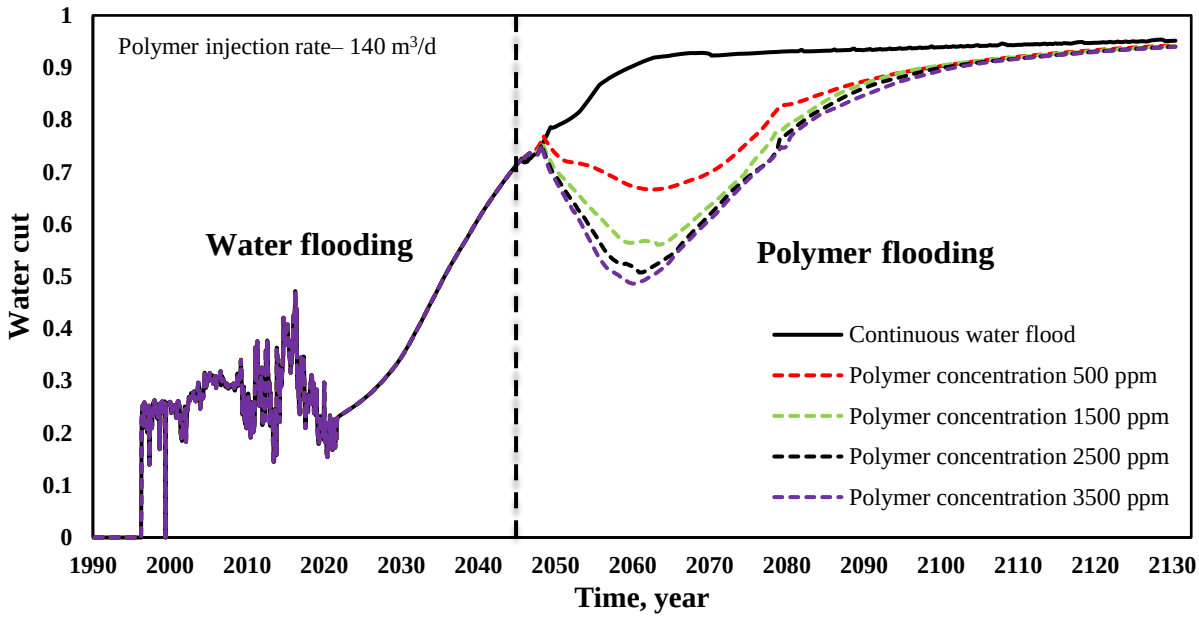

Figure 42. Water cut at different polymer concentrations.

Figure 43 shows how different concentrations of polymer impact the oil recovery factor. Even though PF starts in 2045, its effects on the oil recovery factor become noticeable after 2055. For polymer concentrations of 500, 1500, 2500, and 3500 ppm, the corresponding oil recovery factors are 57%, 60%, 62.3%, and 63%, respectively, by the end of numerical simulation. There is a significant difference of 15% in oil recovery factors between continuous water injection scenario and a polymer concentration of 500 ppm. However, the oil recovery difference reduces to 0.7% between polymer concentrations of 2500 and 3500 ppm.

The incremental difference in oil recovery between polymer concentrations of 2500 ppm and 3500 ppm of 0.7%, could be due to the optimal reservoir conditions. At 2500 ppm, the polymer concentration might already be within a range that optimally addresses the reservoir's specific characteristics, such as permeability and heterogeneity. Increasing the concentration to 3500 ppm doesn't yield significant additional benefits due to the reservoir conditions already being near their optimum for PF.

Figure 44 depicts the influence of varying polymer concentrations on reservoir pressure in 2070 and the subsequent changes in reservoir pressure a decade later in 2080. Examination of the graphs reveals a discernible positive correlation between polymer concentration and reservoir pressure. However, it is notable that the magnitude of increase in

reservoir pressure diminishes with increasing polymer concentration. Specifically, the increase in reservoir pressure decreases as 97%, 38%, and 15% for polymer concentrations of 500, 1500, 2500, and 3500 ppm, respectively.

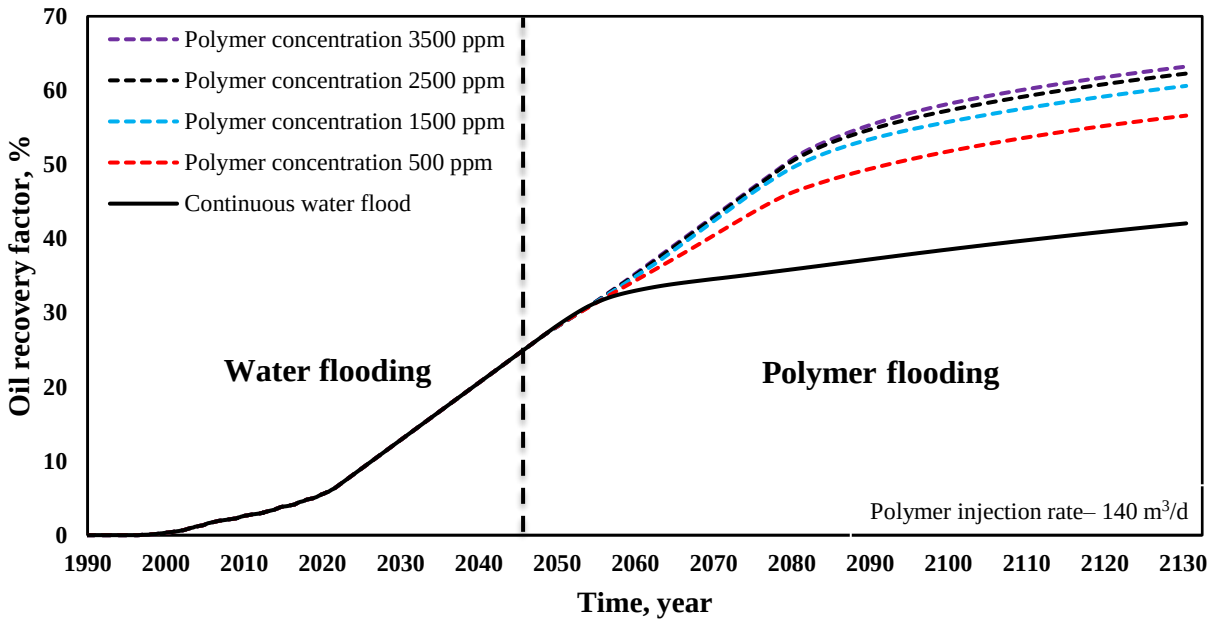

Figure 43. Oil recovery at different polymer concentrations.

Moreover, over the subsequent decade, reservoir pressure experiences a reduction, at different extend across different polymer concentrations. Notably, the reduction is relatively lower for a polymer concentration of 2500 ppm compared to others, standing at 33% as opposed to 38%, 39%, and 34% for concentrations of 500 ppm, 1500 ppm, and 3500 ppm, respectively.

Consequently, it is evident from the data that a polymer concentration of 2500 ppm emerges as the most optimal concentration. Because this concentration achieves a substantial increase in reservoir pressure while also demonstrating relatively lower reductions over time, thus maximizing reservoir pressure efficiently.

Figure 45 illustrates the impact of polymer concentration on water cut in 2060, as well as the subsequent changes in water cut observed over the following decade in 2070. Analysis of this graph reveals an inverse correlation between polymer concentration and water cut, wherein higher concentrations of polymer are associated with lower water cut and consequently reduced water production.

Over the specified period, the water cut increases, with varying percentages across different polymer concentrations. Specifically, the increase in water cut is observed to be 3%, 12%, 17%, and 25% for polymer concentrations of 500, 1500, 2500, and 3500 ppm, respectively.

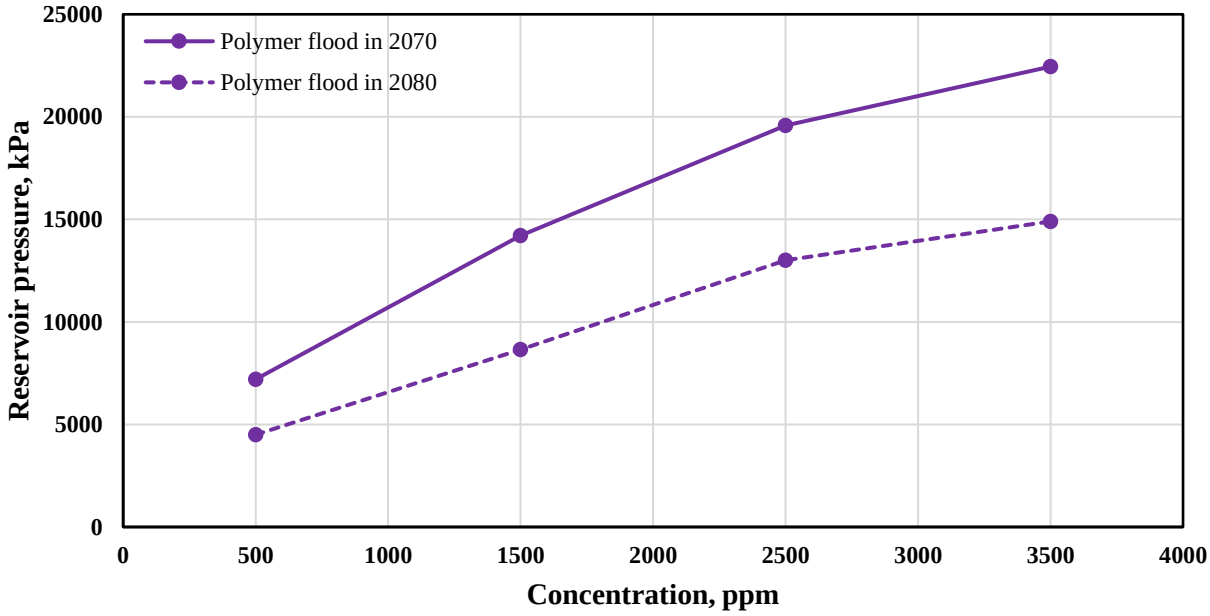

Figure 44. Reservoir pressure at different polymer concentrations in 2070 and 2080 at polymer injection rate of 140 m^3/d.

From this analysis, it is evident that a polymer concentration of 2500 ppm represents a balanced solution. This concentration exhibits relatively lower water cut compared to lower polymer concentrations, while also demonstrating a comparatively smaller increase in water cut in comparison to higher polymer concentration. Such findings suggest that a polymer concentration of 2500 ppm optimally balances the objective of minimizing water cut while avoiding excessive concentrations that lead to increases in water cut.

Upon comparison of the lowest water cut values attained, as illustrated in Figure 42, it is discerned that the disparity in water cut between the minimum values achieved, specifically 0.5 obtained with a polymer concentration of 2500 ppm and 0.49 attained with a concentration of 3500 ppm, is relatively insignificant. Additionally, the reduction in water cut attributed to an increase in concentration to 1000 ppm amounts to merely 2%. Consequently, based on these considerations, a polymer concentration of 2500 ppm represents the optimal choice.

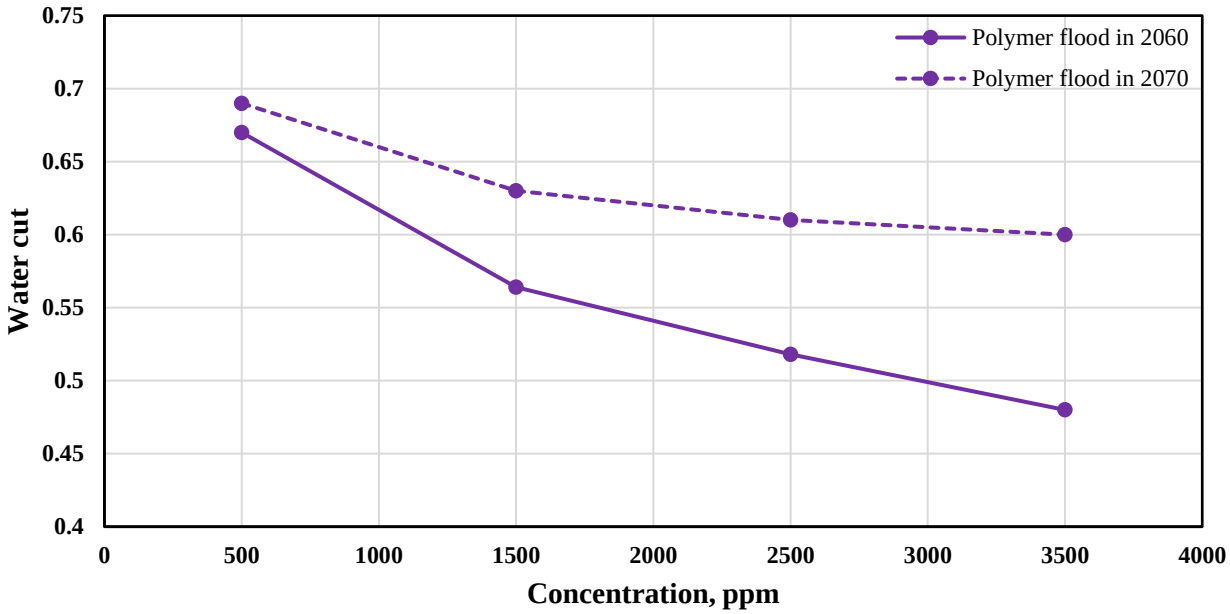

Figure 45. Water cut at different polymer concentrations in 2060 and 2070 at polymer injection rate of 140 m^3/d.

Figure 46 delineates the impact of varying polymer concentrations on the oil recovery factor. Analysis of the graph reveals a discernible positive correlation between polymer concentration and oil recovery. However, it becomes evident that as the concentration increases, the effectiveness of the polymer in enhancing oil recovery diminishes. Specifically, the increase in oil recovery factor diminishes as the concentration rises from 500 to 3500 ppm. Notably, escalating the concentration from 500 to 1500 ppm yields a 6% increase, while further increasing it from 1500 to 2500 ppm results in a 4% increase. However, the subsequent increase from 2500 ppm to 3500 ppm only yields a marginal 1% increase.

Considering the broader context of reservoir pressure maintenance, achieving higher reservoir pressure than the initial reduction and minimizing reductions in reservoir pressure over time are paramount. In this regard, a polymer concentration of 2500 ppm emerges as the most optimal choice. Additionally, in the context of water cut reduction, the polymer concentration of 2500 ppm demonstrates the low water cut values and the least increase in water cut over time.

Moreover, when prioritizing the most crucial factor of oil recovery, the effective polymer concentration is determined to be 2500 ppm. This conclusion arises from the

observation that increasing the concentration to 3500 ppm yields only a marginal 1% increase in oil recovery, which may not be economically viable.

Taking all these considerations into account, the polymer concentration of 2500 ppm emerges as the most optimal concentration for maximizing oil recovery while considering economic feasibility.

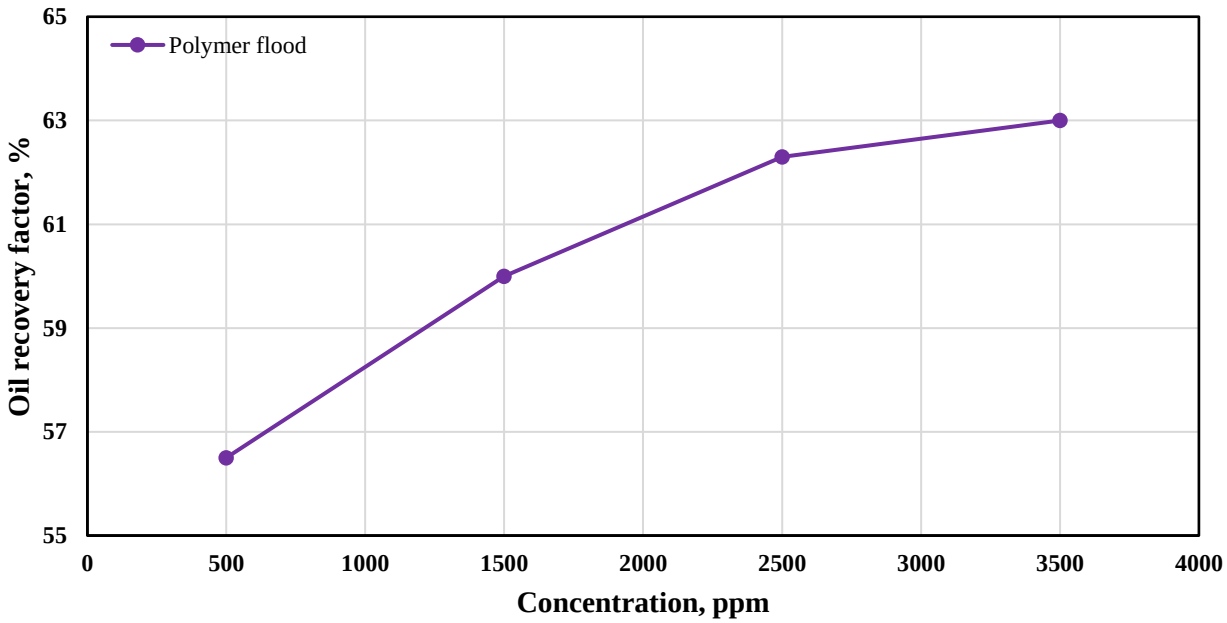

Figure 46. Oil recovery factor at different polymer flood durations at polymer concentration of 2500 ppm.

4.4 Hot polymer flooding

This section undertakes an evaluation and comparison of the efficacy of oil recovery through both hot water flood (HWF) and HPF techniques. The commencement of the evaluation of hot water and HPF techniques is instigated by the oil characteristics prevalent in the Uzen field. Notably, the oil within this reservoir exhibits high viscosity and contains substantial quantities of paraffinic and asphaltene compounds. These properties underscore the challenges inherent in extracting oil from the Uzen field and motivate the exploration of new EOR methods. Considering the prior utilization of HWF in Uzen field, now we decided to evaluate the hybrid application of PF and thermal EOR such as HWF. The chosen methods were selected based on their operational feasibility within the prevailing technological framework.

To accomplish this assessment, data derived from laboratory core flood experiments conducted by our team served as the basis for constructing a core flooding model within a simulator. Subsequent numerical simulations were conducted to validate the effectiveness of HPF at the core scale.

In the laboratory core flood experiment designed to evaluate the efficacy of HPF, the temperature of the polymer solution was incrementally raised from 63°C to 85°C. This elevation in temperature was undertaken with the objective of reducing the viscosity of the oil, thereby augmenting both the recovery efficiency and the mobility of the oil phase.

The effectiveness of HPF can be inferred from the observed increase in oil recovery during the implementation of the core scale HPF, as demonstrated in Figure 47. Initially, during the WF phase, the oil recovery stood at 43%, indicating the limited efficacy of the conventional WF method alone. However, upon the introduction of HPF, a substantial improvement in oil recovery is observed, with the recovery rate soaring to 95%. This significant enhancement underscores the potency of HPF in mobilizing and displacing additional oil from the reservoir. Furthermore, even during the subsequent post-flush phase, where the additional oil production is relatively minor, the overall oil recovery remains impressively high at 96%.

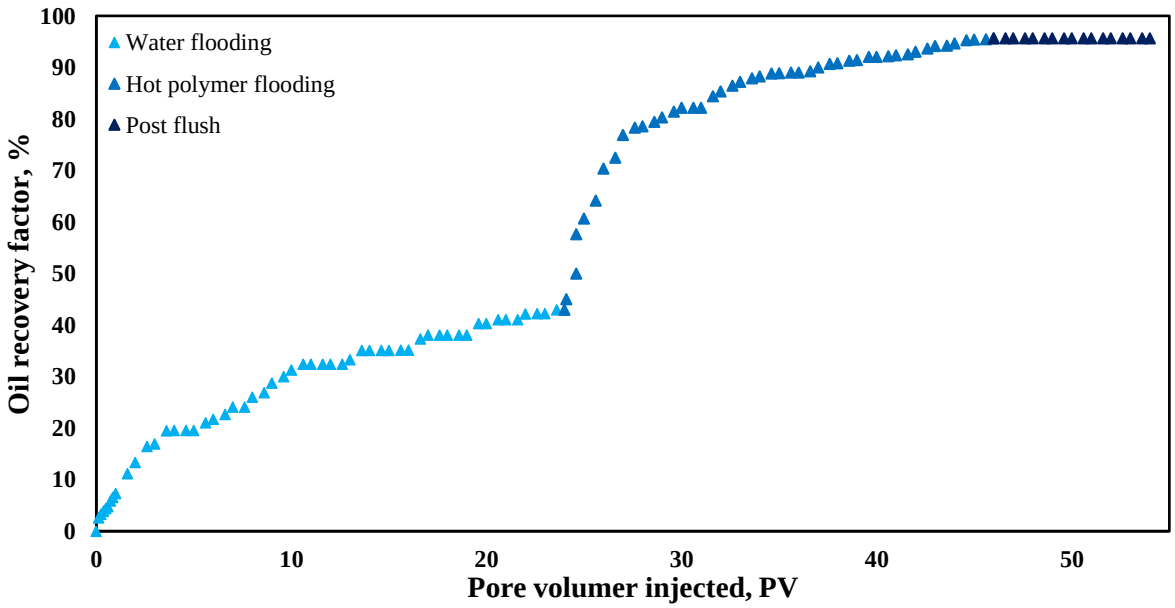

Figure 47. Hot polymer flood oil displacement test result in Uzen fields core.

The subsequent phase within the validation process of the core scale model entails the incorporation of laboratory displacement test outcomes into core model and subsequent numerical simulations. Illustrated in Figure 48 is a comparative analysis between the findings derived from laboratory core flood experiments and those generated through numerical simulations. Within this graphical representation, the laboratory data points are distinctly depicted, while the numerical simulation core flood results are represented by continuous solid lines. This comparison serves to elucidate the concordance or divergence between experimental observations and computational predictions, thereby facilitating a comprehensive assessment of the model's accuracy and predictive capabilities.

According to the graph, during the WF phase, a notable alignment between laboratory data and simulation data is observed, with both datasets mostly coinciding. By the conclusion of this phase, they exhibit similar levels of recovery. Throughout the HPF phase, there is a significant agreement between laboratory data and simulation data, indicating the accuracy of the model. Despite minor discrepancies towards the conclusion of this phase, the overall alignment remains evident. During the post-flush phase, there is a consistent trend observed in both laboratory data and simulation lines, with no discernible changes in trend for either dataset.

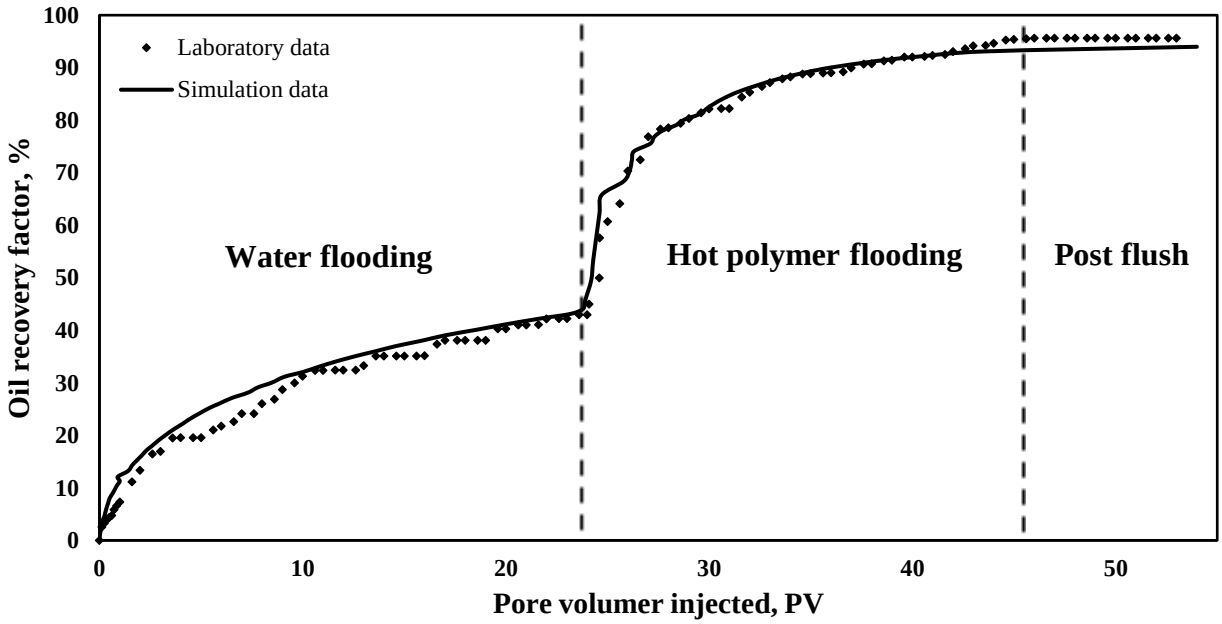

Figure 48. Oil recovery factor of laboratory core flood and simulation core flood of hot polymer.

The calculation of the Average Error, as determined by Eq. 2, yields a value of 4%. This low average error value serves as an indicator of the accuracy and reliability of the simulation model. Such a result suggests that the simulation model effectively captures and reproduces the behavior of the system under investigation, enhancing confidence in its validity and utility for further analysis and interpretation.

Having successfully validated the core scale model to simulate HPF, the next step is to extend the analysis to the field scale. By conducting field-scale simulations, we aim to assess whether the implementation of the hybrid method offers tangible benefits in terms of oil recovery.

The findings depicted in Figure 49 highlight interesting insights into the effectiveness of different flooding techniques in enhancing oil recovery. One notable observation is the marginal discrepancy of 1.7% in oil recovery between water and HWF methods. This minor difference suggests that while HWF may offer a slight advantage over conventional WF, its impact on overall oil recovery is relatively modest.

On the other hand, the absence of a discernible difference in oil recovery between polymer and HPF approaches is apparent. Increasing polymer temperature is expected to decrease the viscosity of the oil, increasing its mobility, thereby displacing more oil from the reservoir. However, the similarity in oil recovery between polymer and HPF methods raises questions about the added benefits of incorporating thermal energy into the process.

Several factors could contribute to these observations. Firstly, it’s possible that the reservoir conditions, such as temperature and permeability, may not significantly favor the utilization of thermal energy in enhancing oil recovery. Additionally, the effectiveness of PF may already be optimized to a point where the introduction of thermal energy provides marginal additional benefits.

Figure 50 presents the water cut profiles obtained from numerical simulations corresponding to different flooding techniques, including WF, PF, HWF, and HPF. Analysis of the data reveals several noteworthy observations. When comparing the water cuts between WF and HWF, a minor difference is observed, with HWF exhibiting slightly lower water cut values throughout the simulation period. Conversely, the comparison between PF and HPF indicates no discernible difference in water cut values over the entire simulation duration.

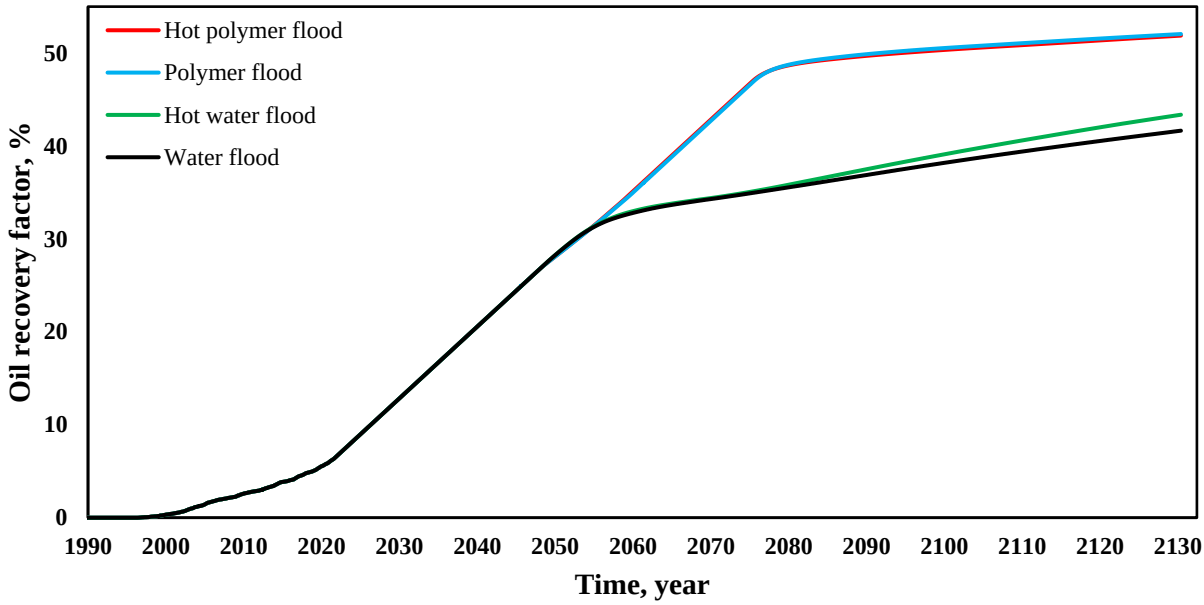

Figure 49. Oil recovery factors of water flood, polymer flood, hot water flood, and hot polymer flood derived from numerical simulation.

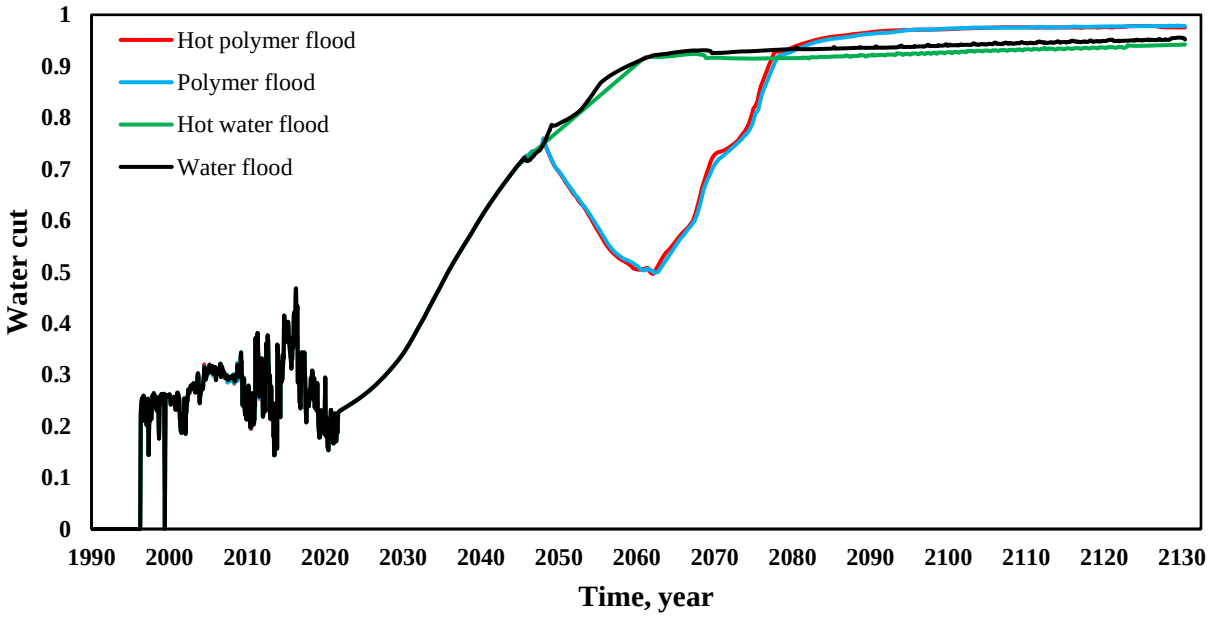

Figure 50. Water cut of water flood, polymer flood, hot water flood, and hot polymer flood derived from numerical simulation.

Figure 51 displays the reservoir pressure profiles obtained from numerical simulations corresponding to different flooding techniques, including WF, PF, HWF, and HPF. Upon examination of the graph, several observations can be made regarding the behavior of reservoir pressure across these techniques.

Firstly, when comparing WF and HWF, a minor difference in reservoir pressure is evident, particularly between the years 2060 and 2070. Specifically, the reservoir pressure appears to be slightly lower in the case of HWF during this time period. This discrepancy may be attributed to the thermal effects introduced by the HWF process, which could alter the fluid properties and reservoir conditions, leading to variations in pressure dynamics.

Conversely, when comparing PF and HPF, the reservoir pressure profiles exhibit similarity throughout the simulation period. This consistency suggests that the incorporation of thermal energy in the flooding process, as observed in HPF, does not significantly impact reservoir pressure dynamics when compared to conventional PF.

Overall, these findings underscore the nuanced interplay between different flooding techniques and their effects on reservoir pressure. While HWF may lead to minor variations in pressure compared to conventional WF, the addition of thermal energy in PF does not seem to significantly influence reservoir pressure behavior.

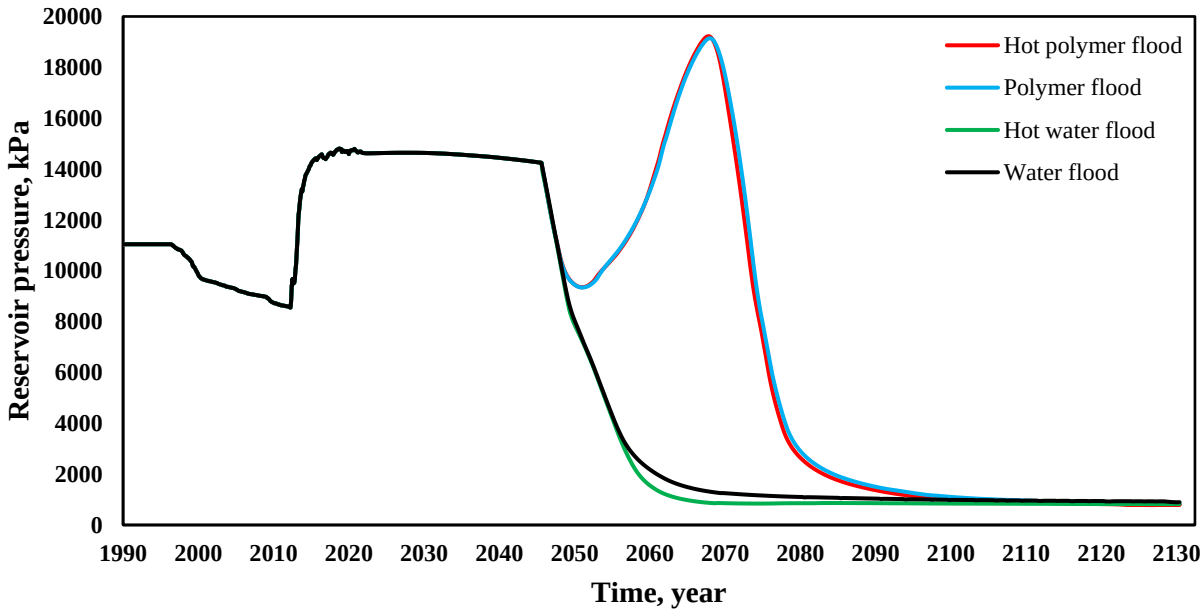

Figure 51. Reservoir pressure of water flood, polymer flood, hot water flood, and hot polymer flood derived from numerical simulation.

5 CONCLUSIONS AND RECOMMENDATIONS

The efficiency of polymer flooding as an EOR approach for the Uzen field in Kazakhstan has been carefully assessed using reservoir-scale simulation model. The study examined the performance of PF using parameters such as injection rate, flood duration, and polymer concentration. Moreover, the investigation extended to explore the potential enhancements achievable through the introduction of thermal energy, specifically via hot water and HPF, and compared its efficacy with conventional WF and PF.

The findings of the study underscored the significant impact of PF in augmenting reservoir pressure, mitigating water cut, and enhancing oil recovery over time. Through numerical simulations, it became evident that PF, when optimized across parameters such as injection rate and concentration, could lead to substantial improvements in oil recovery factors. However, when considering the introduction of thermal energy through hot water and HPF, the results were less promising.

The results of the comprehensive analysis indicate that the polymer concentration of 2500 parts per million (ppm) emerges as the most optimal concentration, PF duration of 20 years represents the most optimal temporal framework for realizing the desired objectives of EOR, and polymer injection rate of 140 m^3/d is the most optimal rate for achieving desired reservoir performance metrics.

The comparison of HPF did not exhibit better performance compared to conventional PF. Despite minor variations in reservoir pressure, HPF demonstrated comparable efficacy in mitigating water production and enhancing oil recovery, suggesting no additional benefits over traditional PF methods. The analysis of numerical simulation results revealed that the integration of thermal energy mostly affected mobility of oil. And the recovery results are the same because viscosity reduction effect due to temperature increase is negligible.

Overall, while PF remains a promising EOR strategy for maximizing oil recovery, the study suggests that the introduction of thermal energy through HPF cannot provide benefits in terms of enhanced performance.

Recommendations:

1. Initiation of Pilot Test program in Sector 14 of Uzen Field. Based on the findings of this thesis, it is recommended to commence a pilot test program in Sector 14 of the Uzen field using defined optimal operational parameters. This pilot program will allow for the practical validation of the identified optimal operational parameters, including injection rate, polymer concentration, and flood duration. By implementing a pilot test in a specific sector, it enables focused observation and data collection, thereby providing valuable insights into the performance of polymer flooding in a bigger field condition.
2. Studies on parameters related to Pilot Test, particularly Polymer Injectivity: Concurrently with the pilot test program, it is recommended to conduct additional studies focusing on polymer injectivity. Moreover, exploring innovative techniques or additives to optimize injectivity while maintaining reservoir integrity. These additional studies will contribute to refining injection strategies, mitigating operational risks, and ultimately maximizing the effectiveness of polymer flooding in the Uzen field.

6 REFERENCES

Abidin, A. Z., Puspasari, T., & Nugroho, W. (2012). Polymers for enhanced oil recovery technology. Procedia Chemistry, 4, 11–16. https://doi.org/10.1016/j.proche.2012.06.002

Ahmed, T., & Meehan, D. N. (2012). Introduction to enhanced oil recovery. In Elsevier eBooks. https://doi.org/10.1016/b978-0-12-385548-0.00006-3

Akın, S. (2005). Polymer/oil relative permeabilities in carbonate reservoirs. https://open.metu.edu.tr/handle/11511/15048

Alamooti, A. M., & Malekabadi, F. K. (2018). An introduction to enhanced oil recovery. In Elsevier eBooks (pp. 1–40). https://doi.org/10.1016/b978-0-12-813027-8.00001-1

Al-Hajri, S., Mahmood, S. M., Abdulelah, H., & Akbari, S. (2018). An overview on polymer retention in porous media. Energies, 11(10), 2751. https://doi.org/10.3390/en11102751

Ameli, F., Moghadam, S., & Shahmarvand, S. (2022). Polymer flooding. In Elsevier eBooks (pp. 33–94). https://doi.org/10.1016/b978-0-12-821931-7.00003-1

Aziz, K., & Settary, A. (1979). Petroleum reservoir simulation. In Elsevier eBooks. https://doi.org/10.1016/c2018-0-04535-1

Bigdeli, A., & Delshad, M. (2023). Strategy for Optimum Chemical Enhanced Oil Recovery Field Operation. *Journal of Resource Recovery*, *1*(1), 0. https://doi.org/10.52547/jrr.2208.1001

Bondor, P. L. (2011). EOR-the time is now: its contribution of world energy supply. Society of Petroleum Engineers. https://www.spe.org/dl/docs/2011/Bondor.pdf

De Sousa Ferreira, V. H., & Moreno, R. B. Z. L. (2018). Workflow for Oil Recovery Design by Polymer Flooding. ResearchGate. https://doi.org/10.1115/omae2018-78359

Delamaide, E. (2014). Polymer flooding of heavy oil – From Screening to Full-Field extension. Semantic Scholar. https://doi.org/10.2118/171105-ms

Dergano, F. (2021, December 25). An overview of recent advances and prospects enhanced oil recovery chemistry. Medium. https://raccomandino.medium.com/an-overview-of-recent-advances-and-prospects-enhanced-oil-recovery-chemistry-8a781efd08db

Fernandes, B. R. B., Pope, G. A., Sepehrnoori, K., & Lashgari, H. (2019). Advances in Chemical EOR Technologies: New Development in Field-Scale Chemical Flooding Simulation. OnePetro. https://doi.org/10.4043/29287-ms

Ferreira, V. H., & Moreno, R. B. Z. L. (2019). Polymer apparent viscosity dependence on inaccessible pore volume: laboratory and field studies of its influence on enhanced oil recovery. Brazilian Journal of Petroleum and Gas, 12(4), 205–218. https://doi.org/10.5419/bjpg2018-0019

Field Evaluation Report. Uzen Field (2010). Former Soviet Union. https://www.twirpx.com/file/1723772/

Gaillard, N., Giovannetti, B., Favero, C., Caritey, J., Dupuis, G., & Zaitoun, A. (2014). New water soluble Anionic NVP acrylamide terpolymers for use in harsh EOR conditions. All Days. https://doi.org/10.2118/169108-ms

Gaillard, N., Giovannetti, B., Leblanc, T., Thomas, A., Braun, O., & Favero, C. (2015). Selection of Customized Polymers to Enhance Oil Recovery from High Temperature Reservoirs. OnePetro. https://doi.org/10.2118/177073-ms

Gbadamosi, A., Junin, R., Manan, M. A., & Yusuff, A. S. (2019). An overview of chemical enhanced oil recovery: recent advances and prospects. International Nano Letters, 9(3), 171–202. https://doi.org/10.1007/s40089-019-0272-8

Gharbi, R., Alajmi, A. F., & Algharaib, M. (2012). The potential of a Surfactant/Polymer flood in a Middle Eastern reservoir. Energies, 5(1), 58–70. https://doi.org/10.3390/en5010058

Green. (2018). File Download Enhanced oil recovery PDF by Green, Don W.; Willhite, G. Paul. https://pdfdrive.to/filedownload/enhanced-oil-recovery-0

Han, B., Cheng, W., & Nian, Y. (2017). Experimental study on effect of temperature field on recovery of reservoir using hot water flooding. Energy Procedia, 142, 3759–3765. https://doi.org/10.1016/j.egypro.2017.12.273

Ibiam, E., Geiger, S., Almaqbali, A. S. H., Demyanov, V., & Arnold, D. (2018). Numerical Simulation of Polymer Flooding in a Heterogeneous Reservoir: Constarained versus Unconstrained Optimization. All Days. https://doi.org/10.2118/193400-ms

Imanbayev, B. A., Kushekov, R., Sagyndikov, M., & Shyrakbayev, D. (2022). Feasibility Study of a Polymer Flood for the Uzen Brownfield Conditions. ResearchGate. https://doi.org/10.2118/212091-ms

Ivanova, A. A., & Cheremisin, A. (2022). Chemical enhanced oil recovery: Where do we stand? Recent advances and applications. In IntechOpen eBooks. https://doi.org/10.5772/intechopen.106732

Jensen, T. B., Harpole, K., & Østhus, A. (2000). EOR screening for 66kofisk. All Days. https://doi.org/10.2118/65124-ms

JPT.SPE.ORG. (2014, December 31). Pelican Lake: First successful application of polymer flooding in a Heavy-Oil reservoir. https://jpt.spe.org/pelican-lake-first-successful-application-polymer-flooding-heavy-oil-reservoir

Kudaivergenov, S., Gusenov, I., Zhappasbayev, B., & Shakhvorostov, A. (2015). Application of polymer flooding technology for enhanced oil recovery. Chemical Bulletin of Kazakh National University, 4, 74–80. https://doi.org/10.15328/cb644

Manrique, E., Thomas, C., Ravikiran, R., Kamouei, M. I., Lantz, M., Romero, J. L., & Alvarado, V. (2010). EOR: Current status and opportunities. All Days. https://doi.org/10.2118/130113-ms

Maratbekkyzy, L., Shakeel, M., Pourafshary, P., & Musharova, D. (2023). Enhancing Polymer Flooding Efficiency in a Sandstone Oilfield in Kazakhstan through Silica Nanoparticle-Based Control of Polymer Adsorption. Energy & Fuels, 37(19), 14727–14740. https://doi.org/10.1021/acs.energyfuels.3c02579

Mukherjee, S., & Suss, M. P. (2014). Performance Evaluation and Design Aspects of Polymer and Hot Water Co-Injection in an Offshore Heavy Oil Field under Challenging Conditions. All Days. https://doi.org/10.2118/169711-ms

Offshore Technology Journal. (2021, November 24). Oil & gas field profile: Uzen Conventional Oil Field, Kazakhstan. https://www.offshore-technology.com/data-insights/oil-gas-field-profile-uzen-conventional-oil-field-kazakhstan/?cf-view&cf-closed

PetroWiki. (2015, June 9). Polymer waterflooding design and implementation – PetroWiki. https://petrowiki.spe.org/Polymer_waterflooding_design_and_implementation

Ragab, A., & Mansour, E. (2021). Enhanced oil recovery: chemical flooding. In IntechOpen eBooks. https://doi.org/10.5772/intechopen.90335

Rego, F. B., Botechia, V. E., & Schiozer, D. J. (2017). Heavy oil recovery by polymer flooding and hot water injection using numerical simulation. Journal of Petroleum Science & Engineering, 153, 187–196. https://doi.org/10.1016/j.petrol.2017.03.033

Safronov, S.V., Stepanov, G.S., Shaevskyi, O.Yu, Kiinov, L.K., Dmitrieev, L.P., and Batirbaiev, M.D., 1993, New methods of oilfield development for complex oilfields: EAPG Improved Oil Recovery Europe Symposium, v. 1, p. 117-128.

Sanches, K. K. M., & Moreno, R. B. Z. L. (2015). Simulation of Polymer Flooding considering Size Model Increase and Economical Evaluation. *Anais Do . . . Congresso Ibero-Latino-Americano De Métodos Computacionais Em Engenharia.* https://doi.org/10.20906/cps/cilamce2015-0709

Sarsenora, A. (2020). SIMULATION STUDY OF IMPROVING OIL RECOVERY BY POLYMER FLOODING IN a KAZAKHSTANI FIELD [Dataset]. https://nur.nu.edu.kz/handle/123456789/4794?show=full

Slater, G., & Ali, S. F. (1970). Simulation of oil recovery by polymer flooding. Journal of Canadian Petroleum Technology, 9(04). https://doi.org/10.2118/70-04-05

Sparke, S. J., Kislyakov, P. Y., & Amirtayev, M. (2005). Significant Production Enhancement in Uzen Field, Kazakhstan through Surface and Subsurface Optimization. All Days. https://doi.org/10.2118/94360-ms

STARS User Guide. (n.d.). Academia.edu. https://www.academia.edu/32418562/STARS_USER_GUIDE

Suleimanov, B. A., & Veliyev, E. F. (2017). Novel polymeric nanogel as diversion agent for enhanced oil recovery. Petroleum Science and Technology, 35(4), 319–326. https://doi.org/10.1080/10916466.2016.1258417

Sun, X., Zhang, Q., Teng, Z., Wang, X., & Cai, J. (2022). Numerical simulation of polymer flooding in water flooding reservoir. E3S Web of Conferences, 352, 01077. https://doi.org/10.1051/e3sconf/202235201077

Thomas, A. (2016). Polymer flooding. In InTech eBooks. https://doi.org/10.5772/64623

Thomas, A. (2019). Essentials of polymer flooding technique. https://doi.org/10.1002/9781119537632

Trujillo, M., Mercado, D., Maya, G., Castro, R. H., Soto, C. ., Quintero, H., Gómez, V. T., & Sandoval, J. (2010). Selection methodology for screening evaluation of Enhanced-Oil-Recovery Methods. All Days. https://doi.org/10.2118/139222-ms

Vishnyakov, V., Suleimanov, B. A., Salmanov, A., & Zeynalov, E. (2020). Oil recovery stages and methods. In Elsevier eBooks (pp. 53–63). https://doi.org/10.1016/b978-0-12-817632-0.00007-4

Wang, D. (2013). Polymer flooding practice in Daqing. In Elsevier eBooks (pp. 83–116). https://doi.org/10.1016/b978-0-12-386545-8.00004-x

Wang, W., Liu, Y., & Gu, Y. (2003). Application of a novel polymer system in chemical Enhanced oil recovery (EOR). Colloid and Polymer Science, 281(11), 1046–1054. https://doi.org/10.1007/s00396-003-0873-6

Xue, L., Liu, P., & Zhang, Y. (2023). Status and prospect of improved oil recovery technology of high water cut reservoirs. Water, 15(7), 1342. https://doi.org/10.3390/w15071342

Yerniyazov, D., Yesmukhambet, M., Kenes, R., Bukayev, A., Shakeel, M., Pourafshary, P., & Musharova, D. (2023). Polymer Screening for Efficient Water Cut Reduction in a Sandstone Oilfield in Kazakhstan. *Polymers*, *15*(8), 1969. https://doi.org/10.3390/polym15081969

Zeito, G. (1968). Three dimensional numerical simulation of polymer flooding in homogeneous and heterogeneous systems. All Days. https://doi.org/10.2118/2186-ms

7 APPENDICES

APPENDIX A

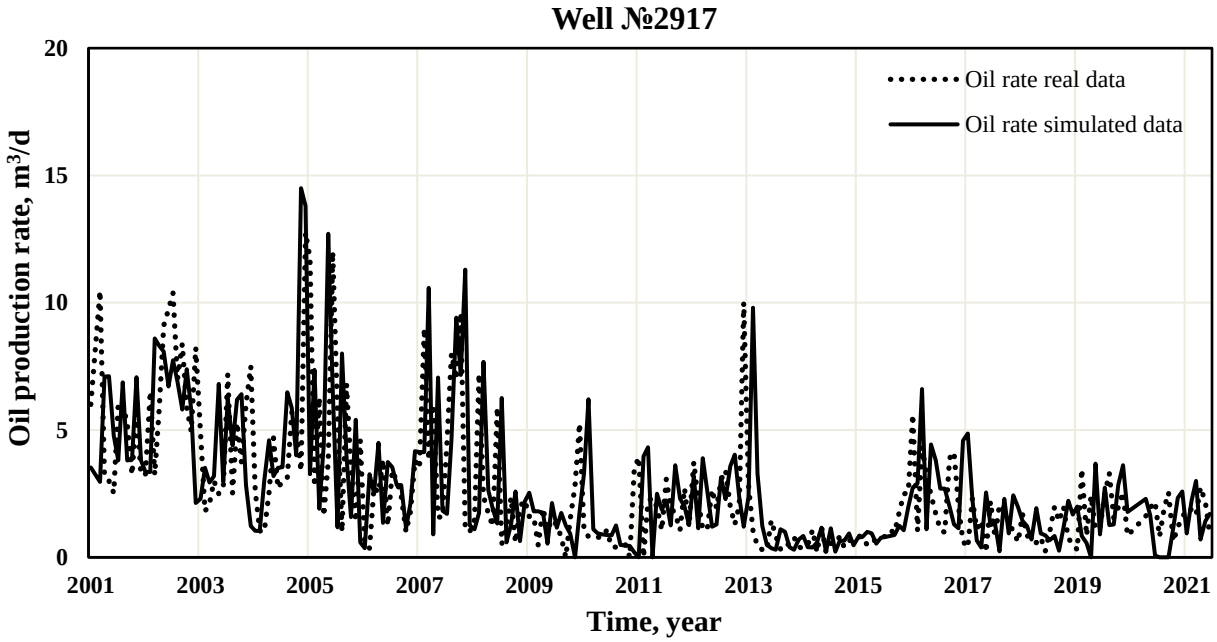

Figure 52. Oil production rate of well №2917 derived from numerical simulation results and real field data.

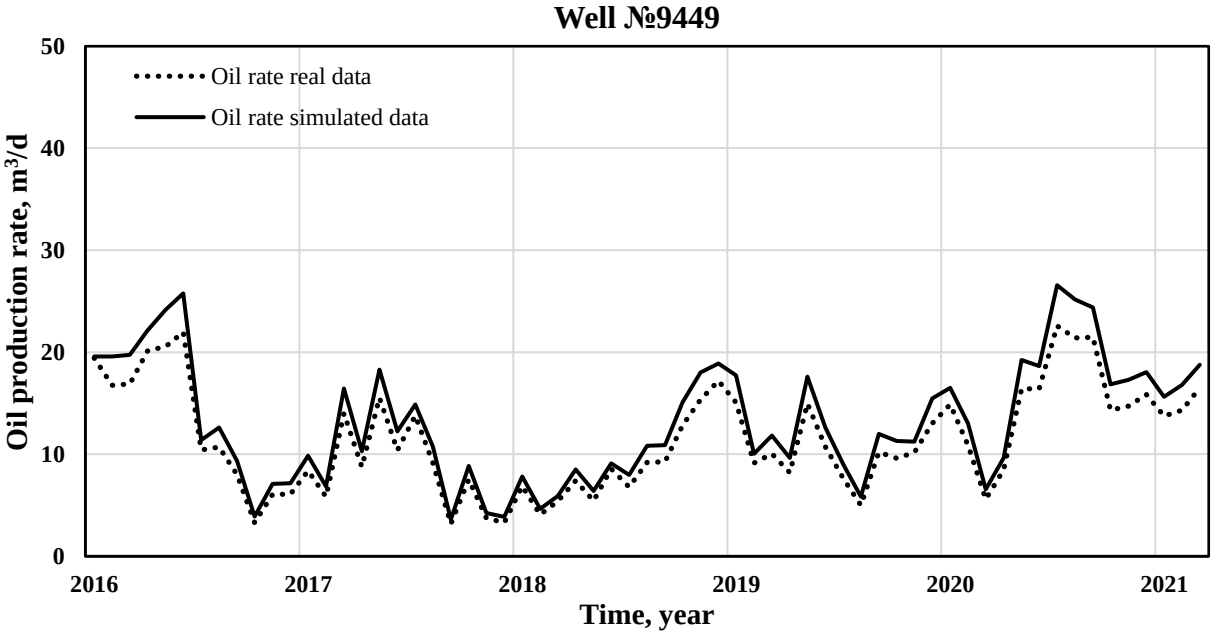

Figure 53. Oil production rate of well №9449 derived from numerical simulation results and real field data.

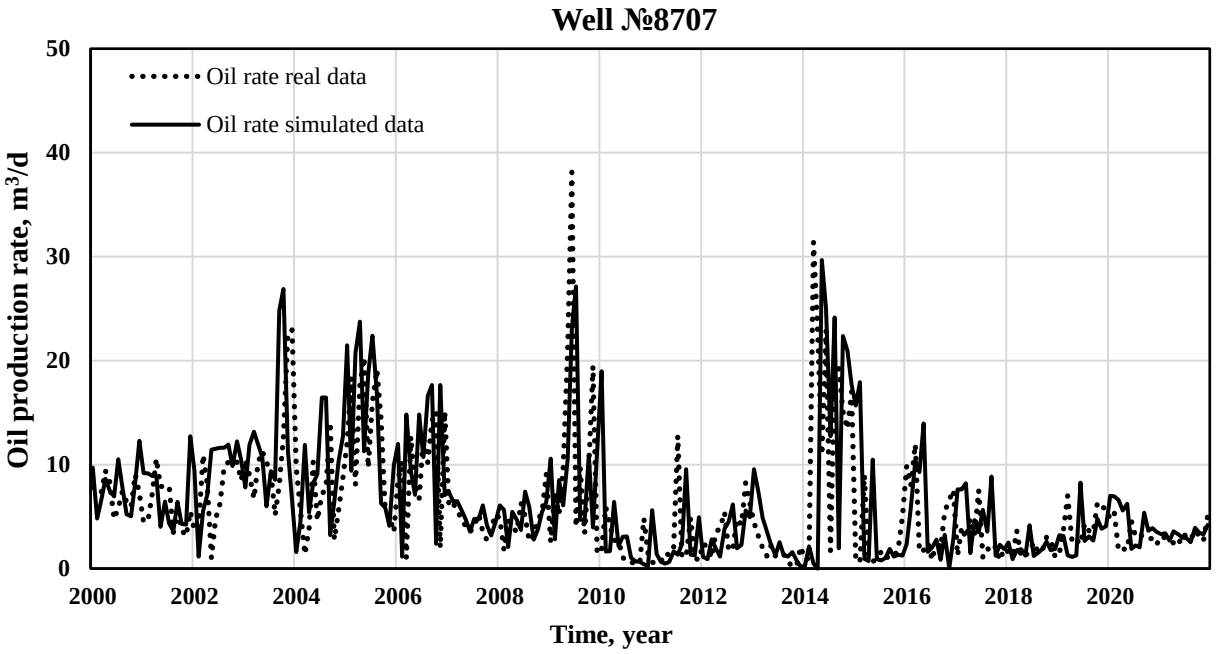

Figure 54. Oil production rate of well №8707 derived from numerical simulation results and real field data.

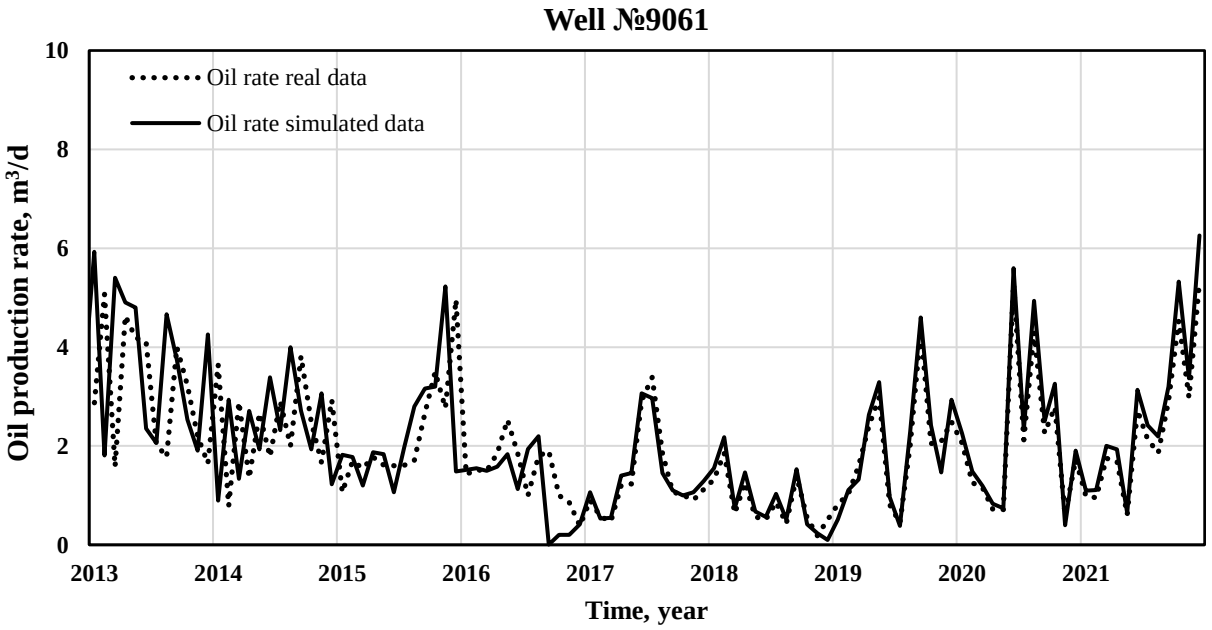

Figure 55. Oil production rate of well №9061 derived from numerical simulation results and real field data.

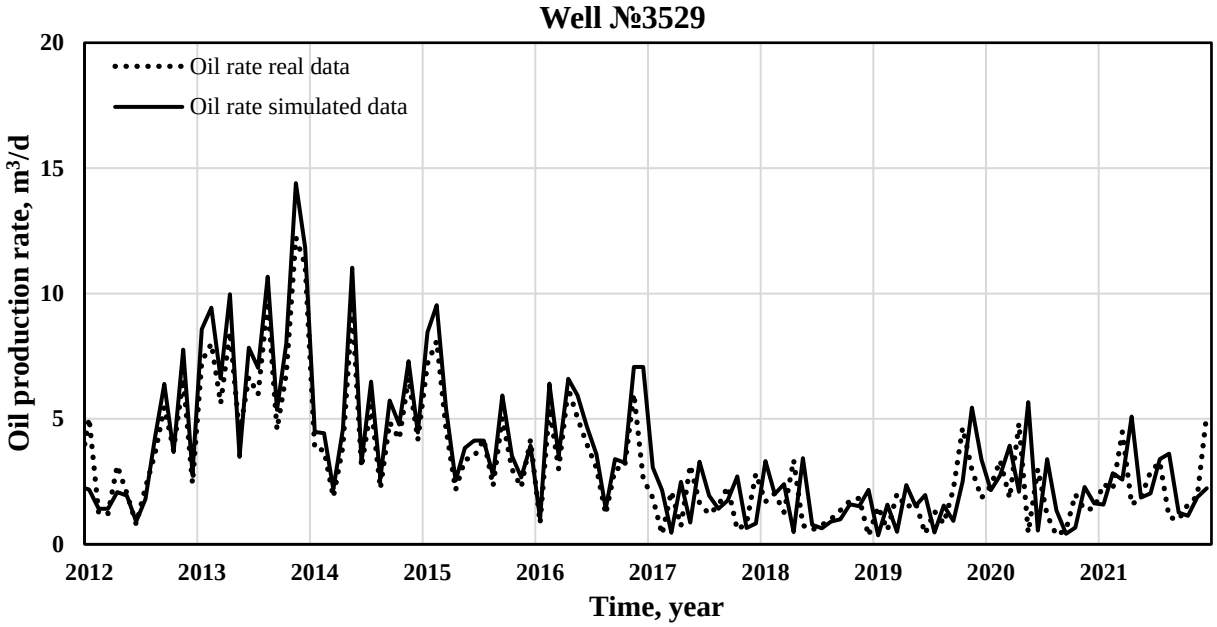

Figure 56. Oil production rate of well №3529 derived from numerical simulation results and real field data.

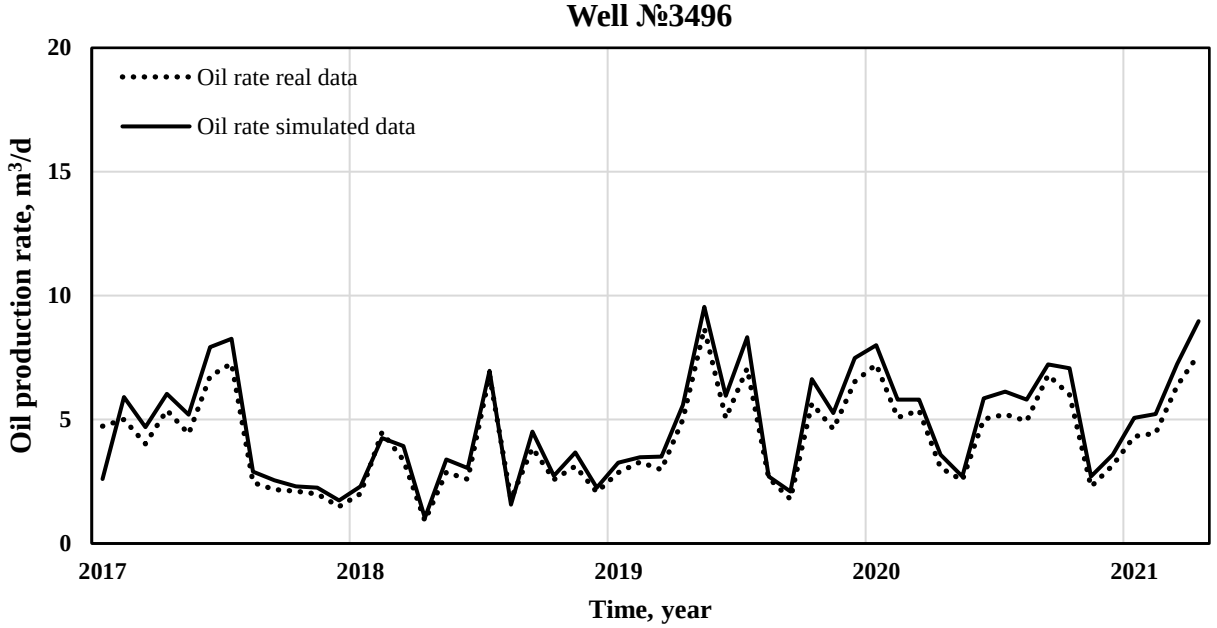

Figure 57. Oil production rate of well №3496 derived from numerical simulation results and real field data.

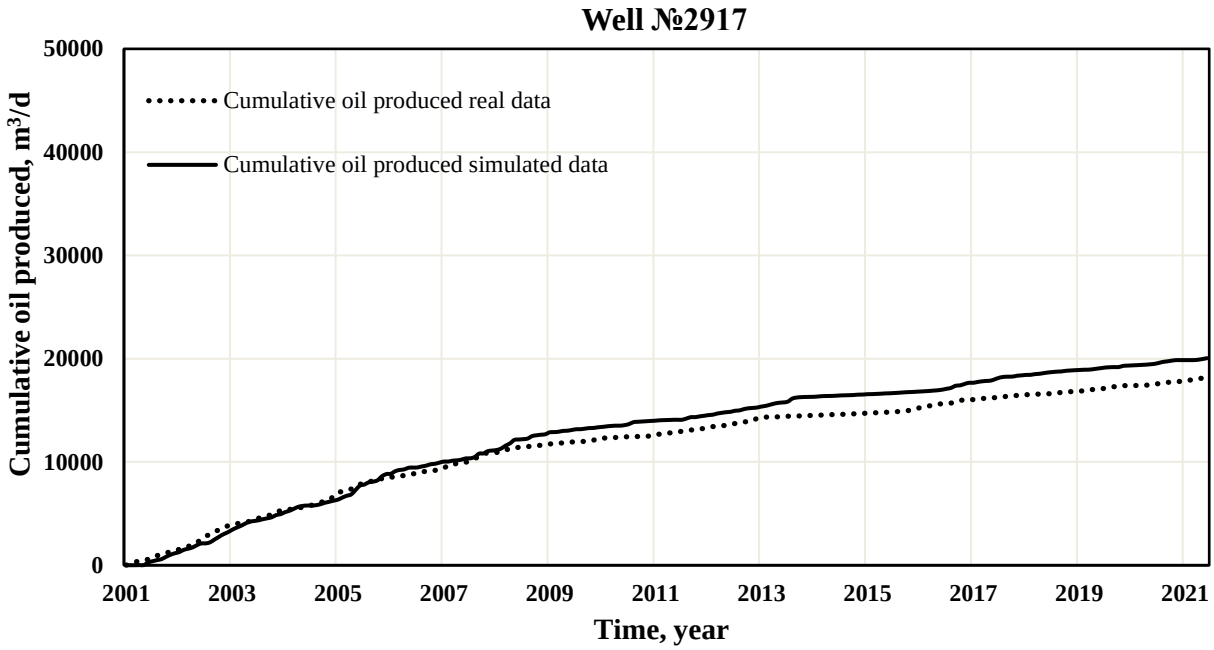

Figure 58. Cumulative oil production of well №2917 derived from numerical simulation results and real field data.

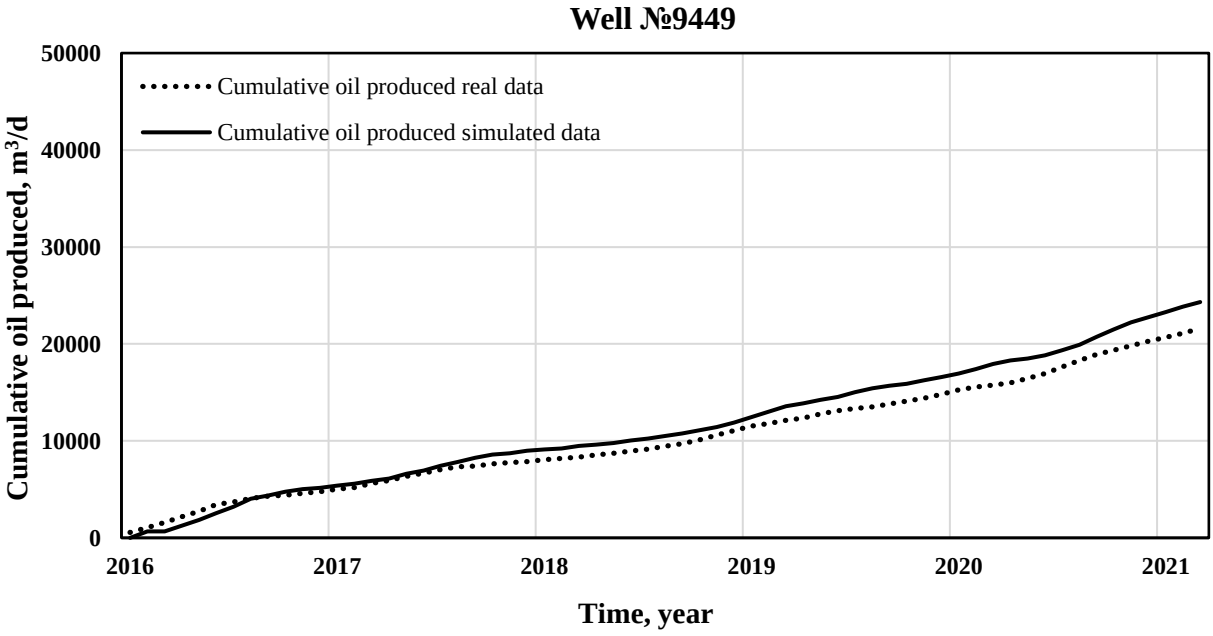

Figure 59. Cumulative oil production of well №9449 derived from numerical simulation results and real field data.

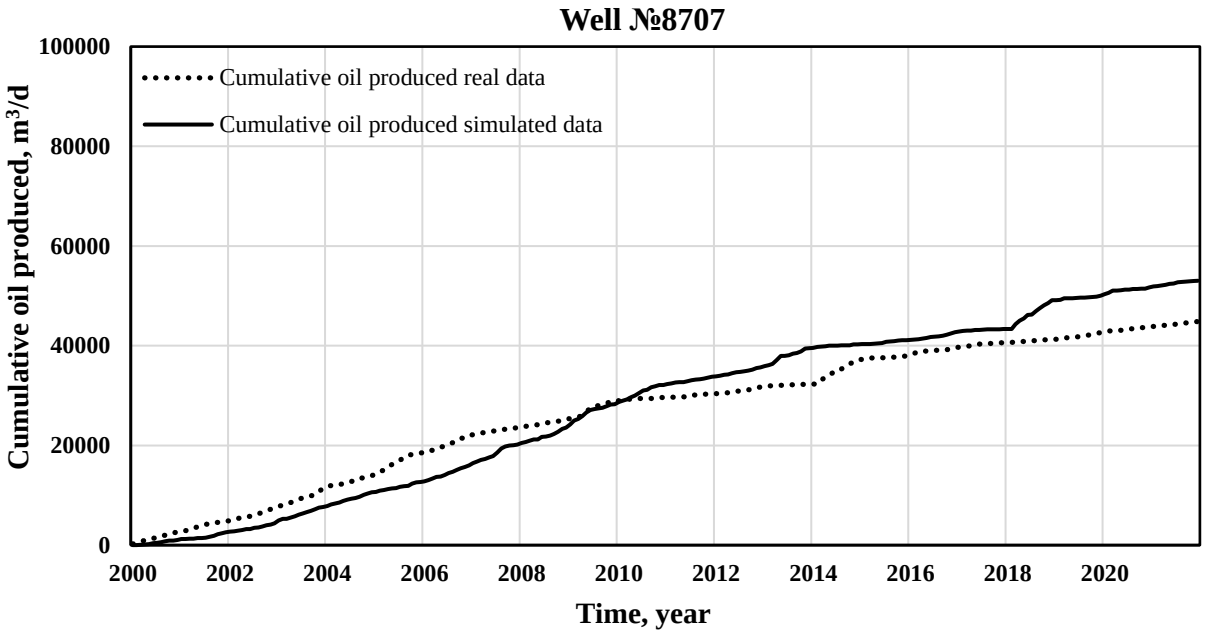

Figure 60. Cumulative oil production of well №8707 derived from numerical simulation results and real field data.

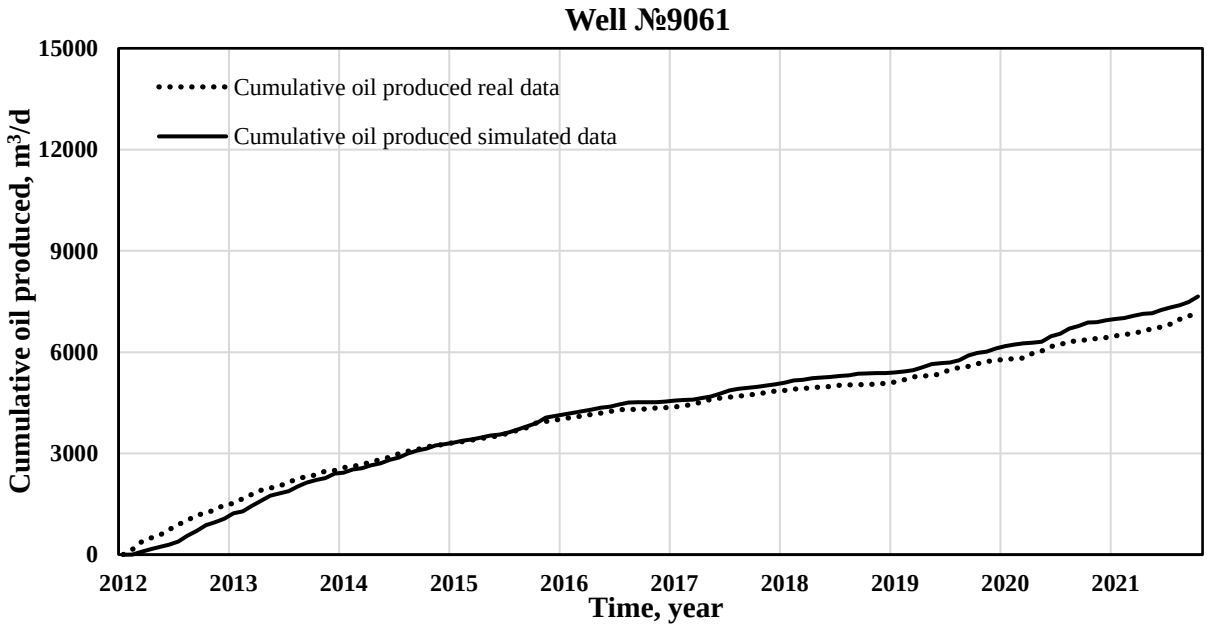

Figure 61. Cumulative oil production of well №9061 derived from numerical simulation results and real field data.

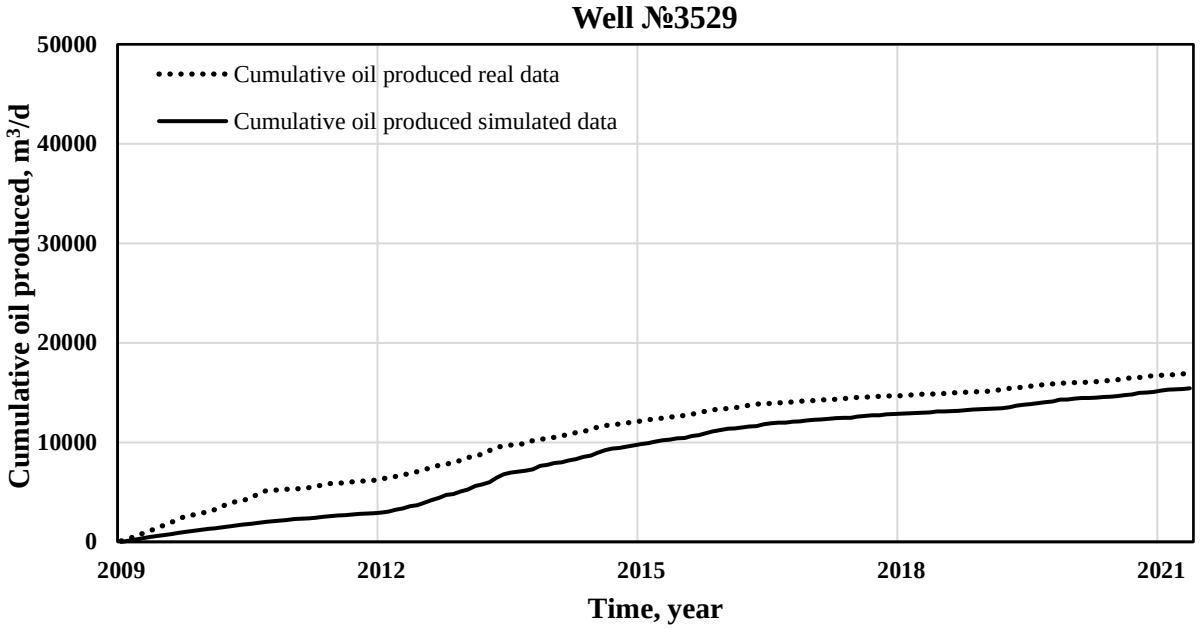

Figure 62. Cumulative oil production of well №3529 derived from numerical simulation results and real field data.

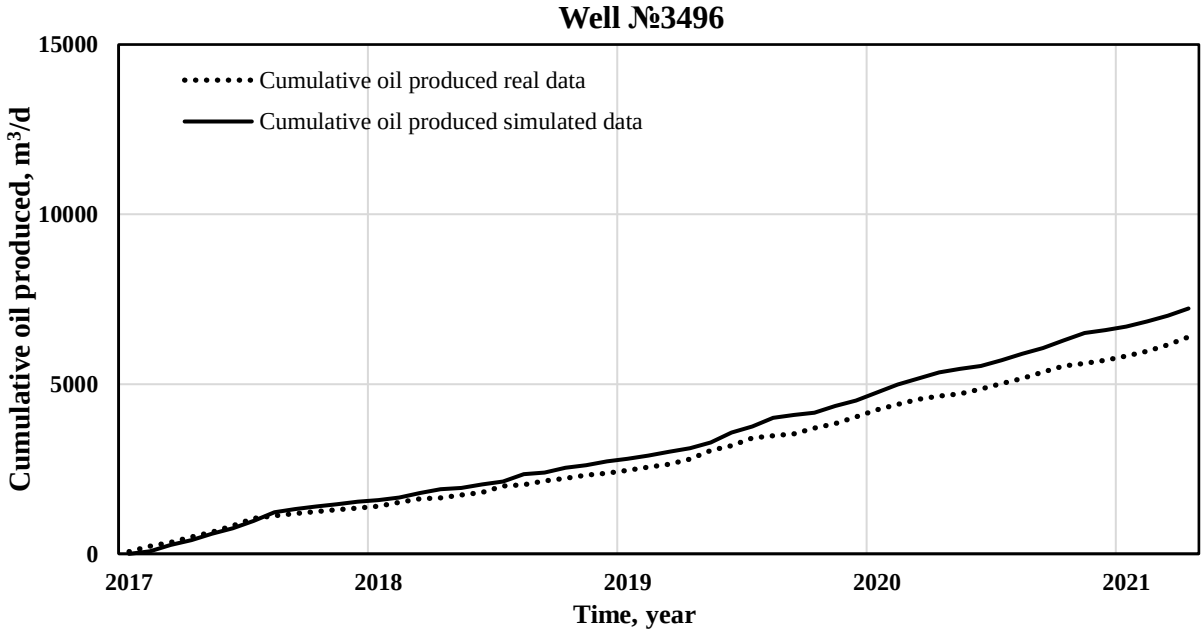

Figure 63. Cumulative oil production of well №3496 derived from numerical simulation results and real field data.

APPENDIX B

1. Conservation Equations

1.1.Volumes and porosities

$$\varphi_f = \frac{V_f}{V_b^0} = \frac{V_v - V_s}{V_b^0} = \frac{V_v}{V_b^0} * \frac{1 - \frac{V_s}{V_v}}{V_v}$$

Where

V_b Current bulk volume

V_0 Initial bulk volume

V_r Rock volume (solid inert matrix, rock grains)

V_v Void volume (fluids & variable solids)

V_s Volume of solid, adsorbed & trapped components

V_f Volume of fluid phases added together

V_w Water (aqueous) phase volume

V_o Oil (oleic) phase volume

V_g Gas (vapour) phase volume

1.2.Accumulation term for energy

$$\frac{d}{dt}\left[V_f\left(\rho_w S_w U_w + \rho_o S_o U_o V_f + \rho_g S_g U_g\right) + V_V C_s U_s + V_r U_r\right]$$

Flow term of energy between two regions

$$\rho_w V_w H_w + \rho_g V_g H_g + \rho_o V_o H_o + K\Delta T$$

1.3.Well source/sink term for energy

$$\rho_w q_{wk} H_w + \rho_g q_{gk} H_g + \rho_o q_{ok} H_o$$

1.4.Heat loss source/sink terms

$$\sum_{k=1}^{n_r} HL_k + HL_V + HL_C$$

1.5.Thermal Aquifer sink/source terms

$$\sum_{k=1}^{n_f}(HA_{CV} + HA_{CD})_K$$

Where

HA_{CV} is a rate of heat transferred by convection to/from the adjacent aquifer

HA_{CD} is a rate of heat transferred by conduction to/from the adjacent aquifer

2. Summary of conservation

$$\frac{d}{dt}\left[V_f\left(\rho_w S_w w_i + \rho_o S_o x_i + \rho_g S_g y_i\right) + V_V A d_i\right] =$$

$$= \sum_{k=1}^{n_f}\left[\left(\rho_w T_w w_i \Delta\emptyset_w + \rho_o T_o x_i \Delta\emptyset_o + \rho_g T_g y_i \Delta\emptyset_g\right) + V\sum_{k=1}^{n_r}(S'_{ki} - S_{ki})r_k\right] + q_w q_{wk} w_i$$

$$+ \sum_{k=i}^{n_f}\left[\varphi D_{wi}\rho_w \Delta w_i + \varphi D_{oi}\rho_o \Delta x_i + \varphi D_{gi}\rho_g \Delta y_i\right] + \delta_{iw}\sum_{k=1}^{n_f} q_w q a q_{wk}$$

$$+ q_o q_{ok} x_i + q_g q_{gk} y_i$$

Where n_f is the number of neighboring regions or grid block faces.

The conservation equation of solid component i is

$$\frac{d}{dt}[V_v C_i] = V\sum_{k=1}^{n_r}(S'_{ki} - S_{ki})r_k$$

The (spatially discretized) conservation equation of energy is

$$\frac{d}{dt}\left[V_f\left(\rho_w S_w U_w + \rho_o S_o U_o V_f + \rho_g S_g U_g\right) + V_V C_s U_s + V_r U_r\right]$$

$$\sum_{k=1}^{n_f}\Bigg[\left(\rho_w T_w H_w \Delta\emptyset_w + \rho_o T_o H_o \Delta\emptyset_o + \rho_g T_g H_g \Delta\emptyset_g\right)$$

$$+\sum_{k=1}^{n_r} K\Delta T + q_w q_{wk} H_w + q_O q_{Ok} H_O + q_g q_{gk} H_g\Bigg]$$

$$+V\sum_{k=1}^{n_r} H_k r_k + HL_o + HL_V + HL_c + \sum_{k=1}^{n_f}(HA_{CV} + HA_{CD})_K$$